Synthesis and Characterization of Iron-Amide and Iron-Imide-Sulfide Clusters

by

Wei Zhang

A thesis

presented to the University of Waterloo

in fulfillment of the

thesis requirement for the degree of

Master of Science

in

Chemistry

Waterloo, Ontario, Canada, 2011

AUTHOR'S DECLARATION

I hereby declare that I am the sole author of this thesis. This is a true copy of the thesis, including any required final revisions, as accepted by my examiners.

I understand that my thesis may be made electronically available to the public.

Abstract

The iron-molybdenum cofactor (FeMo cofactor) is the catalytic center of nitrogen fixation in molybdenum-dependent nitrognease enzymes. The resting state cofactor is a complex [$MoFe_7S_9X$] cluster, in which the central ligand X is a central hexacoordinated monoatomic light atom (2p), and the exact identity of X is uncertain. The heteroligated, nitrogen-containing core environment of the cofactor cluster may also be relevant to active states, as several mechanistic proposals for cofactor catalysis incorporate substrate-derived nitrogenous moeities into the cluster core during turnover. To this end, we have explored synthetic pathways to the dinuclear and tetranuclear nitrogen-containing iron-sufur clusters, which may mimic the heteroligated core environment of the cofactor. Dinuclear iron-amide clusters $Fe_2(\mu\text{-}NH^tBu)_2[N(SiMe_3)_2]_2$ (**46**) and $Fe_2(\mu\text{-}NH^tBu)_2(\mu\text{-}S)[N(SiMe_3)_2]_2$ (**47**) are useful precursors for the preparation of $[Fe_4(N^tBu)_n(S)_{4-n}Cl_4]^z$ cubane complexes that span all mixed imide/sulfide core compositions between the classic [Fe_4S_4] and the more recently reported [$Fe_4(N^tBu)_4$] homoleptic motifs. The [Fe_4NS_3] core of the $n = 1$ cluster is particularly noteworthy in being essentially isometric with the analogous [Fe_4S_3X] subunit of the FeMo cofactor structure. Synthetic compounds are characterized by single crystal X-ray crystallography, cyclic voltammetry, and UV-Vis, ^{1}H NMR spectroscopies.

Acknowledgements

This research project would not have been possible without the support of the following people: first and foremost I wish to express my gratitude to my supervisor, Prof. Sonny C. Lee, who was abundantly helpful and offered invaluable assistance, support and guidance. Deepest gratitude is also due to the members of my supervisory committee, Prof. Richard T. Oakley and Prof. Holger Kleinke, without their knowledge and assistance this study would not have been successful. Special thanks also to all my lab mates: Xudong Chen, Dipesh Prema, Lay Ling Tan, Melanie Chiu and Emily Chan, for their time in helping with my thesis presentation and always being there to answer questions. I also wish to express my gratitude to my family and friends who helped me get through every day with their understanding and endless help.

Table of Contents

List of Figures

List of Schemes

List of Tables

List of Abbreviations

BNF	Biological nitrogen fixation
ENDOR	Electron-nuclear double resonance
ESEEM	Electron spin echo envelope modulation
EDX	Energy-dispersive X-ray spectroscopy
Et_2O	Diethyl ether
Fe-N	Iron-nitrogen
Fe-NR	Iron-imide
Fe-NR-S	Mixed iron-imide-sulfide
Fe-S	Iron-sulfur
HSTip	2,4,6-triisopropylphenylthiol
HSDmp	2,6-dimesitylphenylthiol
HMDSO	Hexamethyldisiloxane
HMDSA	Hexamethyldisilazane
MeCN	Acetonitrile
Mes	Mesityl
Am	Amyl
NMR	Nuclear magnetic resonance
Ph	Phenyl
TMS	Trimethylsilyl
THF	Tetrahydrofuran

UV-Vis	Ultra-violet and visible

Table of Compounds

Number	Formula	Number	Formula
1(a/b/c)	Biological iron-sulfur clusters	**28**	$[Et_4N]_2[Fe_2(\mu\text{-NAr})_2Cl_4]$
2(a/b/c)	Synthetic iron-sulfur clusters	**29**	$[Et_4N]_2[Fe_3(\mu\text{-NAr})_4Cl_4]$
3	$[Et_4N]_3[Mo_2Fe_7S_8(SEt)_{12}]$	**30**	$[Et_4N]_2[Fe_4(\mu_3\text{-NAr})_4Cl_4]$
4	$[Et_4N]_4[Mo_2Fe_6(cat)_2(SEt)_6]$	**31**	$Li[Fe_4(\mu_3\text{-N}^t\text{Bu})_4Cl_4]$
5a	$[Et_4N]_2[(cat)(solv)MoFe_3S_4(SEt)_3]$	**32**	$[Fe_4(\mu_3\text{-N}^t\text{Bu})_4Cl_4]$
5b	$[Et_4N]_2[(cat)(solv)MoFe_3S_4(SCl)_3]$	**33**	$[Fe_4(\mu_3\text{-N}^t\text{Bu})_4(\text{N}^t\text{Bu})Cl_3]$
5c	$[Et_4N]_2[(Meida)MoFe_3S_4(SCl)_3]$	**34**	$Li[Fe(\text{NH}_2{}^t\text{Bu})_2Cl_2]$
6	$[Et_4N]_3[Fe_3S_4(SEt)_4]$	**35**	$Li_2[Fe_2(\mu\text{-N}^t\text{Bu})_2Cl_4]$
7	$Mo(CO)_3(MeCN)_3$	**36**	$Li[Fe_3(\mu_3\text{-N}^t\text{Bu})(\mu\text{-N}^t\text{Bu})(\mu\text{-NH}^t\text{Bu})_2Cl_3]$
8	$[Et_4N]_3[Fe_3S_4(SEt)_3Mo(CO)_3]$	**37**	$[Et_4N]_4[Fe_4N_2Cl_{10}]$
9	$[NH_4]_3[VFe_2S_4Cl_4]$	**38**	$[Et_4N]_5[Fe_{10}N_8Cl_{12}]$
10	$[NH_4][(solv)_3VFe_3S_4Cl_3]$	**39**	$[Et_4N]_4[Fe_{14}N_8(NSnMe_3)_4Cl_{12}]$
11	$[NH_4][(solv)_3VFe_3S_4SR_3]$	**40**	$Fe_2(\mu\text{-N}^t\text{Bu})_2Cl_2(\text{NH}_2{}^t\text{Bu})_2$
12a	$[NH_4]_3[(Meida)VFe_3S_4(SCl)_3]$	**41**	$[Et_4N]_2[Fe_2(\mu\text{-N}^t\text{Bu})(\mu\text{-S})Cl_4]$
12b	$[NH_4]_2[(Tp)VFe_3S_4(SCl)_3]$	**42**	$[Et_4N][Fe_4(\mu_3\text{-N}^t\text{Bu})_3(\mu_3\text{-S})Cl_4]$
13	$(Tp)MoS(S_4)$	**43**	$[Et_4N]_2[Fe_4(\mu_3\text{-N}^t\text{Bu})_2(\mu_3\text{-S})_2Cl_4]$
14a	$Na[(Tp)MoFe_3S_4Cl_3]$	**44**	$[Et_4N]_2[Fe_4(\mu_3\text{-N}^t\text{Bu})_2(\mu_3\text{-S})_2Cl_4]$
14b	$[BPh_4][(Tp)MoFe_6S_8PEt_3]$	**45**	$[Et_4N]_2[Fe_4(\mu_3\text{-N}^t\text{Bu})(\mu_3\text{-Se})_3Cl_4]$
15a	$(Tp)_2Mo_2Fe_6S_8(PEt_3)_4$	**46**	$Fe_2(\mu\text{-NH}^t\text{Bu})_2[N(SiMe_3)_2]_2$
15b	$[Et_4N]_4[(Tp)_2Mo_2Fe_6S_8Cl_3]$	**47**	$Fe_2(\mu\text{-N}^t\text{Bu})_2(\mu\text{-S})[N(SiMe_3)_2]_2$

16 $[Et_4N]_3[(Tp)_2Mo_2Fe_6S_9(SH)_2]$

17 $(Tp)_2V_2Fe_6S_8(PEt_3)_4$

18 $[Et_4N]_3[(Tp)_2V_2Fe_6S_9(SH)_2]$

19 $[\{N(SiMe_3)_2\}\{SC(NMe_2)_2\}Fe_4S_3]_2(\mu_6\text{-S})\{\mu\text{-SN}(SiMe_3)_2\}_2$

20 $Fe_3\{N(SiMe_3)_2\}_2(\mu\text{-Stip})_4$

21 $[Fe_4S_3(SDmp)]_2(\mu\text{-SDmp})_2(\mu\text{-STip})(\mu_6\text{-S})$

22 $[Fe_4S_3(STip)]_2(\mu\text{-SDmp})_2\{\mu\text{-N}(SiMe_3)_2\}(\mu_6\text{-S})$

23 $Fe[N(SiMe_3)_2]_2$

24 $Fe[N(SiMe_3)_2]_2(SAr)$

25 $[Fe_4(\mu_3\text{-NPh})_4SAr_4]$

26 $[FeCl[N(SiMe_3)_2]_2(THF)]$

27 $Li[Fe[N(SiMe_3)_2]_2(Cl)_2]$

48 $Fe_2(\mu\text{-NH}^t\text{Bu})[\mu\text{-N}(SiMe_3)_2][N(SiMe_3)_2]_2$

49 $Fe_3(\mu\text{-NH}^t\text{Bu})_4[N(SiMe_3)_2]_2$

50 $Fe_2(\mu\text{-NH}^t\text{Am})_2[N(SiMe_3)_2]_2$

51 $Fe_3(\mu\text{-NHMes})_4[N(SiMe_3)_2]_2$

52 $Fe_2(\mu\text{-N}^t\text{Bu})_2(\mu\text{-Se})[N(SiMe_3)_2]_2$

53 $Fe_2(\mu\text{-N}^t\text{Bu})_2(\mu\text{-I})[N(SiMe_3)_2]_2$

CHAPTER 1. INTRODUCTION

1.1 Metalloclusters in Biological Nitrogen Fixation

The element nitrogen is essential to all life because it is a basic component of many biochemical compounds, such as amino and nucleic acids.[1] Dinitrogen, while highly abundant, is chemically inaccessible to most organisms. Therefore, most biochemical processes require the use of "fixed" forms of nitrogen, such as ammonia (NH_3) or nitrate ion (NO_3^-). The conversion of dinitrogen into ammonia (NH_3) is critical for life because it makes naturally abundant nitrogen, which is around 78% of the atmosphere, available for biological use. This process is commonly termed "nitrogen fixation", and can be accomplished both industrially and biologically.[2]

Industrial nitrogen fixation is achieved by the Haber-Bosch process, which allows for the economical synthesis of ammonia from dinitrogen and dihydrogen on a large scale. This process is accomplished at 15–25 MPa (150–250 bar) between 300 and 550 °C with iron as the catalyst.[3] In contrast, biological nitrogen fixation (BNF) is achieved by microorganisms at atmospheric pressure and ambient temperatures.[4] The currently known minimal stoichiometry for this reaction can be represented by Equation 1.1.[5]

$$N_2 + 8H^+ + 8e^- + 16MgATP \longrightarrow 2NH_3 + H_2 + 16MgADP + 16P_i \quad \text{(eq 1.1)}$$

BNF is catalyzed by the nitrogenase enzymes, which occur in Mo-dependent, V-dependent and Fe-only forms.[6] The Mo-dependent nitrogenase is the most widely studied enzyme form of this class, and it consists of two distinct proteins: the Fe protein, and the MoFe protein. The former is an approximately 60 kDa homodimer, responsible for electron transfer and MgATP hydrolysis. A single [Fe_4S_4] cluster bridges the two subunits through cysteinate residues.[7, 8] The MoFe protein is an approximately 250 kDa

$\alpha_2\beta_2$ tetramer; this protein is the site of dinitrogen reduction.[9] It contains two structurally complex metalloclusters not found elsewhere in nature: the P-cluster and the FeMo-cofactor (Figure 1.1).

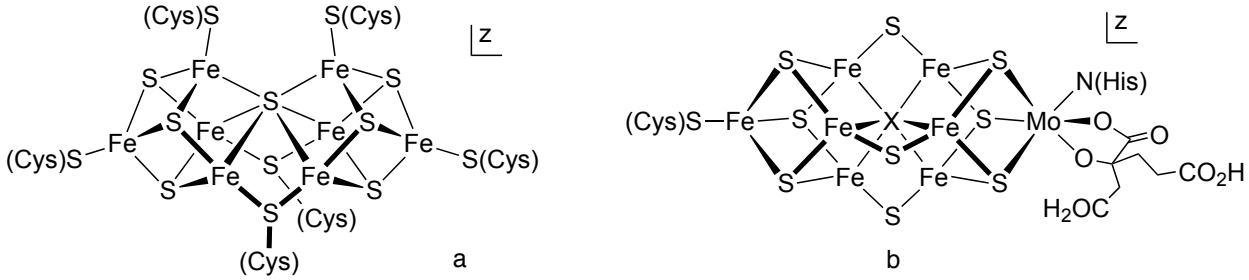

Figure 1.1. The P-cluster and the FeMo-cofactor

Two P-clusters are present in the MoFe protein. Each P-cluster is located between an α- and β-subunit interface, where it participates in the electron transfer from the Fe protein to the FeMo cofactor. The reduced form (P^N) of the P-cluster consists of two [Fe_4S_3] incomplete cubanes linked by a hexacoordinate (μ_6) sulfide ligand and two bridging cysteinate ligands.[10, 11] All the iron atoms in the P^N state are believed to be weak-field Fe(II).[12]

One FeMo cofactor is localized within each α-subunit of the MoFe protein; the cofactor is almost certainly the active site where the binding and reduction of N_2 and other substrates occur. The overall structure of the FeMo cofactor is complex and can be viewed as subunits [Fe_4S_3] and [$MoFe_3S_3$] bridged by three inorganic sulfide ligands.[13, 14] The iron atoms are believed to be high-spin in this cofactor, although their exact oxidation states are uncertain. The latest high-resolution (1.16 Å) X-ray structural analysis of the MoFe protein reveals the presence of a μ_6 interstitial light atom X in the center of the cofactor.[15, 16] This atom can be assigned as carbon, oxygen or nitrogen, and the latter was proposed to be the most likely candidate because the experimental resolution-dependent electron density profile best matches the calculated curve when the interstitial atom is set to be nitrogen.[16] Although a significant

amount of work has been performed to assign X since it was discovered in 2002, the identification of this light atom is still an open question and remains controversial.[16] After comparing the redox data from measurements and calculations of the FeMo cofactor by using density functional theory (DFT), Noodleman and co-workers suggest that X = N,[17] which is also supported by Dance[18] and Nørskov[19] from theoretical studies. However, electron spin echo envelope modulation (ESEEM) and electron−nuclear double resonance (ENDOR) measurements on $^{14/15}$N and $^{12/13}$C isotopomers of the FeMo cofactor by Hoffman and co-workers,[20, 21] provide no evidence of hyperfine couplings from carbon or nitrogen. There are still many details about the FeMo cofactor that remain uncertain at present, such as the substrate binding site, the cluster charge state, the structural relationship between the resting state enzyme and catalytically-active forms, and the assembly, both biological and synthetic, of the cofactor.

Although the P-cluster and the FeMo-cofactor consist of different metal-sulfide cluster frameworks and play different roles in the enzymatic function of nitrogenase, their cluster cores share some structural similarities. First, they are both constructed from two incomplete cubanes, each of which consists of four metal atoms and three sulfur atoms. Second, they each have a hexacoordinated central atom encapsulated in the cluster framework.

1.2 Iron-Sulfur Clusters

The clusters found in nitrogenase are iron-sulfur clusters. In general, iron-sulfur clusters play important roles in numerous biological processes, including electron transfer and catalysis.[22, 23] The three dominant kinds of iron-sulfur clusters are presented in Figure 1.2: (1a) [Fe_2S_2], (1b) [Fe_4S_4], (1c) [Fe_3S_4]. These clusters all contain tetrahedrally coordinated weak-field Fe(II, III) centers, bridged by inorganic sulfide ligands and terminally ligated by four cysteinate residues.

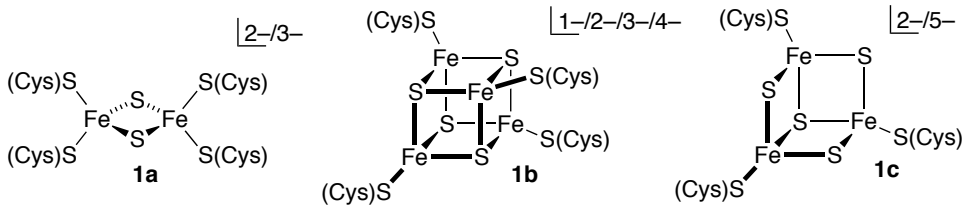

Figure 1.2. Biological iron-sulfur clusters

These biological clusters have been studied by the preparation of synthetic analogues. The synthetic analogues are relatively small molecules that reproduce the structure and chemical properties of the biological metal centers.[24] The investigation of these low-molecular-weight analogues, which are available in highly pure, crystalline form and share essential properties with the biological molecules is expected to be useful in understanding the synthesis and structural chemistry of these complexes, their physical properties, and their roles in catalysis.[25]

With respect to the biological iron-sulfur clusters, many synthetic analogues (Figure 1.3) have been prepared in the last 40 years.[26] Cluster **2a** contains a planar rhombic core, could be found in $[Fe_2S_2(S_2\text{-o-xyl})_2]^{2-}$, which first mimicked the geometry of biological $[Fe_2S_2]$ cluster (**1a**) and was reported in 1973.[27] The oxidized form $[Fe_2S_2(S_2\text{-o-xyl})_2]^{-}$ was also synthesized in 1975.[28] However, the X-ray structure of the protein-bond $[Fe_2S_2]$ core was not proved by crystallography until 1978.[29, 30] Cluster **2b**, obtained as $[Fe_4S_4(SCH_2Ph)_4]^{2-}$, contains a cubane-type structure,[31] which shared the full molecular connectivity with the biological $[Fe_4S_4]$ cluster (**1b**).[32] A broader range of $[Fe_4S_4]$ synthetic analogues has also been achieved through multiple oxidation state changes and ligand substitution.[33, 34] The structure of protein site $[Fe_3S_4]$ (**1c**) cluster was first confirmed in 1989,[35] but it was not until 1995 that the topological analogue (**2c**) was prepared as it was stabilized by a unique ligand.[36, 37] The successful syntheses of these clusters have allowed the exploration of metal sites in iron sulfur proteins at a molecular level and have

developed chemistry for the subsequent construction of high-nuclearity compounds related to the P-cluster and the FeMo cofactor.

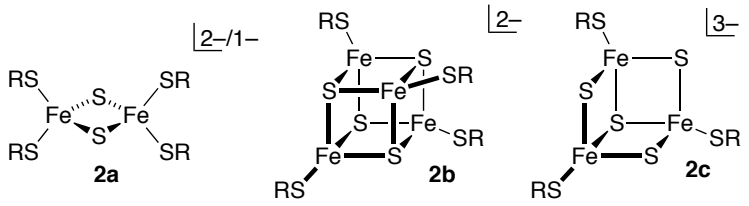

Figure 1.3. Synthetic analogues of iron-sulfur clusters

Scheme 1.1 Syntheses of $[MoFe_3S_4]$ clusters

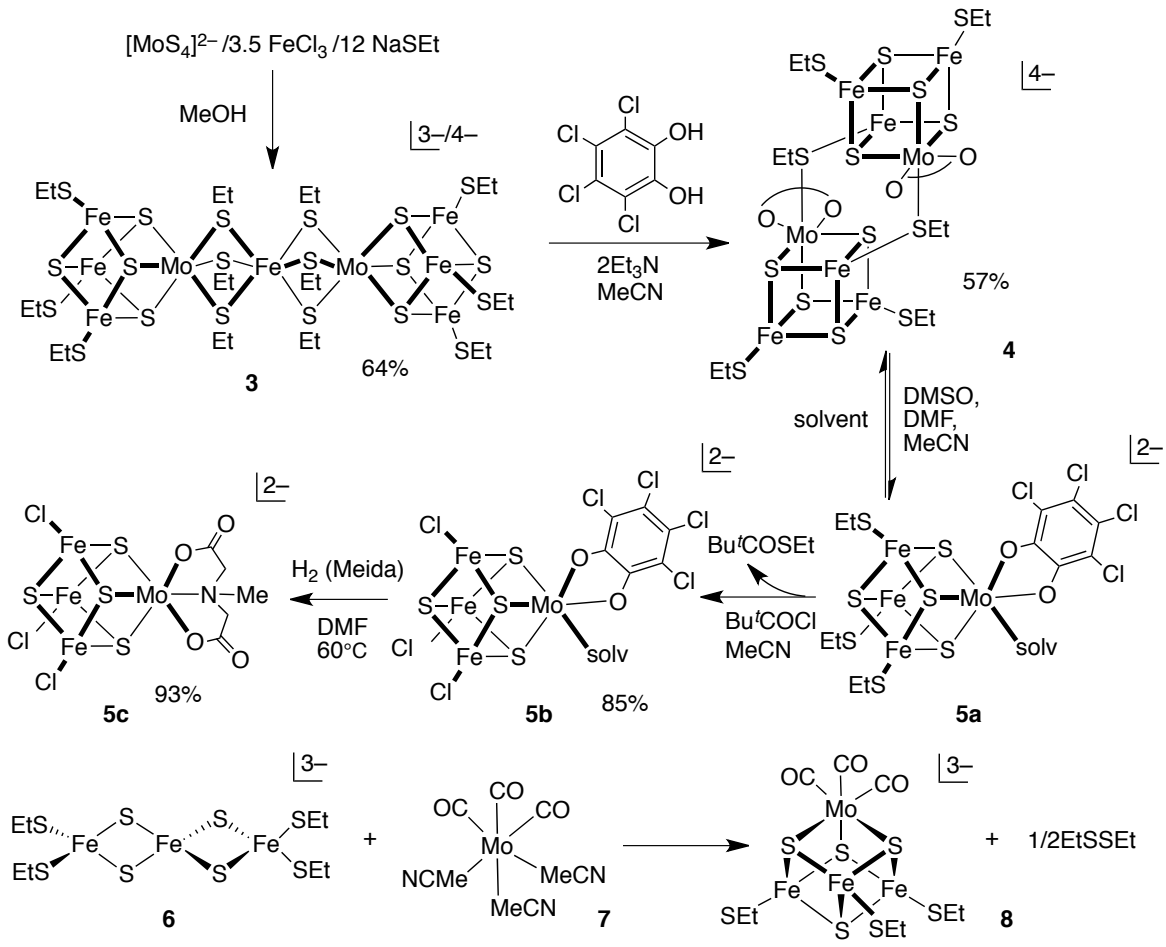

In addition to these dinuclear, voided cuboidal, and cuboidal tetranuclear iron-sulfur complexes, partial synthetic analogues of the more complicated P-cluster and FeMo cofactor (Figure 1.1) forms have

been prepared. To better mimic the bimetallic system in the FeMo cofactor, the incorporation of molybdenum into iron-sulfur clusters to form the $[MoFe_3S_4]$ core was developed by Holm and Garner in 1981.[38-40] Currently, there exist two major routes to the construction of this heterometallic cubane cluster framework, which are summarized in Scheme 1.1. The first route proceeds through the synthesis of a double $[MoFe_3S_4]$ cubane cluster **3** by self-assembly, followed by core rearrangement to form cluster **4** and a single $[MoFe_3S_4]^{2-}$ cubane **5a** was obtained by bridge cleavage of the double cubane. Treatment of **5a** with different ligands yielded the other ligated clusters **5b** and **5c**.[41–43] The second route is the integration of a molybdenum mononuclear cluster **7** into a preassembled $[Fe_3S_4(SEt)_4]^{3-}$ compound **6** to afford the $[Fe_3S_4(SEt)_3Mo(CO)_3]^{3-}$ cluster **8**.[44–46]

Scheme 1.2. Syntheses of $[VFe_3S_4]$ clusters

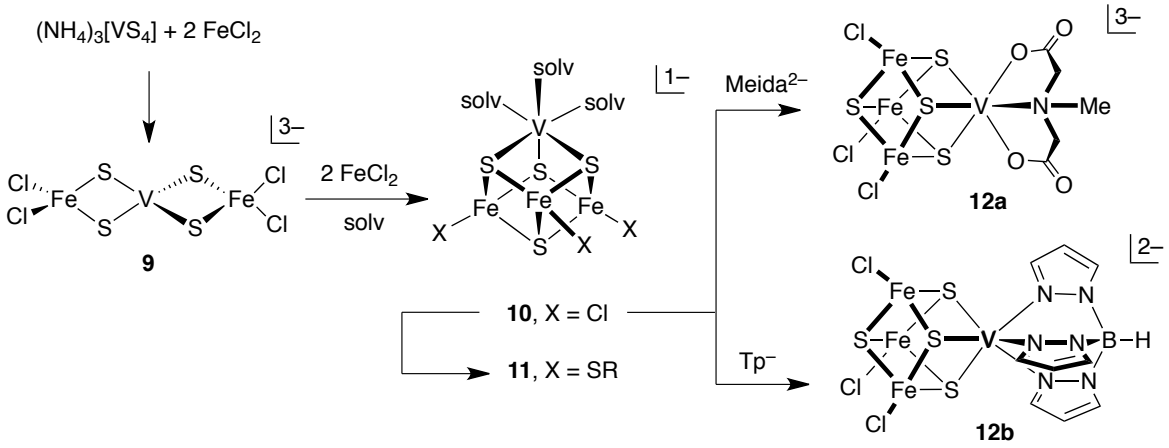

The successful incorporation of the heterometal molybdenum into iron-sulfur clusters raises another question, the possibility of inserting another metal, vanadium, into iron-sulfur clusters. This work was motivated by the existence of another type of nitrogenase, the V-dependent form, which contains vanadium. Clusters described in Scheme 1.2 were first synthesized by Holm in 1986.[47-49] This reaction was started from a mononuclear cluster $(NH_4)_3[VS_4]$ which reacted with $FeCl_2$ to form a linear complex **9**,

which is further reduced by $FeCl_2$ and rearranged the core geometry to generate complex **10**. The solvent in cluster **10** is MeCN. Ligand substitution of cluster **10** can generate cluster **11**, which contains a different solvent ligand as DMF or Me_2SO. Cluster **10** is also the starting material for making the other two V-Fe-S complexes, **12a** and **12b**. These two clusters can be obtained by compound **10** reacting with Tp [hydrotris(pyrazolyl) borate(1–)] and MeIDA [methylimidodiacetate(2–)] respectively.

Scheme 1.3. Synthesis of a $[Mo_2Fe_6S_9]$ cluster

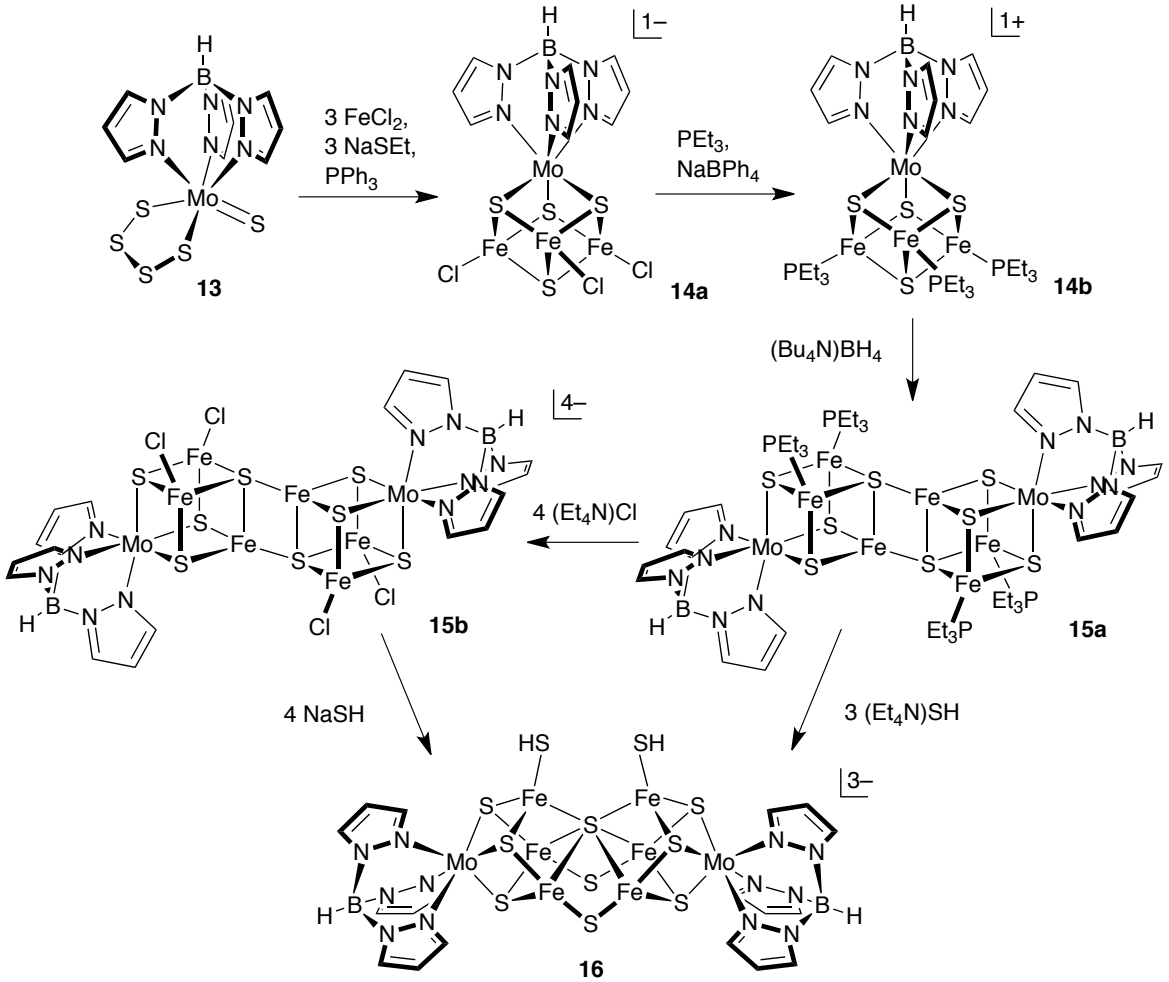

Tetranuclear heterometallic clusters $[MFe_3S_4]$ (M = Mo, V) have proven to be useful in constructing higher-nuclearity clusters that are more related to the FeMo cofactor in nitrogenase. More

recent progress in this area is the synthesis of a Mo-containing P^N-cluster topological analogue, which was prepared via core conversion by Holm in 2002.[50] The detailed synthetic pathway is described in Scheme 1.3. The scheme started with the self-assembly of mononuclear cluster **13** and $FeCl_2$ to form a $[MoFe_3S_4]$ single cubane **14a**. Cluster **14a** was converted to **14b** by reductive substitution. The reduction of **14b** with borohydride yielded a neutral double cubane **15a**. Substitution of the terminal ligand of **15a** with chloride gave **15b**. The reaction of hydrosulfide with **15a** or **15b** lead to: substantial core rearrangement with the incorporation of one additional sulfide, substitution of the terminal ligands, and one electron oxidation of the cluster. This reaction formed a new cluster **16**, which was the first synthetic cluster shown to simulate the core structure of the P^N-cluster of nitrogenase: the $[Mo_2Fe_6S_9]$ core contains two $MoFe_3(\mu_3\text{-}S)_3$ cuboidal fragments which are connected by two μ_2-S atoms and one μ_6-S atom, whereas in the P^N-cluster, two $Fe_4(\mu_3\text{-}S)_3$ cuboidal fragments are linked by two μ_2-SCys bridges and one μ_6-S atom.[31]

Scheme 1.4. Synthesis of a $[V_2Fe_6S_9]$ cluster

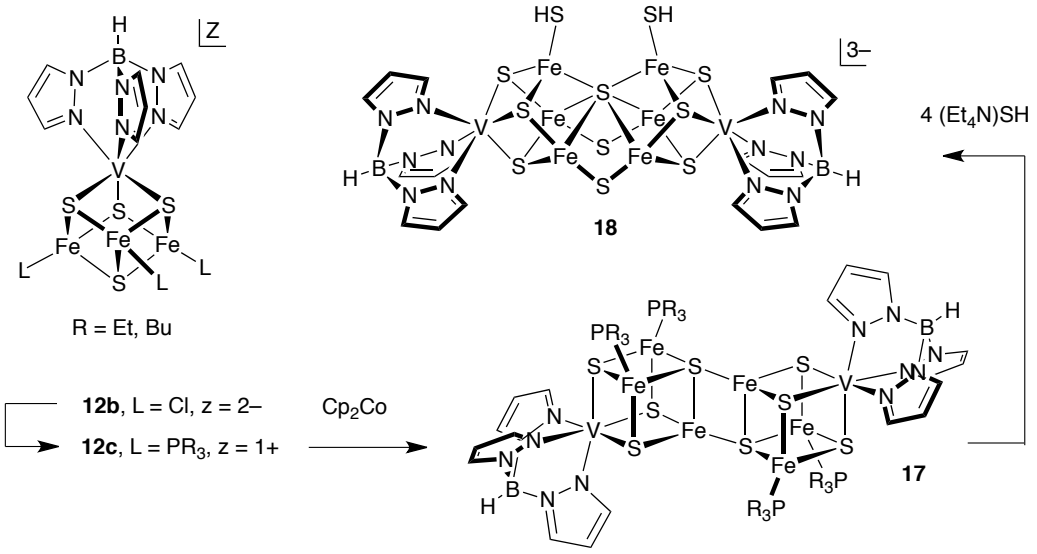

To examine whether the P^N-cluster structure can be prepared in other molecules, the V-containing P^N-cluster topological analogue has been synthesized. Scheme 1.4 summarized the reaction

route, which parallels Scheme 1.3.[51, 52] The phosphine substitution of **12b** yielded cluster **12c**. Reduction of cluster **12c** with cobaltocene gives a double cubane **17**. Reaction of **17** with hydrosulfide leads to $[V_2Fe_6S_9]$ cluster **18,** which is a V-containing iron-sulfur cluster partially reproducing the P^N-cluster core.

Scheme 1.5. Syntheses of $[Fe_8S_7]$ clusters

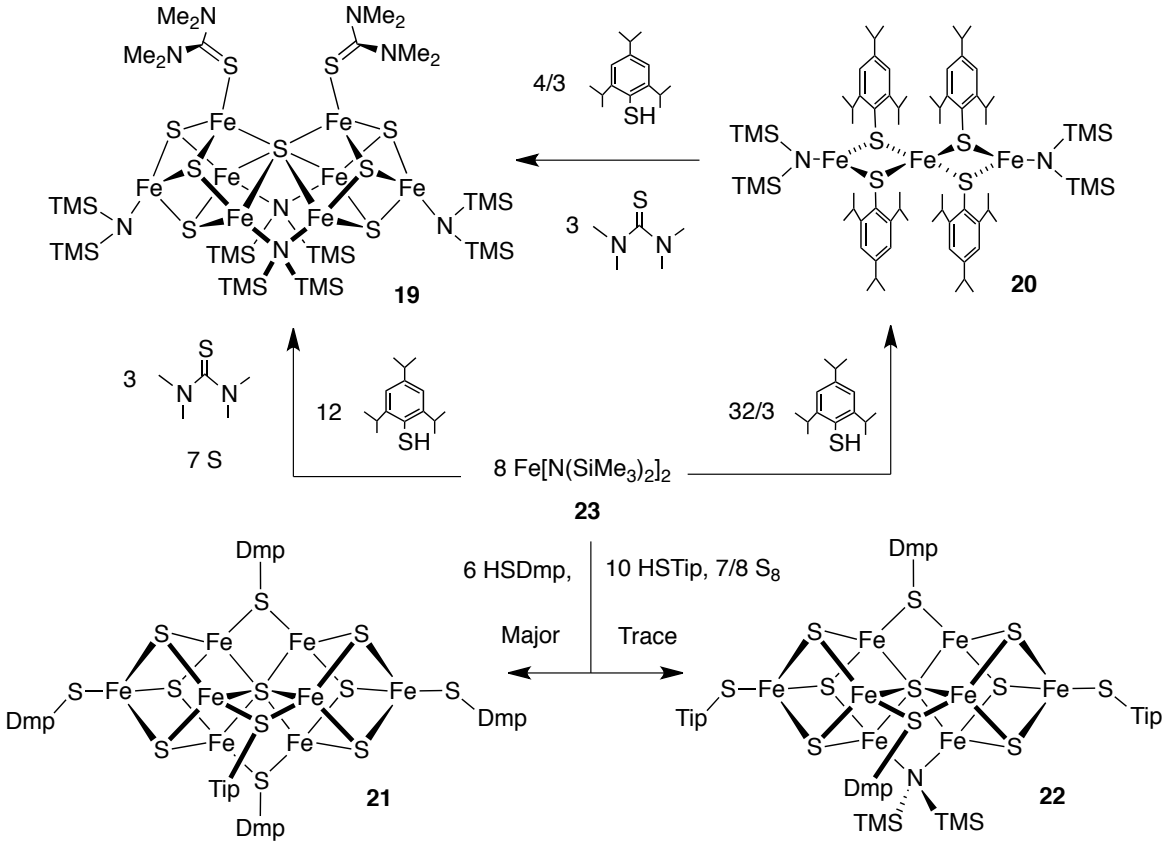

Compared with the core structure of the P^N-cluster, one of the differences in these two clusters $[M_2Fe_6S_9]$ (M = Mo, V) is the presence of the heterometal instead of an all-Fe_8 metal version. A related discovery reported by Tatusmi involves self-assembly of a ferrous precursor **23** to a new $[Fe_8S_7]$ cluster **19**, which better reproduces the $[Fe_8S_7]$ core geometry of the P^N-cluster.[53-55] The linear trinuclear cluster **20** is also made by assembling complex **23**, and **20** can be further reacted to obtain cluster **19**. Although this new cluster has all-Fe_8 metal content, the two $Fe_4(\mu_3\text{-}S)_3$ cuboidal fragments are linked by two

μ_2-N(TMS)$_2$ bridges and one μ_6-S atom instead of two μ_2-SCys bridges and one μ_6-S atom. Another difference is that the iron oxidation states in **19**, formally assigned as 6Fe(II)/2Fe(III), differ from the P^N-cluster.

Similarly, Tatsumi and coworkers have synthesized another class of [Fe_8S_7] clusters (**21** and **22**) through self-assembly, which are topological analogues of the FeMo cofactor.[55] The molecule of cluster **21** consists of two Fe_4S_3 cuboidal units, which are connected by one μ_6-S atom, two μ_2-SDmp bridges and one μ_2-STip bridge. In cluster **22**, one μ_2-N(TMS)$_2$ bridge, one μ_6-S atom and two μ_2-SDmp bridges link the two incomplete Fe_4S_3 cores, whereas incomplete [Fe_4S_3] and [$MoFe_3S_3$] subunits in FeMo-cofactor are bridged by three inorganic sulfide ligands and possibly one μ_6-N atom. Clusters **19**, **21** and **22** in Scheme 1.5 only partially mimic the geometry of P^N-cluster and FeMo-cofactor. The development of new synthetic routes to complicated cluster frameworks structurally similar to the nitrogenase metalloclusters, however, is a significant advancement.

1.3 Iron-Nitrogen Clusters

Previous investigations of nitrogenase-related synthetic metalloclusters are mostly based on the well-known iron-sulfur clusters and considerable contributions have been made in this area. Meanwhile, iron-nitrogen clusters are also potentially important in exploring the chemistry of the FeMo cofactor for three reasons: (i) the iron sites are currently considered to be the sites of dinitrogen binding and reduction, although the substrate transformation is not understood; (ii) the heteroligated, nitrogen-containing core environment of the cofactor cluster may also be relevant to active states, as several mechanistic proposals for cofactor catalysis incorporate substrate-derived nitrogenous moeities into the cluster core during turnover by computational studies;[56] and (iii) nitrogen (as nitride) is one of the candidates that may be

located at the center of the Fe_6 trigonal prism in the FeMo cofactor. The study of the interaction of iron centers and nitrogen anions in an FeMo cofactor-like environment, i.e., weak-field, tetrahedral Fe(II, III), can therefore provide the enzymatic and chemical connection to the process of biological nitrogen fixation.

Scheme 1.6. Syntheses of Fe-NR clusters from a ferrous precursor

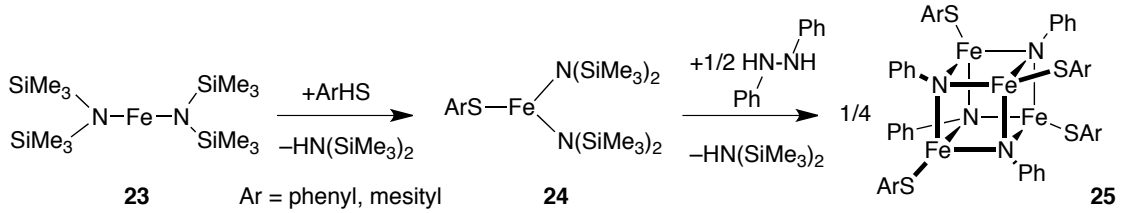

23 Ar = phenyl, mesityl **24** **25**

Scheme 1.7. Syntheses of Fe-NR clusters from a ferric precursor

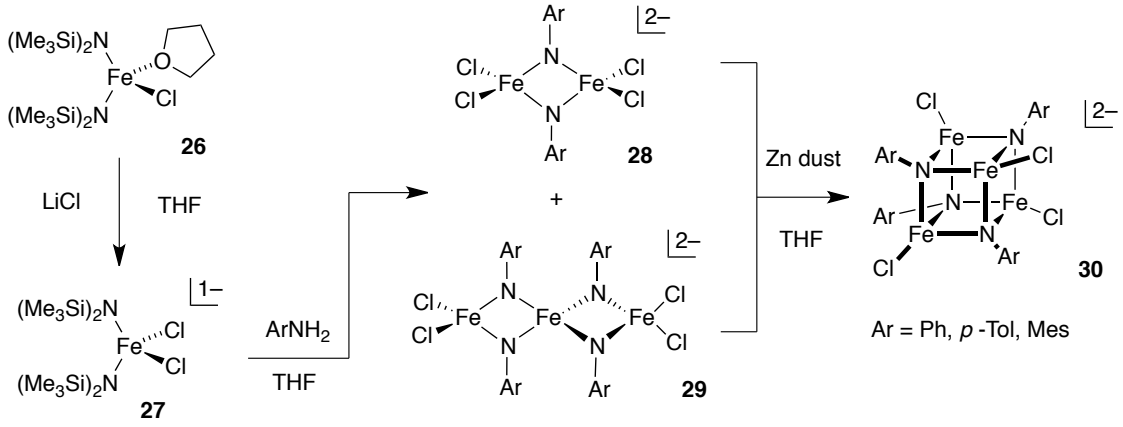

The first weak-field iron-nitrogen clusters were reported by Lee in 1999;[57] their syntheses start from the protonolysis of a ferrous precursor **23** by an aryl thiolate to **24**, followed by the oxidative addition of a diarylhydrazine to produce all-ferric clusters **25**. These ferric imide thiolate clusters **25** (Ar = phenyl, mesityl) provided an opportunity to investigate the iron-nitrogen bond chemistry that is potentially relevant to the nitrogenase mechanism (Scheme 1.6).

Since then, an extensive number of iron-imide (Fe-NR) clusters have been synthesized and characterized in the Lee lab (Scheme 1.7).[58] More recent examples derive from ferric precursor **26**, which contains a labile ligand, THF, that can be easily substituted by chloride to afford **27**. The protonolysis of **27** is an effective pathway to dinuclear cluster **28** and trinuclear cluster **29**. Subsequent reduction of **28** and **29** by Zn dust yields **30**, a heterocubane with iron atoms in formal oxidation states of 2Fe(II)/2Fe(III).

Scheme 1.8. Syntheses of Fe-NR clusters from $FeCl_3$ and Li(NH^{t}Bu)

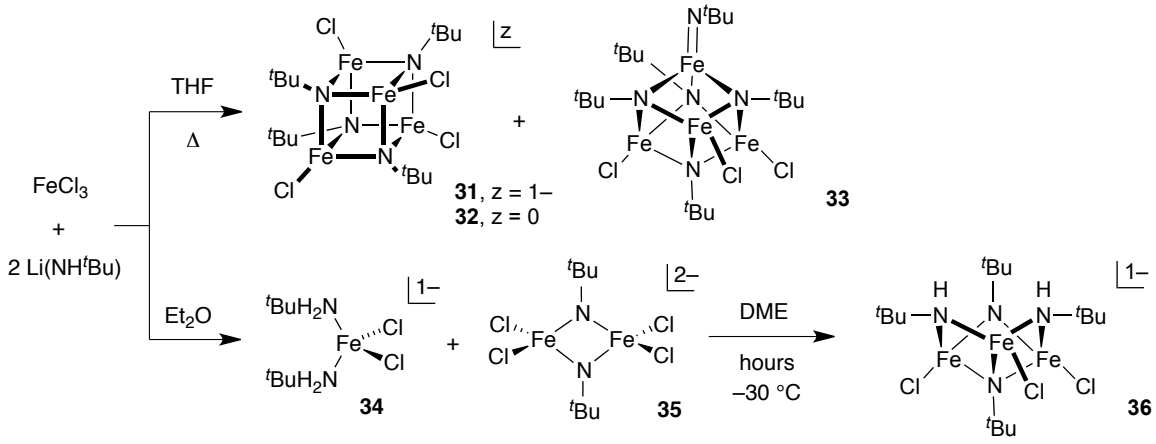

Another synthetic route to the iron-nitrogen clusters is presented in Scheme 1.8.[59] The reaction of $FeCl_3$ with Li(NHBu^t) in THF at 80 to 90 °C yields a mixture of clusters through self-assembly. The major product in this reaction is cluster **31**, which contains 3Fe(III)/1Fe(II). The oxidized form of **31** is an all-ferric compound **32**, which is isolated with **33** as minor components. Cluster **33** is special since it contains both terminal and bridging imides. When the reaction is carried out in Et_2O, the outcome is completely different: two dominant compounds mononuclear **34** and dinuclear **35** are obtained instead of tetranuclear clusters. Dissolution of the mixture of **34** and **35** in DME, followed by crystallization at –30 °C, generated a cuboidal tetranuclear cluster **36** with mixed amide/imide core-ligands.

From the synthetic iron-nitrogen clusters prepared in the Lee lab, the following examples

parallel the biological iron-sulfur clusters as structural analogues (Figure 1.2): compounds $[Fe_4(\mu_3\text{-NPh})_4SAr_4]^{2-}$ (**25**), $[Fe_2(\mu\text{-NPh})_2Cl_4]^{2-}$ (**28**), $[Fe_4(\mu_3\text{-NPh})_4Cl_4]^{2-}$ (**30**), $[Fe_4(\mu_3\text{-N}^t\text{Bu})_4Cl_4]^z$ (**31, 32**), $[Fe_2(\mu\text{-N}^t\text{Bu})_2Cl_4]^{2-}$ (**35**) and $[Fe_3(\mu_3\text{-N}^t\text{Bu})(\mu\text{-N}^t\text{Bu})(\mu\text{-NH}^t\text{Bu})_2Cl_3]^-$ (**36**). Besides the structural commonality, these iron-imide complexes parallel in many other respects the well-established iron-sulfur systems, such as cluster reactivity, and they both contain weak-field Fe(II/III) centers. In addition, the FeMo cofactor framework has been partially duplicated in a cobalt-imide cluster. This nitrogen-anion-ligated complex, $[Co_8(NPh)_9(PPh_3)_2]^-$ (Figure 1.4) is structurally analogous to the $[MoFe_7(\mu_3\text{-S})_6(\mu_2\text{-S})_3]^z$ framework of the FeMo cofactor core, without the central atom. This work was accomplished by Fenske and coworkers, who also prepared dinuclear and tetranuclear iron-imide clusters through similar reactions.[60]

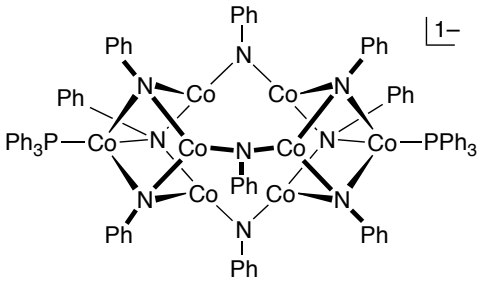

Figure 1.4. $[Co_8(NPh)_9(PPh_3)_2]^-$ cluster

In addition to these mono-, di-, and tetranuclear iron-imide complexes, nitride-containing clusters **37**, **38** and **39** have been synthesized by Holm and coworkers through self-assembly in 2005 (Scheme 1.9).[61, 62] The clusters are produced in the reaction between $[FeCl_4]^-$ and $(Me_3Sn)_3N$ in MeCN; the reaction is controlled by the molar ratio of the reactants. **37** is a nitride-containing tetranuclear iron cluster. **38** contains 9Fe(III)/1Fe(IV) bridged by six μ_4-nitrides and two μ_3-nitrides, and terminally ligated by chloride. Cluster **39** also contains a mixed-valent composition of 12Fe(III)/2Fe(II) and has two types of

nitride: eight interior μ_4-nitrides are bound only to iron atoms, and four exterior μ_3-nitrides are bound to two iron atoms and one tin atom. The successful syntheses of these clusters show the possibility of nitride-containing, high-nuclearity weak-field iron clusters.

Scheme 1.9. Syntheses of nitride-containing iron clusters

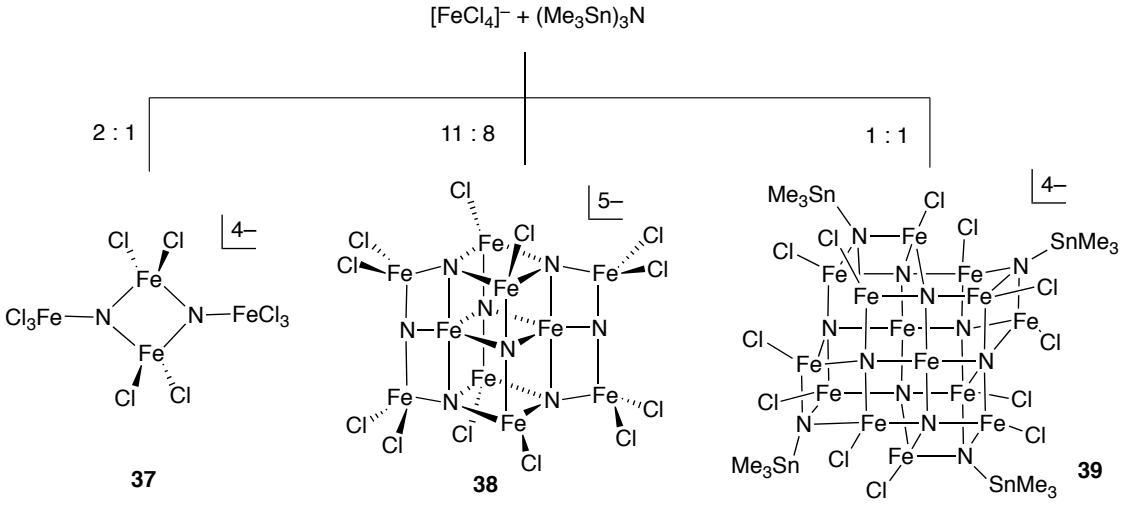

1.4 Iron-Sulfur Clusters with Heteroleptic Cores or Nitrogen-Anion Ligation

The heteroleptic core composition of the FeMo cofactor is unique in the biological iron-sulfur clusters, and its central ligand X is still unknown. The incorporation of new core-ligands into the iron-sulfur clusters is potentially useful to understand FeMo cofactor chemistry and are thus worth investigating. Holm and co-workers have prepared a series of Mo-containing iron-sulfur clusters inspired by the heterometal composition of the FeMo cofactor ($MoFe_7S_9X$; X = C, N, or O).

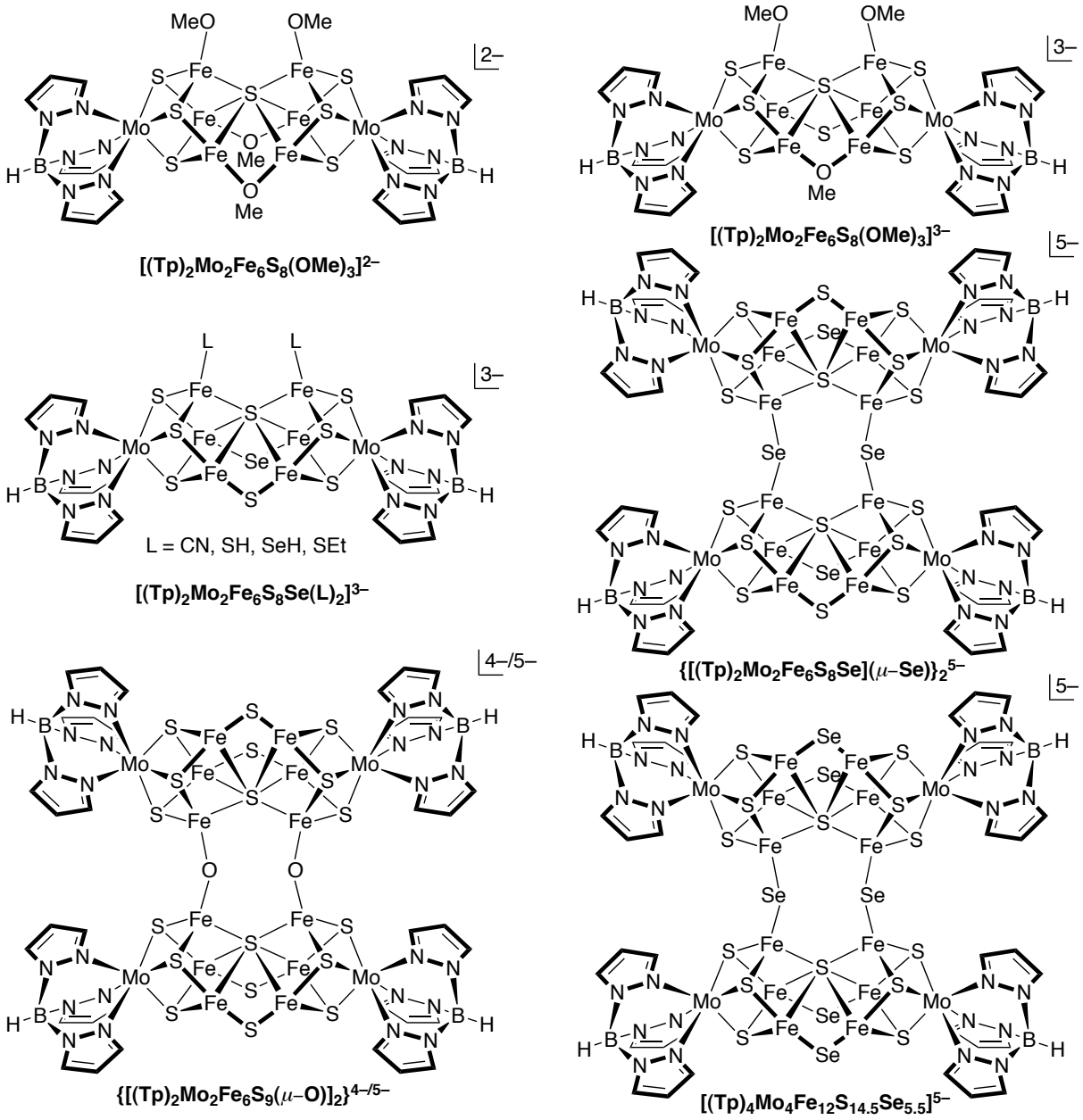

Figure 1.5. Synthetic Mo-Fe-S-X clusters

The current studies of Mo-Fe-S-X clusters are all shown in Figure 1.5.[63-66] These clusters were synthesized from a Mo-Fe-S edge-bridged double cubane **15a** via core conversion. $[(Tp)_2Mo_2Fe_6S_7(OMe)_4]^{2-}$ was made by **15a** reacted with NaOMe in MeCN. It contains four methoxide ligands, two of them are in terminal positions, and the other two are bridging. Treatment of **15a** with 4 equivalents of methoxide in DMF generated $[(Tp)_2Mo_2Fe_6S_7(OMe)_3]^{3-}$, which contains two terminal

methoxide and one μ-OMe. Reaction of **15a** with nucleophiles SeH^- yielded $[(Tp)_2Mo_2Fe_6S_8Se(SeH)_2]^{3-}$, which underwent terminal ligand substitution with retention of core geometry to afford clusters $[(Tp)_2Mo_2Fe_6S_8Se(L)_2]^{3-}$ (L = CN, SH, SEt). Also, terminal ligand elimination of compound $[(Tp)_2Mo_2Fe_6S_8Se(SeH)_2]^{3-}$ produced the bridged cluster $\{[(Tp)_2Mo_2Fe_6S_8Se](\mu\text{-}Se)\}_2^{5-}$. Another selenide bridged cluster $[(Tp)_4Mo_4Fe_{12}S_{14.5}Se_{5.5}]^{5-}$ formed directly from reaction of **15a** with 3 equivalents of SeH^- in MeCN. A doubly oxo-bridged cluster $\{[(Tp)_2Mo_2Fe_6S_9(\mu\text{-}O)]_2\}^{5-}$ was obtained by treating **15a** with Me_3SnOH and fluoride, and its oxidized form $\{[(Tp)_2Mo_2Fe_6S_9(\mu\text{-}O)]_2\}^{4-}$ was also prepared.

Although the complexes in Figure 1.5 mimic the FeMo cofactor-like core composition (Mo-Fe-S-X), they only reproduce the P^N-cluster geometry. Meanwhile, since the central atom X is possibly nitrogen, and iron is believed to be the site of dinitrogen binding and formation of iron-nitrogen bonds in the FeMo cofactor, the integration of nitrogen anions and iron-sulfur clusters may provide insight into the cofactor properties. However, because of the combination of labile ligands and weak-field redox-active iron centers leads to complicated, difficult-to-control chemistry, the construction of such clusters is difficult and they are rare in the literature. Figure 1.6 presents all the known synthetic weak-field iron-sulfur clusters with nitrogen-anion ligands.[67-71] The first example $[Fe_2(\mu\text{-}S)_2(NC_4H_4)_4]^{2-}$ contains an $[Fe_2S_2]$ core and terminally ligated by pyrrole. Another example, $[Tp_2Mo_2Fe_6S_8(NHR)_4]^{4-}$, was prepared by ligand substitution of a preassembled edge-bridged double cubane. More recently, bis(trimethylsilyl)amide has been used as a nitrogen-anion ligand to synthesize weak-filed iron-sulfur clusters, such as $Fe_2S_2(N\{SiMe_3\}_2)_2(tmtu)_2$, $Fe_3S(SR)_3(N\{SiMe_3\}_2)_3$, $[Fe_4S_4(N\{SiMe_3\}_2)_4]^{0,1-,2-}$, $Fe_8S_7(N\{SiMe_3\}_2)_4(tmtu)_2$ and $Fe_8S_7(N\{SiMe_3\}_2)(SR)_2(SR')_2$.

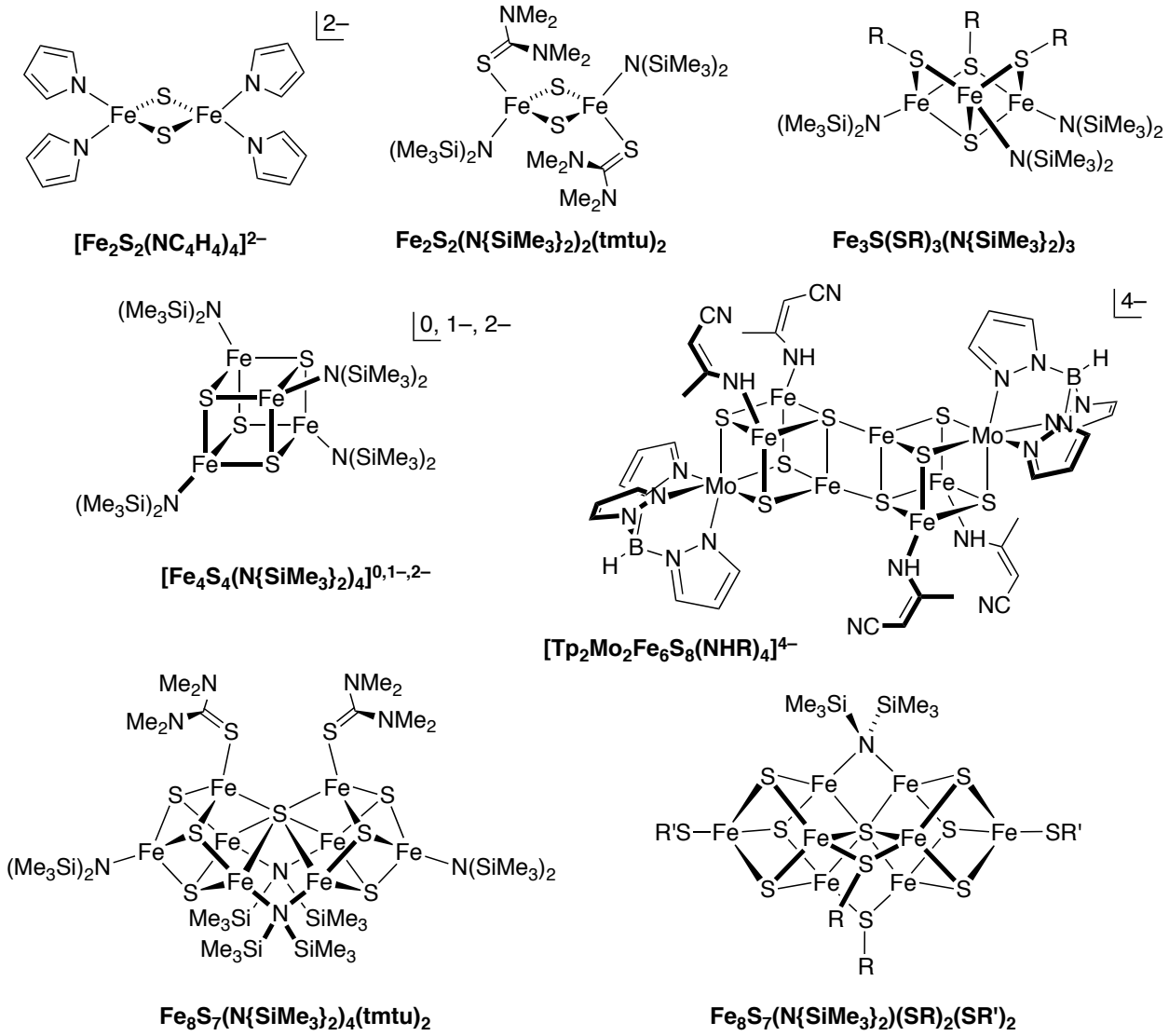

Figure 1.6. Synthetic weak-field iron-sulfur clusters with nitrogen-anion ligands

1.5 Mixed Iron-Imide-Sulfide Clusters

Iron-sulfur clusters with nitrogen-containing, heteroleptic cores are of interest since it is believed that the nitrogen atom is reacted with the iron and incorporated as a core-ligand to form the Fe-S-N core composition of the FeMo cofactor. The preparation of the mixed iron-imide-sulfide (Fe-NR-S) clusters offers the next logical step to investigate the FeMo cofactor-related problems. However, the

systematic, controlled construction of heteroligated cores with such ligands and iron centers is a challenging synthetic problem and they are almost nonexistent in the literature. The development of pathways to these heteroligated cores requires insight into existing iron-sulfur and iron-nitrogen chemistry. The only type of mixed iron-imide-sulfide clusters previously synthesized was reported by Dahl in 1982; the synthetic strategy is described in Scheme 1.10.[72, 73]

Scheme 1.10. Syntheses of Fe-NR-S clusters with low-spin, low-valent iron centers

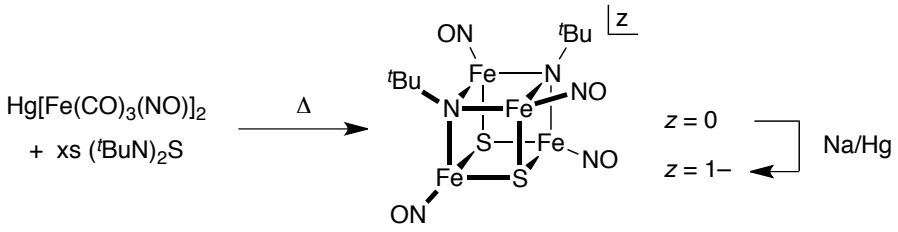

Although $[Fe_4(\mu_3\text{-}N^tBu)_2(\mu_3\text{-}S)_2(NO)_4]^z$ cores prove the existence of mixed iron-imide-sulfide clusters with tetrahedral iron coordination, the iron sites in these clusters are low-spin, low-valent, and poorly mimic the weak-field electronic environment of the FeMo-cofactor.[74-76]

Nothing was known about the syntheses of weak-field, nitrogen-containing iron-sulfur clusters with potential relevance to nitrogen fixation by the FeMo-cofactor in nitrogenase until recently reported results from the Lee lab. Thus, the topic of this thesis is the detailed explanation of the selective synthesis and characterization of dinuclear and tetranuclear iron clusters with heteroligated cores.

CHAPTER 2. TETRANUCLEAR MIXED IRON-IMIDE-SULFIDE CLUSTERS

2.1 Introduction

Among the well-known iron-sulfur clusters, $[Fe_4S_4Cl_4]^{2-/3-}$ has been studied for years,[77] and in the iron-nitrogen clusters, $[Fe_4(N^tBu)_4Cl_4]^{0/1-}$ has recently been prepared.[58] In this project, we investigate the selective syntheses of the $[Fe_4(N^tBu)_n(S)_{4-n}Cl_4]^z$ cubane clusters, which span all mixed imide/sulfide core compositions between the $[Fe_4S_4]$ and the $[Fe_4(N^tBu)_4]$ homoleptic core motifs. This new realm of synthetic tetranuclear clusters with mixed Fe(II/III) oxidation states, mixed core ligands and relatively high nuclearity may mimic the heteroligated environment of the FeMo cofactor better than simple iron-sulfur or iron-nitrogen clusters. A detailed research investigation is presented here.

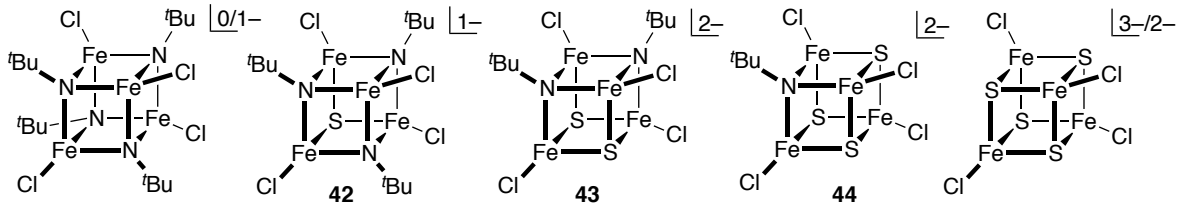

Figure 2.1. $[Fe_4(\mu_3\text{-}N^tBu)_4Cl_4]^{0/1-}$, $[Fe_4(\mu_3\text{-}N^tBu)_3(\mu_3\text{-}S)Cl_4]^{1-}$, $[Fe_4(\mu_3\text{-}N^tBu)_2(\mu_3\text{-}S)_2Cl_4]^{2-}$, $[Fe_4(\mu_3\text{-}N^tBu)(\mu_3\text{-}S)_3Cl_4]^{2-}$ and $[Fe_4(\mu_3\text{-}S)_4Cl_4]^{2-/3-}$ cores.

2.2 Synthetic Considerations

The synthetic method of constructing weak-field metal clusters, especially with homometallic and homoleptic cores is dominated by self-assembly, which involves the combination of precursors that separately provide metal ions, bridging and terminal ligands.[40, 41, 53, 54] However, to achieve heteroleptic cores, strict self-assembly may not be useful because different core ligand components, which are the imide and sulfide ligands of interest here, will have fairly different reactivities. The introduction of a

second core ligand by self-assembly therefore seems unpromising.

Two routes to synthesizing clusters with the $[Fe_4(N^tBu)_n(S)_{4-n}Cl_4]^z$ cores can be devised: (i) core imides of Fe-NR compounds may be replaced with sulfides while maintaining overall cluster structure; and (ii) dinuclear iron precursors may be aggregated into tetranuclear iron clusters whose nitrogen and sulfur content can be manipulated by varying the choice of dimers. The imide replacement method (i) has been successfully applied to the synthesis of a dinuclear iron-imide-sulfide specie, which was achieved by Duncan in the Lee lab and illustrated in Scheme 2.1.[78]

Scheme 2.1. Synthesis of a dinuclear iron-imide-sulfide cluster

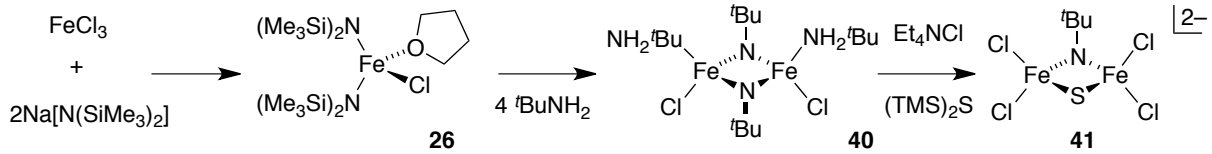

The synthesis of this dinuclear iron-imide-sulfide cluster starts from a ferric precursor $[FeCl[N(SiMe_3)_2]_2(THF)]$ (**26**), which is prepared in high yield (ca. 75%) by anion metathesis of $FeCl_3$ with 2 equivalents of $Na[N(SiMe_3)_2]$ in THF. The coordinated THF is labile and is easily replaced. The reaction of compound **26** with 4 equivalents of $^tBuNH_2$ formed a Fe(III) dimer $Fe_2(\mu\text{-}N^tBu)_2Cl_2(NH_2{}^tBu)_2$ (**40**), which consists of three ligand types: bridging imides, terminal amines and terminal chlorides. The reaction of Et_4NCl and $(Me_3Si)_2S$ with **40** yields the dinuclear hetero-core-ligated iron-imide-sulfide cluster **41**. This route can also be expanded to construct tetranuclear clusters. However, it may potentially result in intractable mixtures because selective core ligand substitution and terminal ligand exchange may be hard to control. The cluster aggregation route (ii) may provide a better pathway for the selective synthesis of $[Fe_4(N^tBu)_n(S)_{4-n}Cl_4]^z$ cubane compounds, as it involves the assembly of preorganized clusters that already contain iron with core-bound nitrogen and/or core-bound sulfur. Moreover, the reductive assembly of heterocubane cores from diferric species is known in both Fe-S and Fe-NR chemistry.[79, 80] The reduction of either diferric $[Fe_2S_2]$ or $[Fe_2(NR)_2]$ dimers can form tetranuclear clusters. Alternatively, the fusion of two diferric Fe-NR clusters can also be achieved thermally, with accompanying redox

changes and some decomposition. These examples are illustrated in Scheme 2.2. From the structures of the dinuclear starting materials and the final tetranuclear products, it is possible that cluster formation in these reactions may be due to fragment condensation, which is the dimerization of preorganized dinuclear $[Fe_2Q_2]$ fragments into the $[Fe_4Q_4]$ cubane structure. This strategy was applied to synthesizing heteroligated cubane complexes by using dinuclear iron-imide-sulfide cluster **41** as the precursor.

Scheme 2.2. Fusion of two diferric clusters

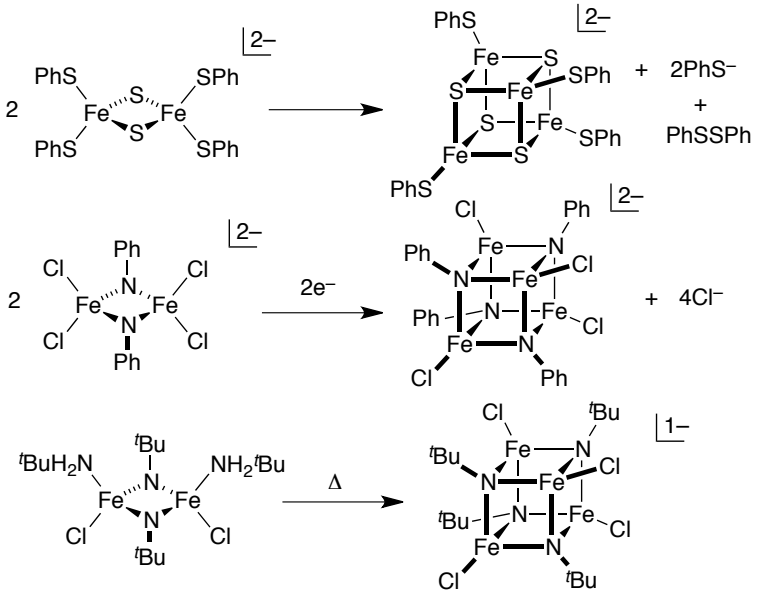

2.3 Results and Discussion

2.3.1 Attempted Syntheses of Mixed Iron-Imide-Sulfide Clusters

Several reactions are proposed in equations 2.1, 2.2 and 2.3: the reduction of **41** to construct tetranuclear compounds **43**; the fusion of dinuclear clusters **41** with $[Fe_2(\mu\text{-}S)_2Cl_4]^{2-}$ to form **44**; and the condensation of **41** with $[Fe_4(\mu\text{-}S)_4Cl_4]^{2-}$ to form **44**.

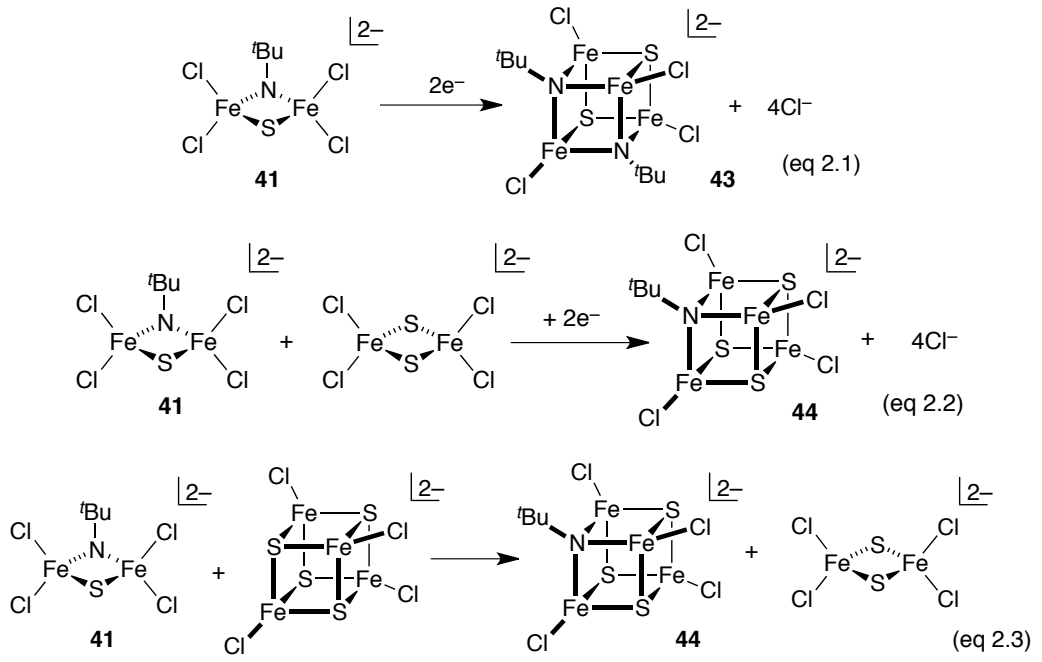

Scheme 2.3. Reduction of compound **41** with 1, 2 or 3 equivalents of $FeCl_2$ in MeCN

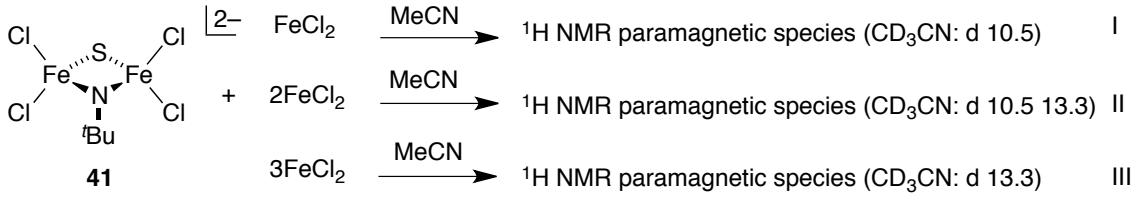

In accordance to the proposed equation 2.1, the reactions in Scheme 2.3 have been attempted by using $FeCl_2$ as a reducing agent and varying the reaction stoichiometry, and ^{1}H NMR spectra of the crude product are shown in Figure 2.2. Reaction I yielded a product with a chemical shift at 10.55 ppm; it has been identified as $[Fe_4(\mu_3\text{-}N^tBu)_3(\mu_3\text{-}S)Cl_4]^{1-}$ (**42**) (the chemical shifts of clusters **42**, **43** and **44** are assigned by further investigation and will be explained later). The formation of **42** suggests that the initial precursor **41** undergoes cluster fragmentation, possibly due to the presence of protic contaminants. When increasing the molar ratio of the reducing agent, reaction II yielded a new compound (Unknown **1**), identified by the chemical shift at 13.3 ppm. Unknown **1** was also synthesized via III, in higher purity. It is

speculated that Unknown **1** may have the same structure as **42**, but as a reduced form $[Fe_4(\mu_3\text{-}N^tBu)_3(\mu_3\text{-}S)Cl_4]^{2-}$, based on its appearance as the quantity of reducing agent is increased. In the ^{1}H NMR spectra of these three reactions, a signal is also observed at a position between –2 ppm to –8 ppm that has been assigned to $FeCl_2(^tBuNH_2)_2$.[49] The signal position changes depending on the concentration of the labile ligand $^tBuNH_2$. The formation of $FeCl_2(^tBuNH_2)_2$ indicates the existence of protic contaminants in the system. The chemical shift at 5.5 ppm common to these three reactions is also indicative of another product of interest, which is identified as $[Et_4N]_2[Fe_4(\mu_3\text{-}N^tBu)(\mu_3\text{-}S)_3Cl_4]$ (**44**). The reduction of **41** with $FeCl_2$ did not give the expected product **43**, and yielded **44** only as minor product.

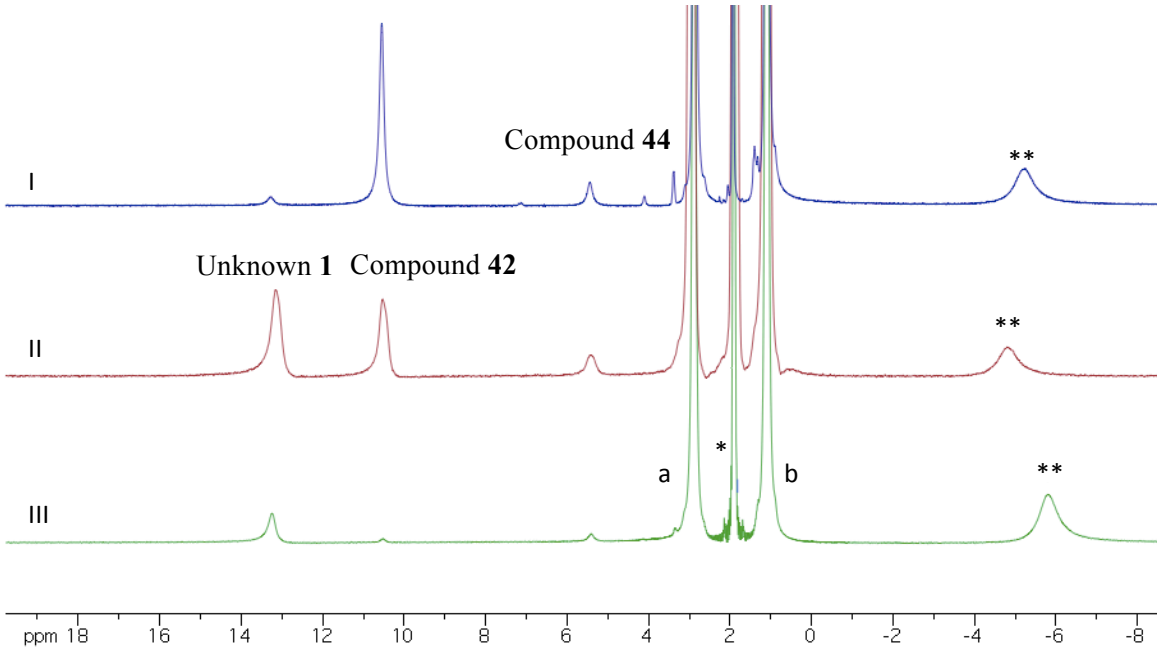

Figure 2.2. ^{1}H NMR spectra (300 MHz) of reactions between **41** with 1 $FeCl_2$ (I), 2 $FeCl_2$ (II) and 3 $FeCl_2$ (III). Residual protio signals of CD_3CN are marked by *, signals of $FeCl_2(^tBuNH_2)_2$ are marked by **, and signals corresponding to the $(Et_4N)^+$ counterions are marked by a and b.

Another iron-based reducing agent, $FeCl_2(THF)_{1.5}$, which has a higher solubility in MeCN than $FeCl_2$, was also tested on the hypothesis that the higher solubility of the reagent may facilitate the

generation of purer products. The ^{1}H NMR spectra of the reaction crudes are shown in Figure 2.3. The products obtained from the reaction between **41** and 1 equivalent of $FeCl_2(THF)_{1.5}$ showed ^{1}H NMR signals at 10.55 ppm and 13.3 ppm, indicating a mixture of the two previously observed components. The presence of two species poses a challenge for compound isolation and crystal growth. When treating **41** with 2 equivalents of $FeCl_2(THF)_{1.5}$, Unknown **1** predominated. However, $FeCl_2(^{t}BuNH_2)_2$ by-product was present in significant quantities. Na_2S is another reducing reagent that was used to react with **41**. In this reaction, the external sulfide functions as the reductant, promoting the fusion of **41**. The product of this reaction showed a ^{1}H NMR signal at 7.01 ppm, assigned to $[Fe_4(\mu_3\text{-}N^{t}Bu)_2(\mu_3\text{-}S)_2Cl_4]^{2-}$ (**43**), which is another cluster of interest, but this reaction is hampered by low yield and poor selectivity. The reactions of cluster **41** with number of other reductants (Zn, $FeCl_2$, Na_2S, NaSH) were also unsuccessful and only some Fe-NR-S cubanes were detected in low yield. The other two proposed reactions (equations 2.2 and 2.3) have also been tested; neither of them generated the desired results.

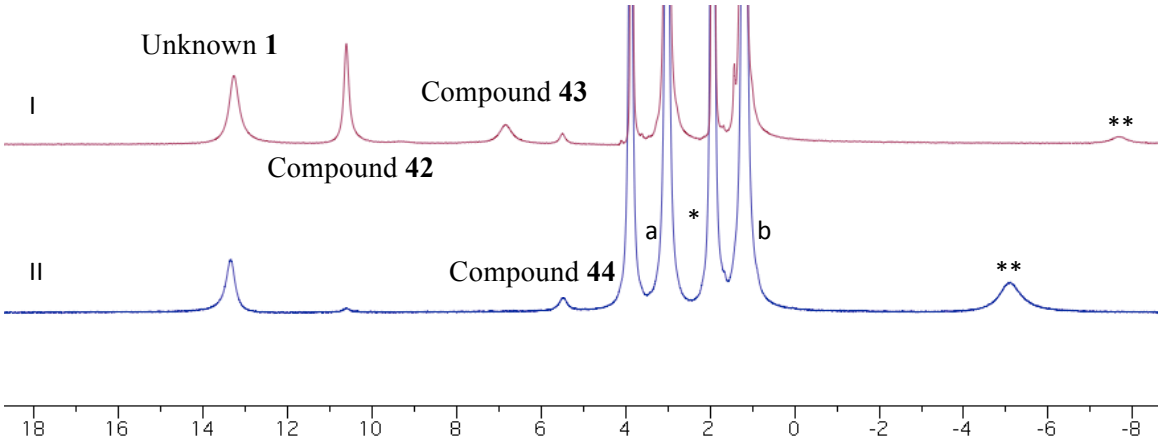

Figure 2.3. ^{1}H NMR spectra (300 MHz) of reactions between **41** with 1 $FeCl_2(THF)_{1.5}$ (I) and 2 $FeCl_2(THF)_{1.5}$ (II). Residual protio signals of CD_3CN are marked by *, signals of $FeCl_2(^{t}BuNH_2)_2$ are marked by **, and signals corresponding to the $(Et_4N)^{+}$ counterions are marked by a and b.

The synthesis of the cluster $[Et_4N]_2[Fe_4(\mu_3\text{-}N^{t}Bu)(\mu_3\text{-}S)_3Cl_4]$ was also attempted through partial

self-assembly (equation 2.4). $FeCl_2(THF)_{1.5}$ and $(Me_3Si)_2S$ serve as iron and sulfur sources, respectively, to construct the core structure **44** from the preexisting dinuclear iron-imide-sulfide framework. However, the ^1H NMR spectrum still shows a signal at 13.3 ppm. Crystalline black blocks were obtained from Et_2O diffusion into a MeCN solution of the reaction mixture at –20 °C for 5 days. X-ray crystal data showed the crystals to be the ^1H NMR silent $[Fe_4S_4Cl_4]^{2-}$. This reaction does not terminate at the target core structure, but instead proceeds with complete sulfide substitution of core *tert*-butylimides.

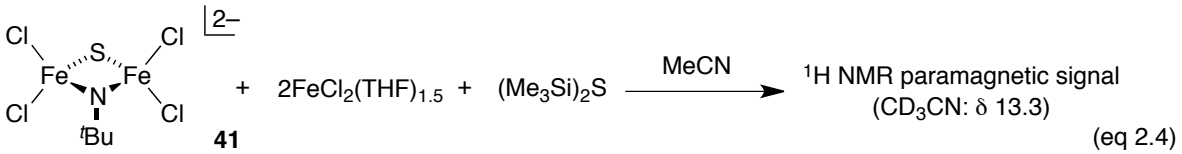

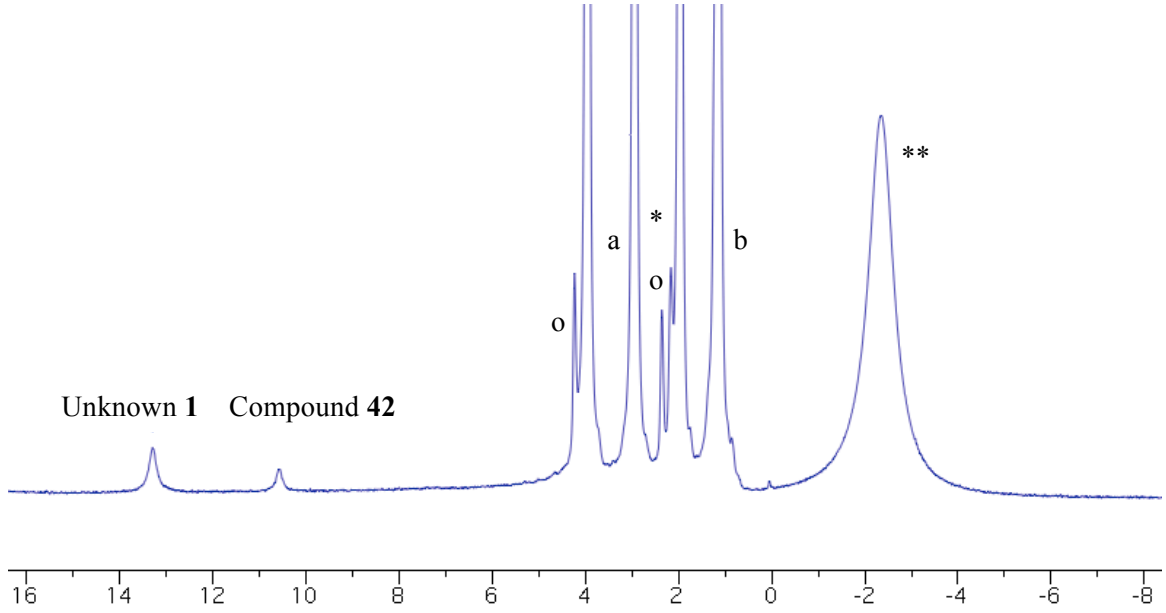

Figure 2.4. ^1H NMR spectra (300 MHz) of reaction between **41** with 2 $FeCl_2(THF)_{1.5}$ and $(Me_3Si)_2S$. Residual protio signal of CD_3CN is marked by *, signal of $FeCl_2(^tBuNH_2)_2$ is marked by **, and signals corresponding to the $(Et_4N)^+$ counterions are marked by a and b. Residual solvent is marked by o.

In general, all of these proposed reactions are contaminated by several difficult to separate species, are not selective for the syntheses of the $[Fe_4(N^tBu)_n(S)_{4-n}Cl_4]^z$ cores, and are constrained by low

yields.

2.3.2 Successful Syntheses of Clusters with $[Fe_4(N^tBu)_n(S)_{4-n}Cl_4]^z$ Cores

Scheme 2.4. Reaction scheme for the production of mixed iron-imide-sulfide/selenide clusters

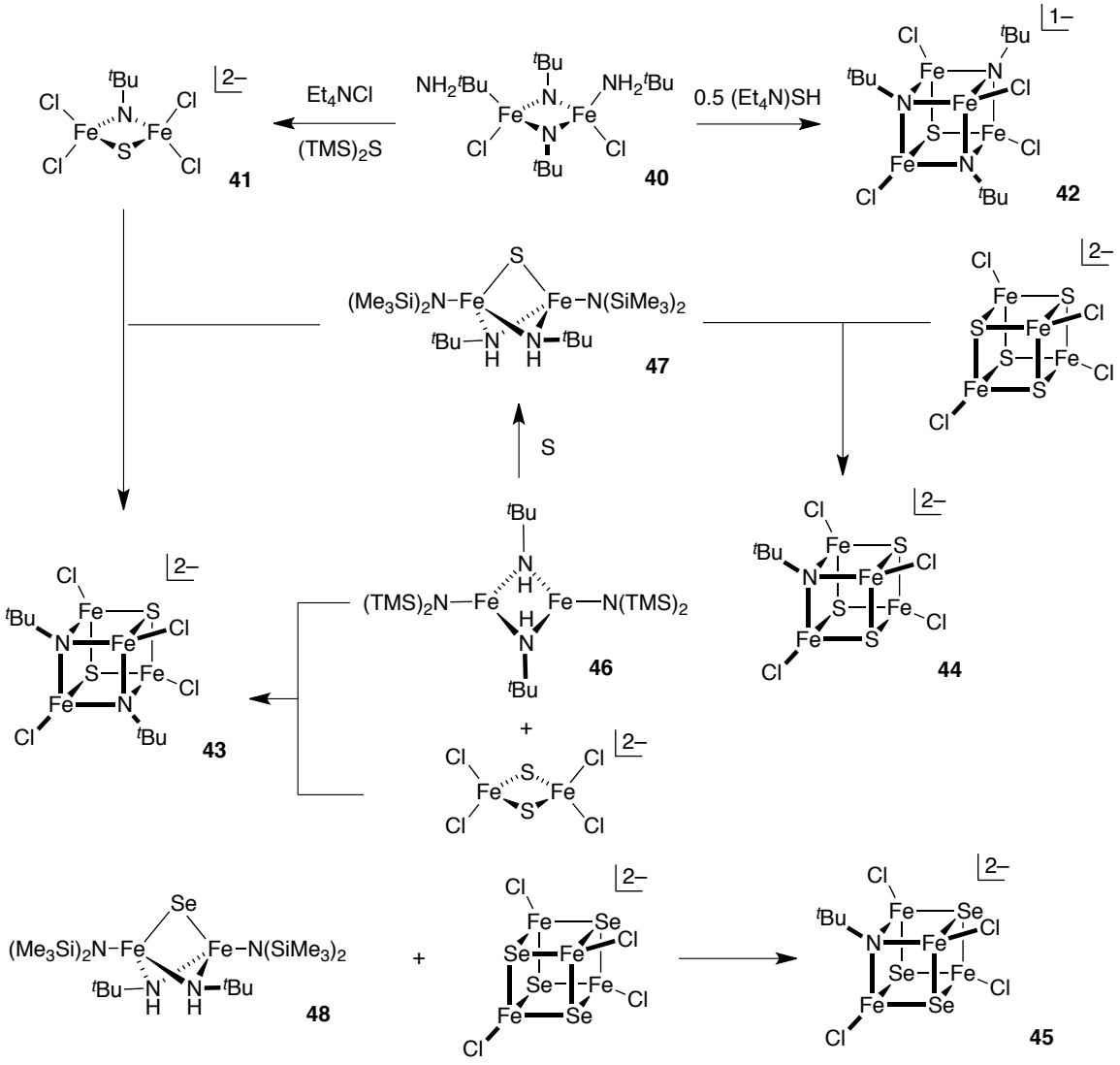

Although the synthetic routes of direct reduction and partial self-assembly of preorganized cluster **41** yielded unpromising results, our efforts to combine two dinuclear iron precursors, or dinuclear and tetranuclear iron clusters, to generate mixed iron-imide-sulfide cubane complexes were successful, as

illustrated in Scheme 2.4. This study has been accomplished by joint work with the postdoctoral fellow Xudong Chen in the Lee lab.[78] The detailed synthetic route to complexes $[Et_4N][Fe_4(\mu_3\text{-}N^tBu)_3(\mu_3\text{-}S)Cl_4]$ (**42**), $[Et_4N]_2[Fe_4(\mu_3\text{-}N^tBu)_2(\mu_3\text{-}S)_2Cl_4]$ (**43**), $[Et_4N]_2[Fe_4(\mu_3\text{-}N^tBu)(\mu_3\text{-}S)_3Cl_4]$ (**44**) and $[Et_4N]_2[Fe_4(\mu_3\text{-}N^tBu)(\mu_3\text{-}Se)_3Cl_4]$ (**45**) and the results of this study are presented here. All reactions in Scheme 2.4 involved the combination of two reactants, with charged species dissolved in MeCN and neutral species dissolved in THF, to ensure homogeneous reaction conditions.

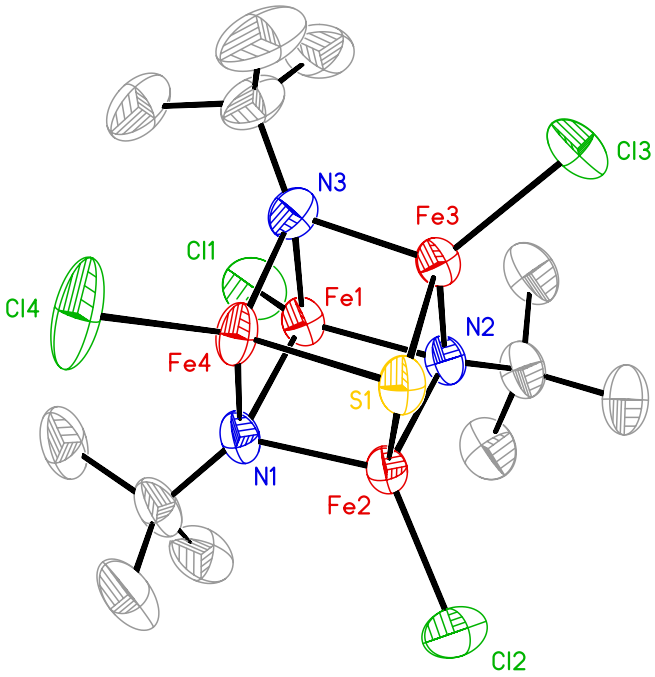

Figure 2.5. Structure of $[Et_4N][Fe_4(\mu_3\text{-}N^tBu)_3(\mu_3\text{-}S)Cl_4]$ (**42**) with thermal ellipsoids (50% probability level) and selected atom labels. Hydrogen atoms are not shown.

$$2\ Fe_2(N^tBu)_2Cl_2(NH_2{}^tBu)_2 + 1\ [SH]^- \longrightarrow [Fe_4(N^tBu)_3(S)Cl_4]^- + 0.5\ {}^tBuNH\text{-}NH^tBu + 4\ {}^tBuNH_2 \qquad \text{(eq 2.5)}$$

When complex **40** is treated with 0.5 equivalent of Et_4NSH, the terminal amines are lost and **40** is reduced to form into a tetranuclear cubane, while one of the bridging imides is replaced by sulfide. The proposed hypothetical reaction is presented in Equation 2.5 (Equations 2.6a, 2.6b, 2.7 and 2.8 are also

hypothetically balanced). This reaction yielded the first mixed-imide-sulfide cluster $[Et_4N][Fe_4(\mu_3\text{-}N^tBu)_3(\mu_3\text{-}S)Cl_4]$ (**42**, Figure 2.5) in 65% yield (all the yields calculated in this thesis are based on the iron content and under the assumption that the dinuclear reactants contributed both irons to the final tetranuclear products). By ^{1}H NMR analysis, we found that cluster **42** was contaminated by another cubane $[Et_4N][Fe_4(\mu_3\text{-}N^tBu)_4Cl_4]$ (ca 8%,), which was formed directly by the reduction of **40** without sulfide substitution. These two clusters are difficult to isolate due to their similarity (they both dissolve in THF and have the same charge state: –1). In preliminary studies, twice the amount of Et_4NSH (1 equivalent) in THF was employed, but we have observed that product selectivity is inconsistent under these heterogeneous conditions, and the current preparation gives a higher yield and better selectivity.

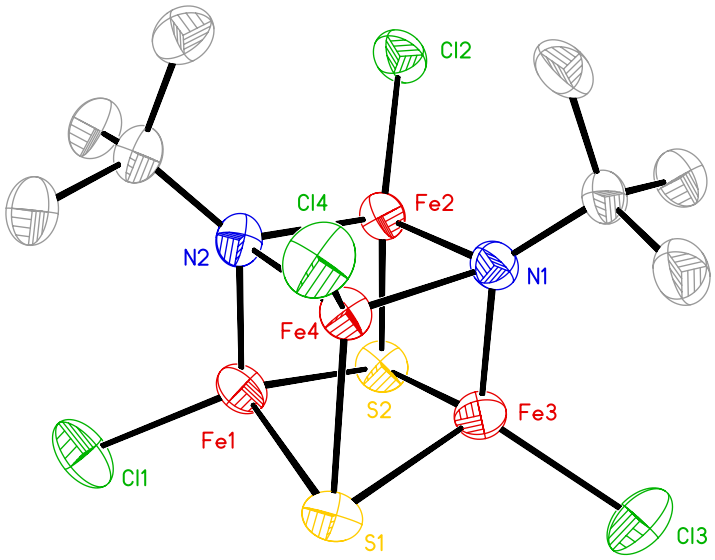

Figure 2.6. Structure of $[Et_4N]_2[Fe_4(\mu_3\text{-}N^tBu)_2(\mu_3\text{-}S)_2Cl_4]$ (**43**) with thermal ellipsoids (50% probability level) and selected atom labels. Hydrogen atoms are not shown.

$$Fe_2(NH^tBu)_2(S)(N\{SiMe_3\}_2)_2 + [Fe_2(N^tBu)(S)Cl_4]^{2-} \longrightarrow [Fe_4(N^tBu)_2(S)_2Cl_4]^{2-} + 2\ HN(SiMe_3)_2 + 0.5\ {}^tBuN{=}N^tBu \qquad \text{(eq 2.6a)}$$

Two routes exist to produce cluster $[Et_4N]_2[Fe_4(\mu_3\text{-}N^tBu)_2(\mu_3\text{-}S)_2Cl_4]$ (**43**, Figure 2.6), both involving the condensation of two different diiron clusters. The first synthesis employed the dinuclear complexes $[Et_4N]_2[Fe_2(\mu\text{-}N^tBu)(\mu\text{-}S)Cl_4]$ (**41**) and $Fe_2(\mu\text{-}N^tBu)_2(\mu\text{-}S)[N(SiMe_3)_2]_2$ (**47**), which both contain mixed sulfide and imide/amide bridges. The proposed balanced stoichiometry is shown in Equation 2.6a. The reaction of **41** with **47** generated tetranuclear cluster **43** (ca. 55%), which is contaminated by another mixed iron-imide-sulfide cluster $[Et_4N]_2[Fe_4(\mu_3\text{-}N^tBu)(\mu_3\text{-}S)_3Cl_4]$ (**44**) (ca. 10%). This contaminated cluster **44** can be removed by extracting product **43** into CH_2Cl_2 solution, and further recrystallization from $MeCN/Et_2O$ afforded microcrystalline pure product **43**. Cluster **47** is a mixed iron-amide-sulfide dinuclear complex and its detailed synthesis and properties will be discussed in the next chapter.

$$Fe_2(NH^tBu)_2(N\{SiMe_3\}_2)_2 + [Fe_2S_2Cl_4]^{2-} \longrightarrow [Fe_4(N^tBu)_2(S)_2Cl_4]^{2-} + 2\ HN(SiMe_3)_2 \qquad \text{(eq 2.6b)}$$

The synthesis of cluster **43** can also be achieved by an alternative reaction, which is more economical since this route involved using more accessible starting materials. Treatment of a THF solution of $Fe_2(\mu\text{-}NH^tBu)_2[N(SiMe_3)_2]_2$ (**46**) with $[Et_4N]_2[Fe_2(\mu\text{-}S)_2Cl_4]$ in MeCN in a 1:1 ratio gives cluster **42** (Equation 2.6b) (ca. 60%). Cluster **46** is a neutral heteroleptic dimer, containing two trigonal planar iron centers and will be discussed in the next chapter. The 2Fe(II) in complex **46** and 2Fe(III) in $[Et_4N]_2[Fe_2(\mu\text{-}S)_2Cl_4]$ lead to a redox balanced equation without intervening ligands redox chemistry. The imide-trisulfide cluster **44** is still present as a minor component (ca. 15%) and product **43** can be extracted into CH_2Cl_2 solution.

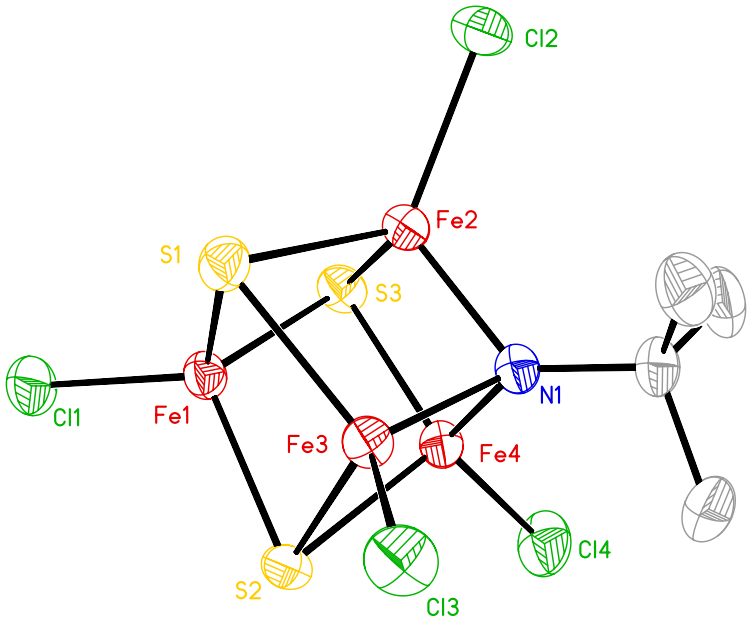

Figure 2.7. Structure of $[Et_4N]_2[Fe_4(\mu_3\text{-}N^tBu)(\mu_3\text{-}S)_3Cl_4]$ (**44**) with thermal ellipsoids (50% probability level) and selected atom labels. Hydrogen atoms are not shown.

$$Fe_2(NH^tBu)_2(S)(N\{SiMe_3\}_2)_2 + [Fe_4S_4Cl_4]^{2-} \longrightarrow [Fe_4(N^tBu)(S)_3Cl_4]^{2-} + 2\ HN(SiMe_3)_2 + 0.5\ {}^tBuN{=}N^tBu + 2\ \text{"FeS"} \qquad \text{(eq 2.7)}$$

The last iron-imide-sulfide cluster $[Et_4N]_2[Fe_4(\mu_3\text{-}N^tBu)(\mu_3\text{-}S)_3Cl_4]$ (**44**), which contains three sulfide and one imide ligands, is prepared by the reaction of $Fe_2(\mu\text{-}N^tBu)_2(\mu\text{-}S)[N(SiMe_3)_2]_2$ (**47**) and $[Et_4N]_2[Fe_4(\mu_3\text{-}S)_4Cl_4]$ (Equation 2.7). Clusters **47** and $[Et_4N]_2[Fe_4(\mu\text{-}S)_4Cl_4]$ were dissolved in THF and MeCN separately; the mixture was stirred overnight. There formed some black insoluble material, which is air-sensitive and contains iron and sulfur, but almost no chlorine, by EDX analysis. We believe that the precipitate is polymeric iron-sulfur material. The soluble fraction contained product **44** (ca. 60%) and was contaminated by cluster **43** (ca. 20%), which could be mostly removed by CH_2Cl_2 extraction, with the remaining material purified by recrystallization.

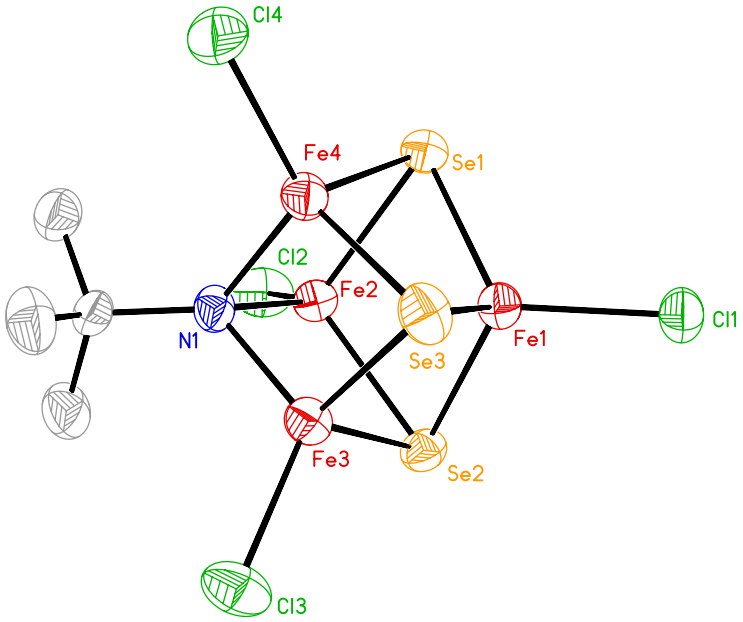

Figure 2.8. Structure of $[Et_4N]_2[Fe_4(\mu_3\text{-}N^tBu)(\mu_3\text{-}Se)_3Cl_4]$ (**45**) with thermal ellipsoids (50% probability level) and selected atom labels. Hydrogen atoms are not shown.

$$Fe_2(NH^tBu)_2(Se)(N\{SiMe_3\}_2)_2 + [Fe_4Se_4Cl_4]^{2-} \longrightarrow [Fe_4(N^tBu)(Se)_3Cl_4]^{2-} + 2\ HN(SiMe_3)_2 + 0.5\ {}^tBuN{=}N^tBu + 2\ \text{"FeSe"} \qquad \text{(eq 2.8)}$$

It is established that planar rhombic dinuclear $[Fe_2Se_2]$ or cubane-type $[Fe_4Se_4]$ analogues can be synthesized by using selenium sources instead of sulfur.[82] Similarly, cluster $[Et_4N]_2[Fe_4(\mu_3\text{-}N^tBu)(\mu_3\text{-}Se)_3Cl_4]$ (**45**) can be prepared as a structural analogue of complex **44**. Precursor clusters $Fe_2(\mu\text{-}N^tBu)_2(\mu\text{-}Se)[N(SiMe_3)_2]_2$ (**52**) and $[Et_4N]_2[Fe_4(\mu\text{-}Se)_4Cl_4]$ also share the structures of complex **47** and $[Et_4N]_2[Fe_4(\mu\text{-}S)_4Cl_4]$. The synthesis and characterization of compound **52** will be presented in the next chapter. Compared with the synthesis of compound **44**, the preparation of cluster **45** generates more insoluble polymeric material. Additionally, a chemical shift of a second cluster is also found in the ^1H NMR spectrum of the unpurified reaction mixture. By analogy, this contaminant cluster is

believed to be $[Et_4N]_2[Fe_4(\mu_3\text{-}N^tBu)_2(\mu_3\text{-}Se)_2Cl_4]$, which can be removed by CH_2Cl_2 extraction and subsequent recrystallization.

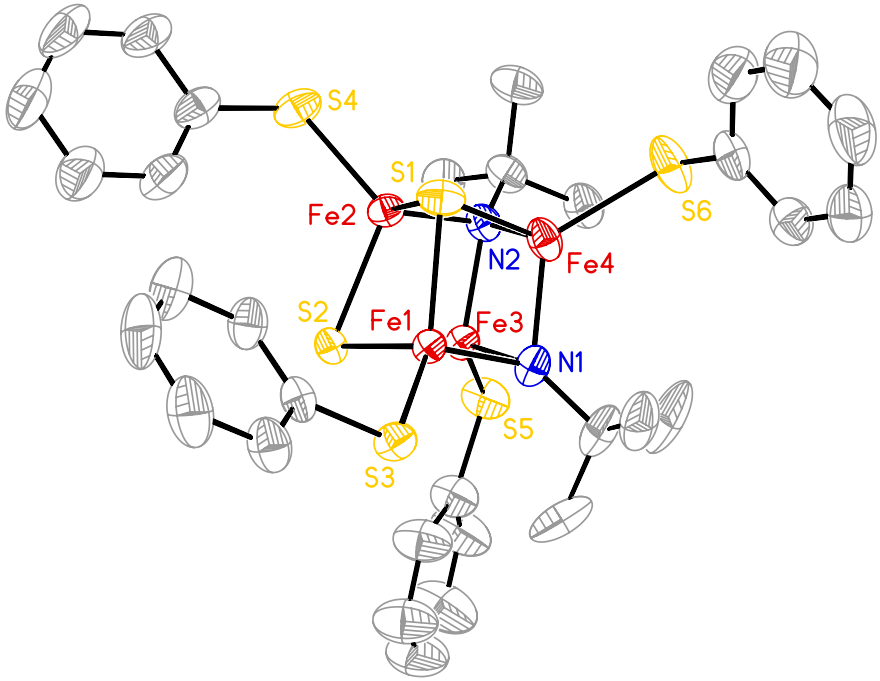

Figure 2.9. Structure of $[Et_4N]_2[Fe_4(\mu_3\text{-}N^tBu)_2(\mu_3\text{-}S)_2(SPh)_4]$ (**43a**) with thermal ellipsoids (50% probability level) and selected atom labels. Hydrogen atoms are not shown.

$$[Fe_4(N^tBu)_2(S)_2Cl_4]^{2-} + 4\ NaSPh \longrightarrow [Fe_4(N^tBu)_2(S)_2(SPh)_4]^{2-} + 4\ NaCl \qquad \text{(eq 2.9)}$$

The terminal chloride ligands can be replaced with thiolates by metathesis with sodium benzenethiolate. Cluster **43** has been tested for the preparation of thiolate-ligated clusters, and the reaction of **43** with 4 equivalents of sodium benzenethiolate leads to the four chloride terminal ligands of **43** being replaced without the loss of the tetranuclear core geometry to form **43a** (Equation 2.9). The ^1H NMR spectrum of **43a** is shown in Figure 2.5 and summarized in Table 3.1.

Table 2.1. ^{1}H NMR spectroscopic data for clusters $[Et_4N]_2[Fe_4(\mu_3\text{-}N^tBu)_2(\mu_3\text{-}S)_2(SPh)_4]$ (**43a**)

Compound	^{1}H NMR (C_6D_6, δ ppm)
43a	5.10 (2 br), 5.56 (2 br), 6.09 (4 br), 6.72 (4 br), 7.10 (18 br), 8.03 (4 br), 8.87 (4 br)

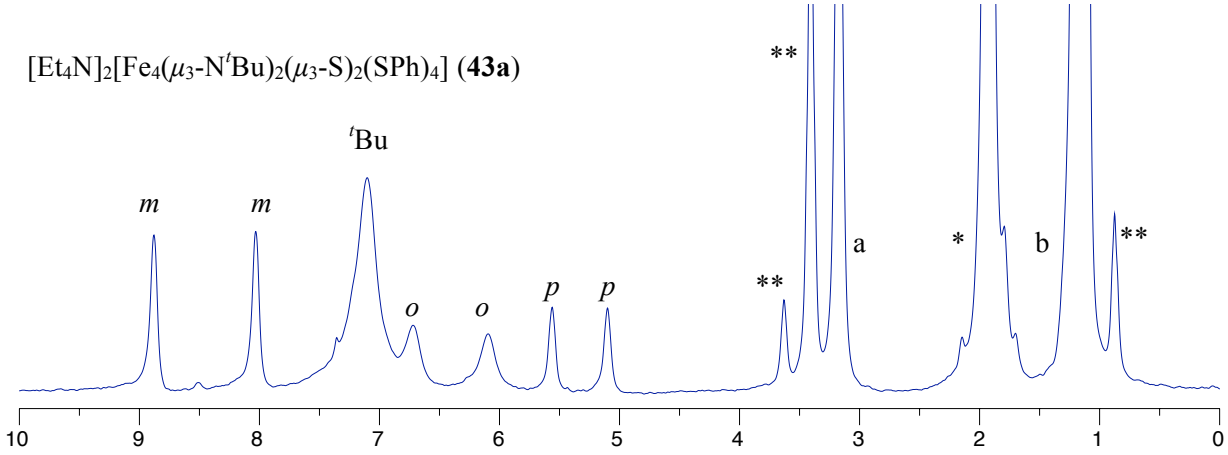

Figure 2.10. ^{1}H NMR spectra (300 MHz) of clusters **43a**. Residual protio signal of CD_3CN is marked by *, signals corresponding to the $(Et_4N)^+$ counterions are marked by a and b, other residual solvent peaks are marked by **.

2.3.3 Cubane Formation: Reaction Analysis and Mechanistic Observations

The tetranuclear mixed iron-imide-sulfide clusters discussed in this chapter all contain weak-field iron centers, redox-active metal and core ligands, and unconstrained metal coordination environments, making the cluster assembly mechanisms difficult to analyze and thus are not well understood. However, important reactions and observations from these studies will be summarized here.

(i) The construction of tetranuclear clusters is relatively selective by the standards of weak-field cluster chemistry. Each $[Fe_4(N^tBu)_n(S)_{4-n}Cl_4]^z$ cubane member can be assembled by its own specific reaction system. By analyzing ^{1}H NMR spectra of the crude reaction systems, we

found that cubane clusters are formed almost exclusively. Total in situ cluster yields are about 60-75%, and the desired product dominates 45-65%.

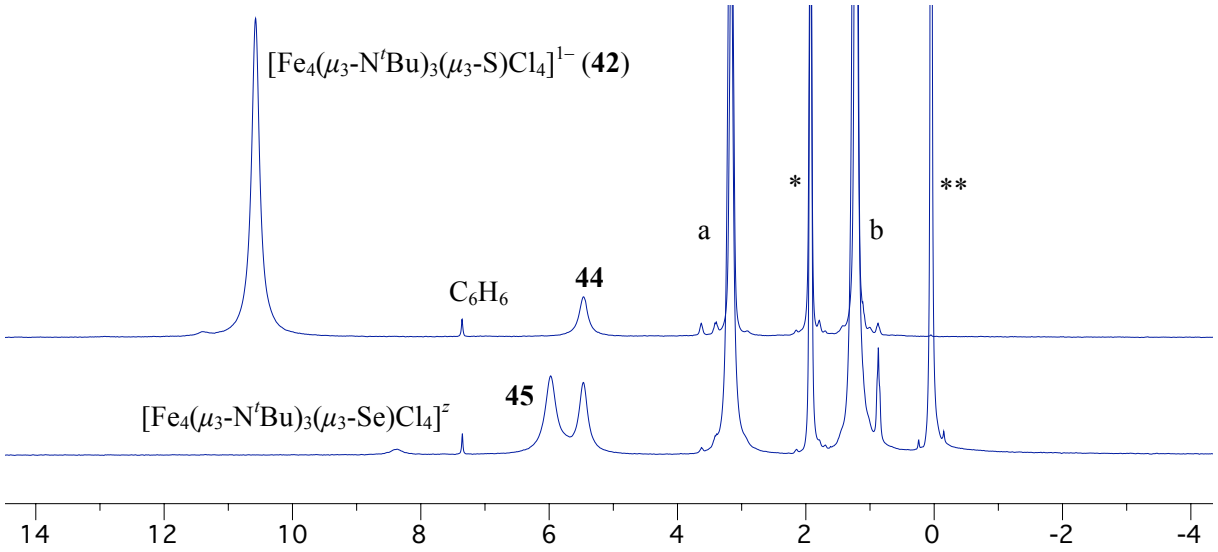

Figure 2.11. ^{1}H NMR spectra (300 MHz) of mixtures of **42** and **44**, and mixtures of **44** and **45** after 2 d. Residual protio signals of CD_3CN are marked by *, internal calibrant HMDSO is marked by **, and signals corresponding to the $(Et_4N)^+$ counterions are marked by a and b.

(ii) ^{1}H NMR assays indicate that all three Fe-NR-S clusters decompose slowly in solution to form NMR-silent products at millimolar concentrations over several days at am temperature. Dianionic clusters **43** and **44** decayed most rapidly, with 10-20% decomposition over 2 days, while monoanionic cluster **42** decayed less than 5% over 2 days. We believe that the cluster degradation may be linked to chloride dissociation; when **44** in MeCN solution was treated with 6 equivalents of Et_4NCl over the same time period, there is no evidence of cluster decomposition, which is verified by Layling Tan in the Lee lab. Under the same conditions after 2 days, there is no evidence of intercluster core ligand exchange, i.e., mixtures of **42** and **44** in MeCN do not generate **43**, and mixtures of **44** and **45** in MeCN do not yield mixed

sulfide/selenide clusters, as demonstrated by NMR assays (Figure 2.11). Also, solutions of pure **42**, **43**, and **44** do not generate other core compositions.

$[Fe_4(N^tBu)(S)_3Cl_4]^{2-}$ (**44**) + $[Fe_4(N^tBu)_3(S)Cl_4]^-$ (**42**)	⟶	$[Fe_4(N^tBu)_2(S)_2Cl_4]^{2-}$ (**43**)
$[Fe_4(N^tBu)(S)_3Cl_4]^{2-}$ (**44**) + $[Fe_4(N^tBu)(Se)_3Cl_4]^-$ (**45**)	⟶	Mixed sulfide/selenide clusters

(iii) In the synthesis of cluster **42**, product selectivity is excellent at 10:1; however, the syntheses of **43** and **44** exhibit only moderate selectivity. In the preparation of cluster **44**, the reaction crude was contaminated by 15% (of the total iron content) of cluster **43**. A time course experiment was performed and monitored by ^{1}H NMR assay, which reveals that **44** is the only product at the beginning of the reaction, with no **43** formed during the first hour. We believe that cluster **47** is not only reacting with the starting material cluster $[Fe_4S_4Cl_4]^{2-}$, but might also further reacts with product **44** to form side product **43**. Indeed, treatment of **44** with 1 equivalent of **47** generates **43** within 5 minutes. Interestingly, cluster **43** also reacts with **47**, but only with cluster decomposition; no other species were identified. On the other hand, cluster **44** is found as a contaminating compound in the synthesis of **43** as well, and appears at similar ratio (ca. 25%, of the iron content) throughout the reaction course. Dinuclear cluster **46** does react with the dominant product **43**, but does not form **44**, and only forms ^{1}H NMR-silent species. Another starting material $[Fe_2S_2Cl_4]^{2-}$ does not react with **44**. The observation summaries of the time-course reactions are presented in Tables 2.5 and 2.6.

Table 2.2. Time-course reaction of the synthesis of cluster **44**

Time \ Reaction	**47** + $[Fe_4S_4Cl_4]^{2-}$	**44** + **47**	**43** + **47**
5 minutes	The only type of cluster formed was **44**.	A large amount of **44** has reacted with **47**, generated 3% of **43** and other minor unidentified species, and 55% of **44** left.	80% of **43** was detected and minor unknown species were found.
30 minutes	The reaction kept forming **44**.	**44** kept reacting with **47** to form 4.5% of **43** and 45% of **44** was left. Minor unidentified species also presented.	Cluster **43** kept decomposing and 67% was left.
2 hours	**44** still dominated the cluster products, but **43** formed as a minor component, and the ratio of **44** to **43** was 4:1.	**44** kept reacting with **47** to form 5.5% of **43** and 38% of **44** was left. Minor unidentified species still presented.	Cluster **43** kept decomposing and 36% was left.
18 hours	The ratio of **44** to **43** continues to diminish, reaching 3:1.	70% of **44** has reacted with **47**, yielded 11% of **43** and other minor unknown components.	Only 34% of **43** was detected and there is no evidence of a second cluster

Table 2.3. Time-course reaction of the synthesis of cluster **43**

Time \ Reaction	**46** + $[Fe_2S_2Cl_4]^{2-}$	**43** + **46**
5 minutes	Three cluster types were formed, including 2% of **43**, 20% of **44** and 6% of **45**.	Cluster **43** decayed by 50% after 2 hours and 80% after 18 hours. There were no signals for other known clusters, only minor unidentified species.
30 minutes	The yields of three clusters remained the same.	
2 hours	The yields of three clusters grew to 3% of **43**, 22% of **44** and 7% of **45**.	
18 hours	Only two clusters **43** and **44** were found in a ratio of 4:1.	

(iv) With the availability of selenium analogues **52** and **45**, which have different chemical shifts relative to their sulfur analogues, several labeling experiments were tested to track core ligand mixing by ^{1}H NMR spectroscopy: (a) **41** + **52**; (b) $[Fe_4S_4Cl_4]^{2-}$ + **52**; (c) $[Fe_4Se_4Cl_4]^{2-}$ + **47**. A typical ^{1}H NMR spectrum from these labeling reactions is given in Figure 2.12 (IV).

The chemical shifts of some mixed-core clusters are assigned based on their positions relative to Se-only and S-only clusters. In reactions (a) and (b), all mixed-core products were detected within the first five minutes; by contrast, in (c), Se-only heteroleptic clusters appear to dominate within the reaction.

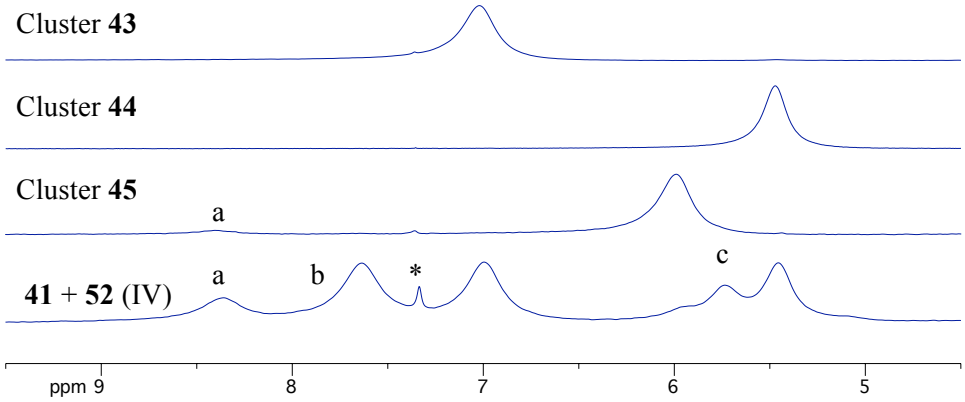

Figure 2.12. ^{1}H NMR spectra (300 MHz) of clusters **43**, **44**, **45** and clusters with mixed sulfide/selenide cores. Residual solvent C_6H_6 is marked by *, signals of $[Fe_4(\mu_3\text{-}N^tBu)_2(\mu_3\text{-}Se)_2Cl_4]^z$ are marked by a, signal of $[Fe_4(\mu_3\text{-}N^tBu)_2(\mu_3\text{-}Se)(\mu_3\text{-}S)Cl_4]^z$ is marked by b, and the signal corresponding to $[Fe_4(\mu_3\text{-}N^tBu)(\mu_3\text{-}Se)_2(\mu_3\text{-}S)Cl_4]^z$ or $[Fe_4(\mu_3\text{-}N^tBu)(\mu_3\text{-}Se)(\mu_3\text{-}S)_2Cl_4]^z$ is marked by c.

2.3.4 Cluster Structures

The crystallographic data for clusters $[Et_4N][Fe_4(\mu_3\text{-}N^tBu)_3(\mu_3\text{-}S)Cl_4]$, $[Et_4N]_2[Fe_4(\mu_3\text{-}N^tBu)_2(\mu_3\text{-}S)_2Cl_4]$, $[Et_4N]_2[Fe_4(\mu_3\text{-}N^tBu)(\mu_3\text{-}S)_3Cl_4]$, $[Et_4N]_2[Fe_4(\mu_3\text{-}N^tBu)(\mu_3\text{-}Se)_3Cl_4]$ and $[Et_4N]_2[Fe_4(\mu_3\text{-}N^tBu)_2(\mu_3\text{-}S)_2(SPh)_4]$ were obtained by single X-ray crystallography. Selected bond distances and angles of these clusters are given in the Tables 2.4 to 2.7. The four Fe–NR–S/Se clusters all contain tetrahedral iron centers, edged fused through μ_3-imide/sulfide/selenide bridges and terminal chlorides complete the ligand sets. The cube cluster **42**, **43** and **44** cores can be viewed as six $[Fe_2N_2]$, $[Fe_2S_2]$ and $[Fe_2NS]$ rhomb units, with shared edges with N belonging to *tert*-butyl imide and S belonging

to sulfide. In these cores, the Fe–N bond distances are much shorter than Fe–S bond distances; and the Fe–S–Fe angles are more acute than the Fe–N–Fe angles. Fe–S bonds and Fe–S–Fe angles are approximately equal to bonds and angles in all-sulfide cubane type structures (mean Fe–S bond lengths and Fe–S–Fe angles for $[Fe_4(\mu_3\text{-}S)_4Cl_4]^{2-}$, 2.283 Å, 71.5°). Fe–N bonds and Fe–N–Fe angles are approximately equal to bonds and angles in all-imide cubane type structures (mean Fe–N bond lengths and Fe–N–Fe angles for $Fe_4(\mu_3\text{-}N^tBu)_4Cl_4$, 1.942 Å, 84.4°). The cube faces of $[Fe_2N_2]$ and $[Fe_2NS]$ rhombs are nearly planar while the $[Fe_2S_2]$ units significantly from the ideal planar. **42** is one electron more oxidized than clusters **43**, **44**, and there is a slight decrease in Fe–Cl bond length (ca. 0.03 Å). Oxidation appears to have little obvious effect on cluster structure. Compared with cluster **43**, its terminal thiolate substituted version **43a** has approximately equal Fe-S and Fe-N bond distances. Also, their Fe–N–Fe and Fe–S–Fe angles are comparable.

Cluster **44**, which contains the heteroligated core with the highest sulfur-to-nitrogen ratio, is the most cofactor-relevant heteroligated cluster as its eight-atom $[Fe_4NS_3]$ core is virtually isometric with the $[Fe_4S_3X]$ (assuming X = N) cubane subunit of the FeMo cofactor. A superposition of the cores from cluster **44** and the FeMo cofactor is shown in Figure 2.8, with comparative metrics listed. The difference of the interatomic distances between the two core fragments is less than 1.5%, with the exception of a 4% deviation in the Fe1···Fe2 separation. Although the μ_3-imide ligand in **44** does not reproduce the μ_6-environment of X in the FeMo cofactor, the *tert*-butylimide ligand shares some of the chemical properties of a nitride ligand and the two core frameworks are an excellent match. These similarities may provide further useful information about the FeMo cofactor, especially if X = N.

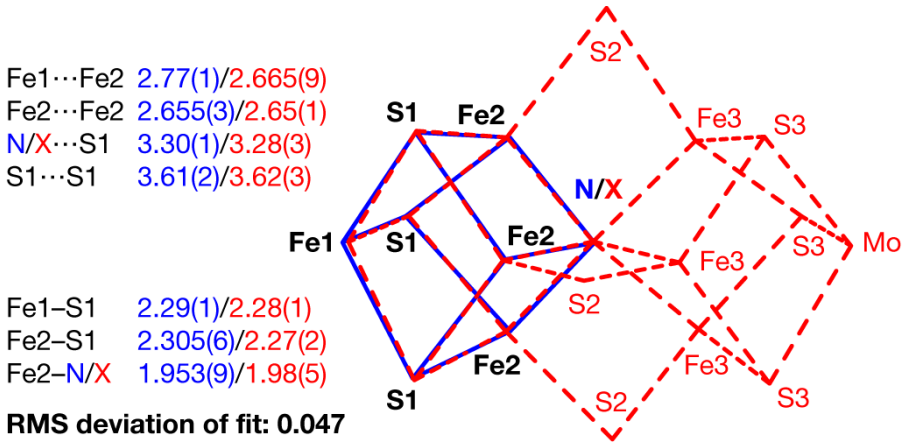

Figure 2.13. Structural comparison between the $[Fe_4(\mu_3\text{-}N^tBu)(\mu_3\text{-}S)_3Cl_4]^{2-}$ core and the FeMo-cofactor

Another tetranuclear cluster **45** is geometrically similar to **44** except that **44** contains μ_3-sulfide ligands and **45** contains μ_3-selenide ligands. Compared with the core structure of clusters **44** and **45**, Fe–N bonds and Fe–N–Fe angles are approximately equal; the Fe–S bond distances are much shorter than Fe–Se bond distances; and the Fe–Se–Fe angles are slightly more acute than the Fe–S–Fe angles.

Table 2.4. Selected interatomic distances (Å) and angles (deg) in $[Et_4N][Fe_4(\mu_3\text{-}N^tBu)_3(\mu_3\text{-}S)Cl_4]$ (**42**)

Fe(1)-N(1/2/3)	1.9582(17)/1.9500(16)/1.9479(17)
Fe(2)-N(1/2)	1.9441(16)/1.9
Fe(3)-N(2/3)	1(16)
Fe(4)-N(1/3)	1.9363(16)/1.9423(17)
Fe(2/3/4)-S(1)	1.9352(18)/1.9539(18)
Fe(1)…Fe(2/3/4)	2.3121(6)/2.3060(6)/2.2986(5)
Fe(2)…Fe(3/4)	2.6043(4)/2.5762(4)/2.5735(4)
Fe(3)…Fe(4)	2.6787(4)/2.6797(4)
Fe(1/2/3/4)-Cl(1/2/3/4)	2.6891(4)
S(1)…N(1/2/3)	2.1959(6)/2.2080(7)/2.1964(6)/2.1857(7)
N(1/1/2)…N(2/3/3)	3.2503(18)/3.2621(17)/3.2410(19)

Cl(1)-Fe(1)-N(1/2/3)		2.897(2)/2.924(3)/2.908(3)	
Cl(2)-Fe(2)-N(1/2)		121.00(5)/120.96(5)/119.86(5)	
Cl(3)-Fe(3)-N(2/3)		123.01(6)/118.18(5)	
Cl(4)-Fe(4)-N(1/3)		117.18(5)/122.72(6)	
S(1)-Fe(2/3/4)-Cl(2/3/4)		119.30(6)/119.84(6)	
N(1/1/3)-Fe(1)-N(2/3/2)		116.15(2)/116.33(2)/117.08(3)	
N(2)-Fe(2)-N(1)		95.72(7)/96.94(7)/96.51(7)	
N(3)-Fe(3)-N(2)		96.24(7)	
N(3)-Fe(4)-N(1)		97.15(7)	
S(1)-Fe(2)-N(1/2)		97.51(7)	
S(1)-Fe(3)-N(2/3)		99.19(5)/99.57(5)	
S(1)-Fe(4)-N(1/3)		100.14(5)/99.12(5)	
Fe(2/3/3)-Fe(1)-Fe(4/4/2)		99.92(5)/99.03(5)	
Fe(3/4/4)-Fe(2)-Fe(1/1/3)		62.330(11)/62.957(11)/62.270(11)	
Fe(2/2/4)-Fe(3)-Fe(4/1/1)		58.349(11)/58.272(11)/60.244(11)	
Fe(3/3/2)-Fe(4)-Fe(2/1/1)		59.896(11)/59.381(10)/58.474(10)	
Fe(1/1/2)-N(1)-Fe(2/4/4)		59.896(11)/58.569(11)/59.398(11)	
Fe(2/2/1)-N(2)-Fe(1/3/3)		83.73(6)/82.75(7)/87.38(6)	
Fe(4/4/1)-N(3)-Fe(1/3/3)		83.84(6)/87.20(6)/83.04(6)	
Fe(3/3/2)-S(1)-Fe(2/4/4)		82.54(7)/87.29(7)/82.94(7)	
C(1)-N(1)-Fe(1/2/4)		70.907(17)/71.463(17)/71.067(17)	
C(5)-N(2)-Fe(1/2/3)		126.74(13)/129.29(15)/130.62(15)	
C(9)-N(3)-Fe(1/3/4)		127.84(13)/129.14(14)/129.67(13)	
		129.64(14)/128.74(15)/129.26(16)	
[Fe(1,3),N(2,3)]	0.038	Planarity[a]	
[Fe(1,4),N(1,3)]	0.0329	[Fe(2,3),N(2),S(1)]	0.1007
[Fe(1,2),N(1,2)]	0.0449	[Fe(2,4),N(1),S(1)]	0.1067
		[Fe(3,4),N(3),S(1)]	0.1203

[a] RMS deviation from the least-squares-fitted $[Fe_2N_2]$ rhomb plane

Table 2.5. Selected interatomic distances (Å) and angles (deg) in $[Et_4N][Fe_4(\mu_3\text{-}N^tBu)_2(\mu_3\text{-}S)_2Cl_4]$ (**43**)

Fe(1)-S(1/2)	2.3283(13)/2.3283(13)
Fe(2)-S(2)	2.2879(13)
Fe(3)-S(1/2)	2.3279(13)/2.3312(13)
Fe(4)-S(1)	2.2882(13)
Fe(2/3/4)-N(1)	1.976(3)/1.903(3)/1.973(3)
Fe(1/2/4)-N(2)	1.897(3)/1.966(3)/1.970(3)
Fe(1)…Fe(2/3/4)	2.6139(8)/2.7954(9)/2.6274(9)
Fe(2)…Fe(3/4)	2.6321(8)/2.6720(8)
Fe(3)…Fe(4)	2.6369(9)
Fe(1/2/3/4)-Cl(1/2/3/4)	2.2406(13)/2.2312(12)/2.2436(13)/2.2394(13)
S(1)…N(1/2)	3.299(3)/3.301(4)
S(2)…N(1/2)	3.306(4)/3.309(4)
S(1)…S(2)	3.6103(16)
N(1)…N(2)	2.889(5)
Cl(1)-Fe(1)-S(1/2)	115.27(5)/114.08(5)
Cl(2)-Fe(2)-S(2)	116.22(5)
Cl(3)-Fe(3)-S(1/2)	113.88(5)/115.44(5)
Cl(4)-Fe(4)-S(1)	117.28(5)
N(1)-Fe(2/3/4)-Cl(2/3/4)	121.68(10)/119.36(11)/119.68(11)
N(2)-Fe(1/2/4)-Cl(1/2/4)	118.70(11)/117.43(10)/118.99(11)
S(1)-Fe(1/3)-S(2)	101.66(5)/101.59(5)
N(1)-Fe(2/4)-N(2)	94.28(14)/94.18(14)
N(2)-Fe(1)-S(1/2)	102.27(10)/102.60(11)
N(1/2)-Fe(2)-S(2)	101.43(11)/101.86(11)
N(1)-Fe(3)-S(1/2)	101.99(11)/102.16(10)
N(1/2)-Fe(4)-S(1)	101.22(10)/101.35(11)
Fe(2/2/3)-Fe(1)-Fe(3/4/4)	61.30(2)/58.12(2)/58.09(2)
Fe(1/1/3)-Fe(2)-Fe(3/4/4)	64.40(2)/59.60(2)/59.62(2)

Fe(1/1/4)-Fe(3)-Fe(2/4/2)		57.48(2)/57.76(2)/60.95(2)	
Fe(3/3/2)-Fe(4)-Fe(2/1/1)		59.44(2)/64.15(2)/59.10(2)	
Fe(1/1/3)-S(1)-Fe(3/4/4)		73.80(4)/69.38(4)/69.67(4)	
Fe(1/1/2)-S(2)-Fe(2/3/3)		68.97(4)/73.73(4)/69.47(4)	
Fe(2/2/3)-N(1)-Fe(3/4/4)		85.45(14)/85.19(13)/85.71(13)	
Fe(1/1/2)-N(2)-Fe(2/4/4)		85.15(14)/85.55(13)/85.49(13)	
C(1)-N(1)-Fe(2/3/4)		126.8(3)/130.5(3)/127.9(3)	
C(5)-N(2)-Fe(1/2/4)		130.3(3)/127.6(3)/127.4(3)	
		Planarity	
[Fe(2,4),N(1,2)]	0.0602	[Fe(1,2),N(2),S(2)]	0.0806
[Fe(1,4),N(2),S(1)]	0.0821	[Fe(3,4),N(1),S(1)]	0.0809
[Fe(2,3),N(1),S(2)]	0.083	[Fe(1,3),S(1,2)]	0.2301

Table 2.6. Selected interatomic distances (Å) and angles (deg) in $[Et_4N][Fe_4(\mu_3\text{-}N^tBu)(\mu_3\text{-}S)_3Cl_4]$ (**44**) and $[Et_4N][Fe_4(\mu_3\text{-}N^tBu)(\mu_3\text{-}Se)_3Cl_4]$ (**45**), in the first column Q = S, and in the second column Q = Se.

	$[Et_4N][Fe_4(\mu_3\text{-}N^tBu)(\mu_3\text{-}S)_3Cl_4]$ (**44**)	$Et_4N][Fe_4(\mu_3\text{-}N^tBu)(\mu_3\text{-}Se)_3Cl_4]$ (**45**)
Fe(1)-Q(1/2/3)	2.2900(10)/2.2823(9)/2.3039(9)	2.3913(10)/2.4240(9)/2.4229(10)
Fe(2)-Q(1/3)	2.3121(9)/2.3048(9)	2.4377(10)/2.4069(10)
Fe(3)-Q(1/2)	2.3029(10)/2.2983(9)	2.4371(10)/2.4362(10)
Fe(4)-Q(2/3)	2.3099(9)/2.2996(9)	2.4362(10)/2.4168(10)
Fe(2/3/4)-N(1)	1.948(3)/1.963(3)/1.948(3)	1.946(4)/1.922(4)/1.956(4)
Fe(1)…Fe(2/3/4)	2.7758(6)/2.7750(6)/2.7587(6)	2.7956(11)/2.7790(11)/2.8171(11)
Fe(2)…Fe(3/4)	2.6549(6)/2.6525(6)	2.6625(11)/2.6935(11)
Fe(3)…Fe(4)	2.6575(6)	6805(11)
Fe(1/2)-Cl(1/2)	2.2310(10)/2.2333(9)	2386(15)/2.2140(17)
Fe(3/4)-Cl(3/4)	2.2288(9)/2.2147(10)	2226(17)/2.2302(17)
N(1)…Q(1/2/3)	3.308(3)/3.299(3)/3.288(3)	3.428(4)/3.403(4)/3.403(4)
Q(1/1/2)…Q(2/3/3)	3.5856(11)/3.6119(12)/3.6208(11)	3.8440(8)/3.8317(9)/3.9083(8)
Cl(1)-Fe(1)-S(1/2/3)	120.57(4)/112.82(4)/110.65(4)	113.94(5)/108.70(5)/114.78(5)

Cl(2)-Fe(2)-S(1/3)	114.45(4)/115.61(4)	112.59(6)/112.28(6)	
Cl(3)-Fe(3)-S(1/2)	117.48(4)/113.14(4)	110.38(6)/113.46(6)	
Cl(4)-Fe(4)-S(2/3)	110.84(4)/116.02(4)	111.03(6)/116.98(6)	
N(1)-Fe(2/3/4)-Cl(2/3/4)	118.97(8)/118.72(8)/121.68(8)	120.68(13)/120.93(13)/118.88(12)	
Q(1/1/3)-Fe(1)-Q(2/3/2)	103.29(3)/103.67(3)/104.27(4)	105.93(3)/105.48(3)/107.48(3)	
Q(3)-Fe(2)-Q(1)	102.95(3)	105.02(4)	
Q(1)-Fe(3)-Q(2)	102.39(3)	106.63(4)	
Q(3)-Fe(4)-Q(2)	103.54(3)	104.28(3)	
Fe(2/2/3)-Fe(1)-Fe(3/4/4)	57.147(15)/57.274(16)/57.399(16)	57.36(3)/57.24(3)/57.06(3)	
Fe(1/1/3)-Fe(2)-Fe(3/4/4)	61.412(15)/61.040(17)/60.094(17)	61.16(3)/61.72(3)/60.54(3)	
Fe(1/1/4)-Fe(3)-Fe(2/4/2)	61.441(15)/60.933(16)/59.909(17)	60.54(3)/61.78(3)/62.10(3)	
Fe(3/3/2)-Fe(4)-Fe(2/1/1)	59.997(17)/61.608(17)/61.686(17)	59.40(3)/60.67(3)/60.92(3)	
Fe(1/1/2)-Q(1)-Fe(2/3/3)	74.19(3)/74.34(3)/70.24(3)	70.74(3)/71.39(3)/67.10(3)	
Fe(3/4/1)-Q(2)-Fe(1/3/4)	74.57(3)/70.43(3)/73.84(3)	70.72(3)/66.68(3)/69.73(3)	
Fe(4/4/1)-Q(3)-Fe(1/2/4)	73.64(3)/70.35(3)/74.07(3)	71.19(3)/67.05(3)/69.77(3)	
Fe(2/3/2)-N(1)-Fe(4/4/3)	85.82(10)/85.61(10)/85.51(10)	87.00(16)/87.44(16)/87.29(16)	
C(1)-N(1)-Fe(2/3/4)	128.3(2)/129.0(2)/127.5(2)	127.9(3)/126.1(4)/127.6(3)	
	Planarity		
[Fe(1,2),S(1,3)]	0.1694	[Fe(3,4),N(1),Se(3)]	0.0938
[Fe(1,4),S(2,3)]	0.1619	[Fe(2,4),N(1),Se(1)]	0.0782
[Fe(1,3),S(1,2)]	0.1734	[Fe(2,3),N(1),Se(2)]	0.0981
[Fe(2,3),N(1),S(1)]	0.078	[Fe(1,2),Se(1,2)]	0.2147
[Fe(2,4),N(1),S(3)]	0.0908	[Fe(1,4),Se(1,3)]	0.216
[Fe(3,4),N(1),S(2)]	0.0838	[Fe(1,3),Se(2,3)]	0.1973

Table 2.7. Selected interatomic distances (Å) and angles (deg) in $[Et_4N][Fe_4(\mu_3\text{-}N^tBu)_2(\mu_3\text{-}S)_2(SPh)_4]$ (**43a**)

Fe(1)-S(1/2)	2.3256(9)/2.3236(9)
Fe(2)-S(1/2)	2.3362(9)/2.3380(9)
Fe(3)-S(2)	2.2825(9)
Fe(4)-S(1)	2.2768(10)
Fe(1/3/4)-N(1)	1.897(3)/1.983(3)/1.990(3)
Fe(2/3/4)-N(2)	1.897(3)/1.988(3)/1.985(3)
Fe(1)…Fe(2/3/4)	2.7598(6)/2.6187(6)/2.6182(6)
Fe(2)…Fe(3/4)	2.6320(6)/2.6309(7)
Fe(3)…Fe(4)	2.6456(7)
Fe(1/2/3/4)-S(3/4/5/6)	2.3015(9)/2.3042(10)/2.2879(10)/ 2.297(2)
S(3)-Fe(1)-S(1/2)	113.68(3)/114.72(3)
S(4)-Fe(2)-S(1/2)	117.13(4)/115.01(4)
S(5)-Fe(3)-S(2)	119.48(4)
S(6)-Fe(4)-S(1)	118.47(16)
N(1)-Fe(1/3/4)-S(3/5/6)	117.79(8)/123.60(8)/126.04(19)
N(2)-Fe(2/3/4)-S(4/5/6)	115.47(9)/110.70(8)/108.95(9)
S(1)-Fe(1/2)-S(2)	103.86(3)/103.09(3)
N(1)-Fe(3/4)-N(2)	96.30(11)/96.16(11)
N(1)-Fe(1)-S(1/2)	102.44(8)/102.56(9)
N(2)-Fe(2)-S(1/2)	101.91(8)/102.12(8)
N(1/2)-Fe(3)-S(2)	101.20(8)/101.21(8)
N(1/2)-Fe(4)-S(1)	101.35(8)/101.23(8)
Fe(2/2/3)-Fe(1)-Fe(3/4/4)	58.526(16)/58.503(17)/60.687(17)
Fe(1/1/3)-Fe(2)-Fe(3/4/4)	58.058(16)/58.057(16)/60.357(18)
Fe(1/1/4)-Fe(3)-Fe(2/4/2)	63.418(16)/59.648(17)/59.800(18)
Fe(3/3/2)-Fe(4)-Fe(2/1/1)	59.843(17)/59.665(17)/63.440(17)
Fe(1/1/2)-S(1)-Fe(2/4/4)	72.60(3)/69.34(3)/69.53(3)
Fe(1/2/2)-S(2)-Fe(3/3/1)	69.29(3)/69.44(3)/72.60(3)

Fe(1/1/3)-N(1)-Fe(3/4/4)		84.86(11)/84.64(11)/83.51(10)	
Fe(3/2/2)-N(2)-Fe(4/3/4)		83.50(10)/85.27(10)/85.31(10)	
C(25)-N(2)-Fe(2/3/4)		127.0(2)/130.5(2)/129.4(2)	
C(29)-N(1)-Fe(1/3/4)		127.5(2)/132.4(2)/127.6(2)	
		Planarity	
[Fe(3,4),N(1,2)]	0.0477	[Fe(2,3),N(2),S(2)]	0.0953
[Fe(2,4),N(2),S(1)]	0.0967	[Fe(1,4),N(1),S(1)]	0.0990
[Fe(1,3),N(1),S(2)]	0.1010	[Fe(1,2),S(1,2)]	0.2117

2.3.5 Spectroscopic Properties

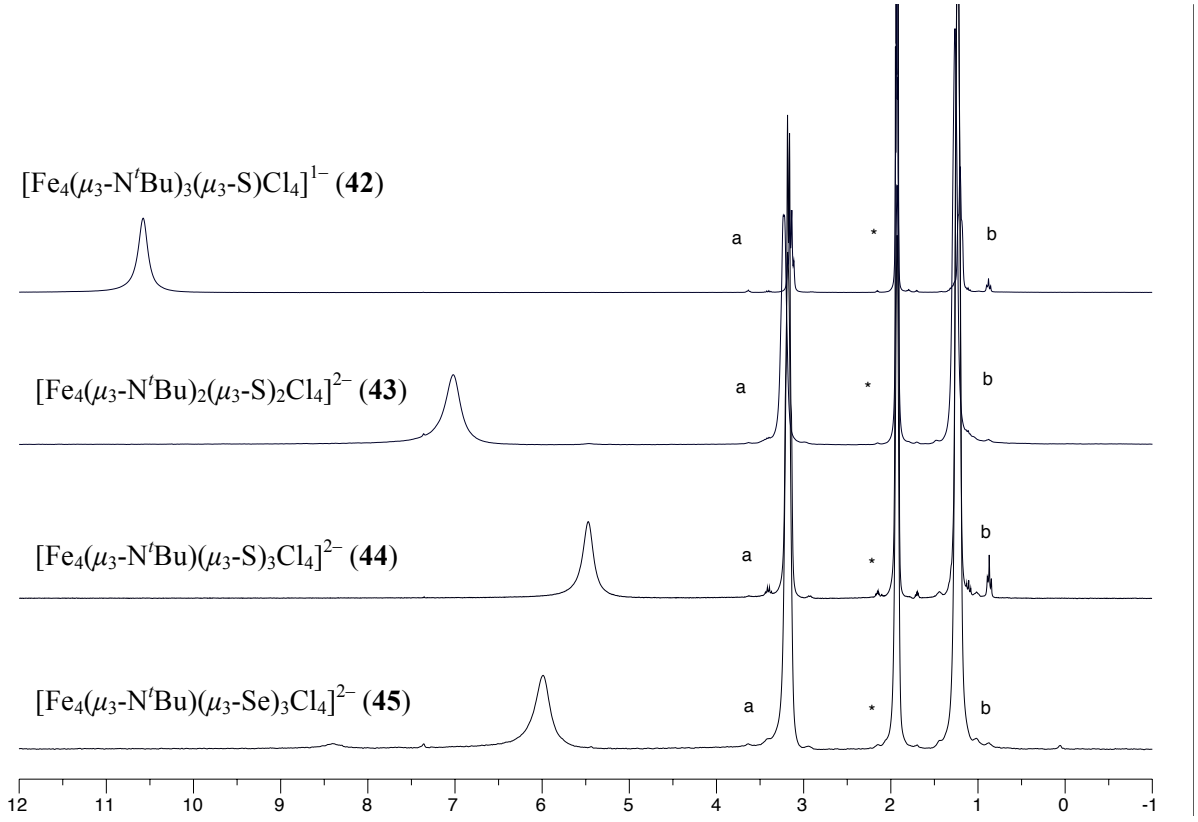

Figure 2.14. ^{1}H NMR spectra (300 MHz) of clusters **42**, **43**, **44** and **45**. Residual protio signal of CD_3CN is marked by *, signals corresponding to the $(Et_4N)^+$ counterions are marked by a and b.

Table 2.8. ^{1}H NMR spectroscopic data for clusters **42**, **43**, **44** and **45**.

Compound	^{1}H NMR (C_6D_6, δ ppm)
42	10.51 (27 br)
43	7.02 (18 br)
44	5.51 (9 br)
45	5.97 (9 br)

Clusters **42**, **43**, **44** and **45** exhibit well-defined isotropically shifted ^{1}H NMR spectra that can be easily distinguished. The clusters are therefore paramagnetic under the measurement conditions, behavior consistent with previously studied Fe-S and Fe-NR clusters. The ^{1}H NMR spectra of these complexes are presented in Figure 2.14 and summarized in Table 2.8.

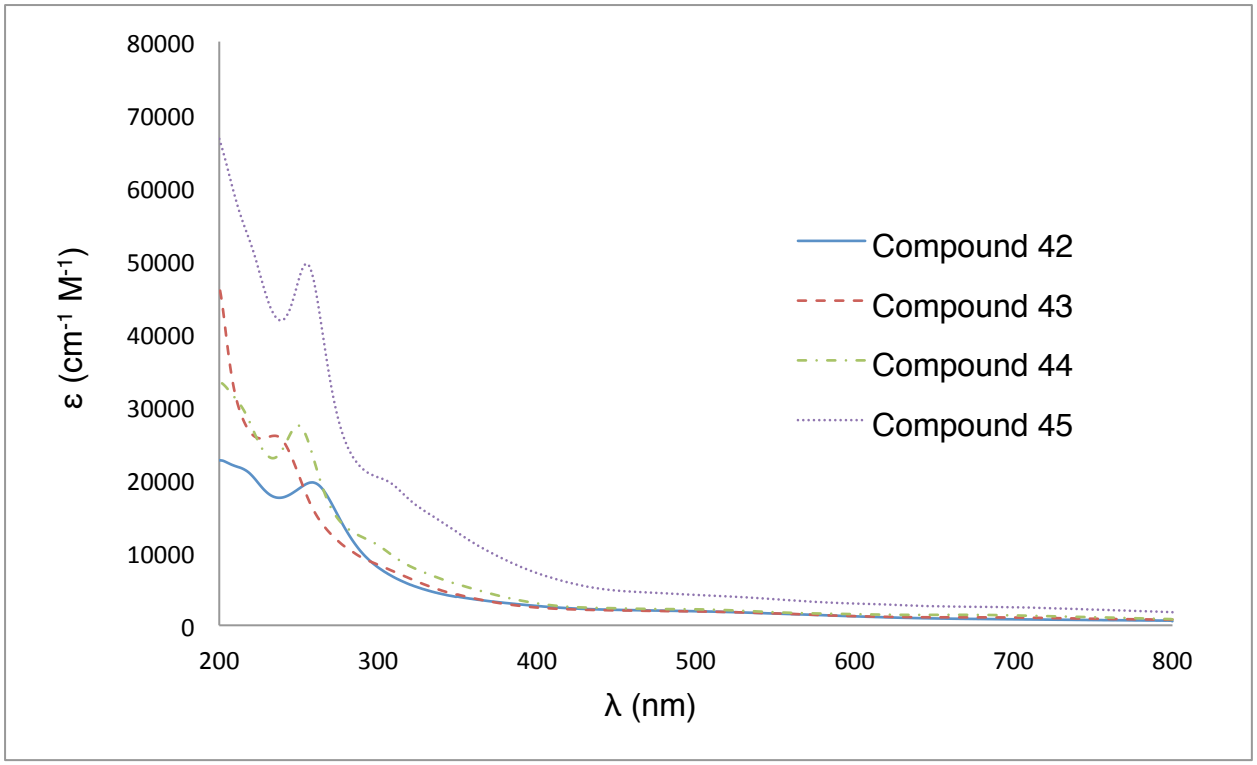

Figure 2.15. Comparative electronic absorption spectra of clusters **42**, **43**, **44** and **45** in MeCN.

Electronic absorption spectra of iron-imide clusters **42**, **43**, **44** and **45** are presented in Figure 2.15 and the data is summarized in Table 2.9. All the compounds were measured in MeCN. These tetranuclear species are black in the crystal form, and dissolve to give deep brown solutions. The spectra of these clusters are characterized by intense charge-transfer bands in the near violet region and trail off into the visible region, which explains why they are deep brown in solution.

Table 2.9. Electronic absorption spectroscopic data for clusters **42**, **43**, **44** and **45**.

Compound	electronic abs: λ_{max}, nm (ε_M, L mol^{-1}·cm^{-1})
42	259 (19500)
43	235 (25900)
44	250 (27300)
45	255 (49500)

2.4.5 Redox Behavior

The redox properties of the isolated $[Fe_4(N^tBu)_n(S)_{4-n}Cl_4]^z$ cubane clusters were explored using cyclic voltammetry; results are summarized in Table 2.10. The following observations are noted:

(i) Cluster $[Fe_4(N^tBu)_3(S)Cl_4]^-$ exhibits chemically reversible behavior at z = 1–/2– (Figure 2.16).

(ii) Clusters $[Fe_4(N^tBu)_2(S)_2Cl_4]^{2-}$ and $[Fe_4(N^tBu)(S)_3Cl_4]^{2-}$ exhibit only quasi-reversible behavior at z = 2–/3–. This behavior has also been found in $[Fe_4S_4Cl_4]^{3-}$ due to chloride dissociation and it is likely that a similar situation occurs in heteroligated imide/sulfide cubanes at the same oxidation state as well.

(iii) Each replacement of sulfide by imide in the $[Fe_4(N^tBu)_n(S)_{4-n}Cl_4]^z$ cubane system leads to a progressive negative shift in potential for a given redox couple[77, 81] as plotted in Figure 2.17:

from $[Fe_4S_4Cl_4]^{2-}$ to $[Fe_4(N^tBu)_2(S)_2Cl_4]^{2-}$ at z = 3–/2– and from $[Fe_4(N^tBu)_2(S)_2Cl_4]^{2-}$ to $[Fe_4(N^tBu)_4Cl_4]^{-}$ to at z = 2–/1–. It is likely that highly basic *tert*-butylimide helps stabilize higher oxidation states in these compounds.

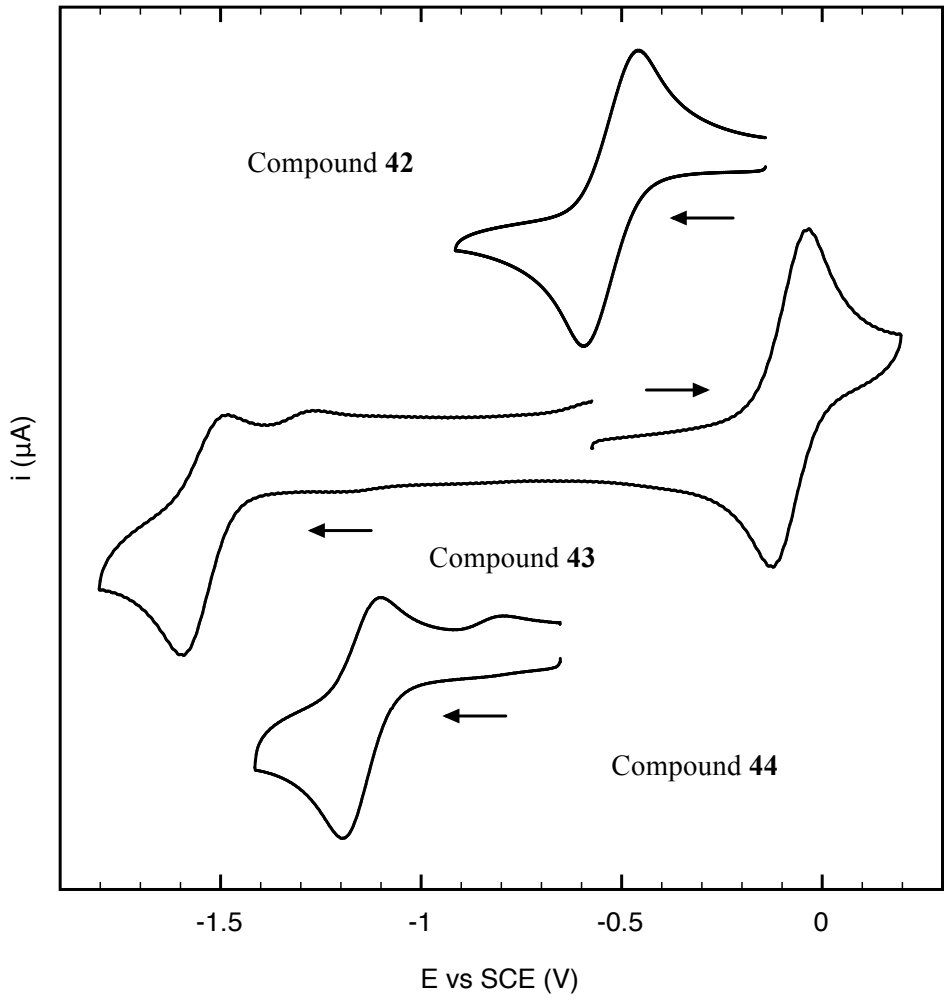

Figure 2.16. Cyclic voltammograms of clusters **42**, **43** and **44**, peak potentials vs SCE are indicated. The data is obtained from 100 mV/s scan rates using 0.1 M (n-Bu_4N)(ClO_4) (TBAP) supporting electrolyte in MeCN.

Table 2.10. Chemically reversible redox couples ($E_{1/2}$) for $[Fe_4(N^tBu)_n(S)_{4-n}Cl_4]^z$ cubane clusters (V vs. SCE)

Compound	z = –2/–1	z = –3/–2
42	–0.529	
43	–0.079	–1.554
44		–1.167

Quasi-reversible behavior: for **43**, ΔE = 64, 66, 83, 97, 110, and 110 mV, and i_p^a/i_p^c = 0.7, 0.8, 1.2, 1.1, 0.7, and 0.6 at 25, 50, 100, 200, 500, and 750 mV/s scan rates, respectively; for **44**, ΔE = 109, 120, 132 and 173 mV, and i_p^a/i_p^c = 0.5, 0.4, 0.3 and 0.3 at 50, 100, 200, and 500 mV/s scan rates, respectively.

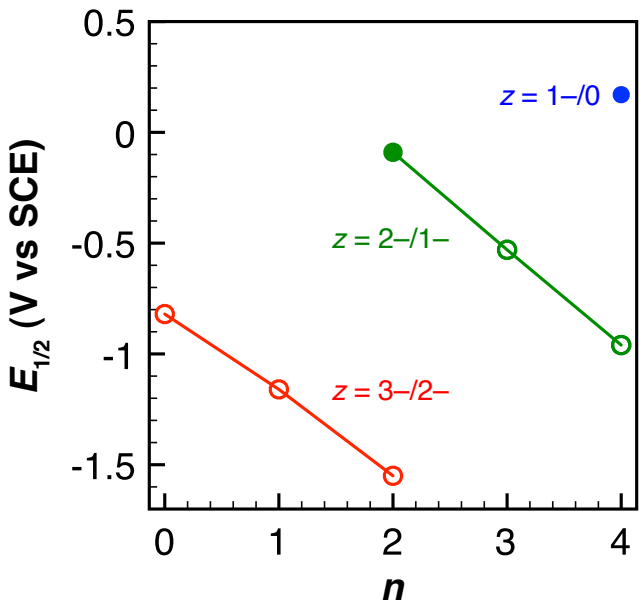

Figure 2.17. Potentials of the $[Fe_4(N^tBu)_n(S)_{4-n}Cl_4]^z$ cubane system for a given redox couple. Solid and open symbols indicate chemically- and quasi-reversible processes, respectively. The data is obtained from 100 mV/s scan rates at 0.1 M (n-Bu_4N)(ClO_4) (TBAP) supporting electrolyte in MeCN.

2.4 Experimental Section

2.4.1 General Experimental Method

Due to the air-sensitive nature of the compounds in this project, all operations were performed under dry, anaerobic conditions (N_2 atmosphere) through the use of inert atmosphere gloveboxes and Schlenk techniques. All glassware were oven-dried directly prior to use. Solvents were purified either by passage through an M. Braun solvent purification system (THF, Et_2O, *n*-pentane and benzene), or by distillation from appropriate scavengers (MeCN from CaH_2 and toluene from Na metal), then degassed and kept over 3 Å molecular sieves. Deuterated NMR solvents (purchased from Cambridge Isotope Laboratories) were kept over 3 Å molecular sieves for at least 24 hours before use. Diatomaceous earth (Celite) was activated by being heated at 150 °C for more than 12 hours and dried under vacuum for more than 12 hours before use. $(Et_4N)_2[Fe_4(\mu_3\text{-}S)_4Cl_4]$, $(Et_4N)_2[Fe_2(\mu\text{-}S)_2Cl_4]$, $(Et_4N)_2[Fe_4(\mu_3\text{-}Se)_4Cl_4]$[82] and $FeCl_2(THF)_{1.5}$[83], were synthesized by published procedures. $(Me_3Si)_2S$ is purchased from Sigma Aldrich.

2.4.2 Preparation of Compounds

Et_4NSH.[84] A commercial H_2S was bubbled into a 20% aqueous Et_4NOH solution in CH_3OH for 30 minutes at 0 ºC; and dried at 50 ºC/0.06 torr overnight. The solid residue was dissolve in CH_3CN, charged with Et_2O to form a light yellow solution, volume reduced to induce crystallization, and cooled to –30 ºC for 3 d. The white microcrystalline precipitate was filtered off and dried in vacuo for 3 h.

$(Et_4N)_2[Fe_2(\mu\text{-}N^tBu)(\mu\text{-}S)Cl_4]$ (41). A solution of $(Et_4N)Cl$ (0.332 g, 2.0 mmol) in MeCN (6 mL) was added to a solution of *cis*-$[Fe_2(\mu\text{-}N^tBu)_2Cl_2(NH_2{}^tBu)_2]$ (**40**) (0.471 g, 1.0 mmol) in MeCN (30 mL). After stirring for 4 h, $(Me_3Si)_2S$ (0.235 mL, 1.1 mmol) was added to the brownish-orange solution. The

reaction mixture was stirred for another 12 h to afford a red-orange solution. Then the solvent was removed in vacuo, and the black residue was taken up by 1:1 MeCN/THF (12 mL). After filtration, the orange-black filtrate was cooled to –30 ºC, and Et_2O was diffused into it for 3 d to afford 0.216 g black crystals, which was isolated by filtration and rinsed with Et_2O (3 x 2 mL). The filtrate was volume reduced in vacuo to ca. 4 mL and diffused by Et_2O at –30 ºC for 7 d to produce a second crop (0.124 g) Total yield: 0.340 g (55%). Anal. Calcd. for $C_{20}H_{49}N_3Cl_4Fe_2S$: C, 38.92; H, 8.00; N, 6.81. Found: C, 38.70; H, 8.04; N, 6.45.

$(Et_4N)[Fe_4(\mu_3\text{-}N^tBu)_3(\mu_3\text{-}S)Cl_4]$ (42). $(Et_4N)SH$ (0.082 g, 0.5 mmol) was added to a solution of *cis*-$[Fe_2(\mu\text{-}N^tBu)_2Cl_2(NH_2{}^tBu)_2]$ (0.471 g, 1.0 mmol) in THF (30 mL). The reaction mixture was stirred for 12 h to give a black solution and allowed to stand at –30 ºC for another 20 h. A black filtrate was then obtained by celite filtration, which was volume reduced to 20 mL and diffused by *n*-pentane at –30 ºC for 5 d to give 202 mg black crystals (Yield: 54.6 %). Anal. Calcd. for $C_{20}H_{47}Cl_4Fe_4N_4S$: C, 32.42; H, 6.39; N, 7.56. Found: C, 32.21; H, 6.20; N, 7.42.

$(Et_4N)_2[Fe_4(\mu_3\text{-}N^tBu)_2(\mu_3\text{-}S)_2Cl_4]$ (43). To a solution of $(Et_4N)_2[Fe_2(\mu\text{-}S)_2Cl_4]$ (0.223 g, 0.4 mmol) in CH_3CN was added $Fe_2(\mu\text{-}NH^tBu)_2[N(SiMe_3)_2]_2$ (0.216 g, 0.4 mmol) in THF. After stirring for 12 hours, filtered the reaction solution was filtered through celite to remove a black precipitate. The solvent was evaporated to leave black oil, which was treated with CH_2Cl_2 and filtered to remove a black precipitate. Then the solvent was then taken to dryness under vacuum, affording a black oil, which was treated with CH_3CN/Et_2O to give black plate-like crystalline product. Yield: 0.124 g (39%). Anal. Calcd. For $C_{24}H_{58}Cl_4Fe_4N_4S_2$: C, 34.64; H, 7.03; N, 6.73. Found: C, 34.45; H, 6.96; N, 6.55.

$(Et_4N)_2[Fe_4(\mu_3\text{-}N^tBu)(\mu_3\text{-}S)_3Cl_4]$ (44). To a solution of $(Et_4N)_2[Fe_4(\mu_3\text{-}S)_4Cl_4]$ (0.301 g, 0.4 mmol) in CH_3CN (30 mL) was added $Fe_2(\mu\text{-}NH^tBu)_2(\mu\text{-}S)[N(SiMe_3)_2]_2$ (0.243 g, 0.4 mmol) in THF (30

mL). The reaction mixture was stirred for 8 hours, and filtered through celite to remove a black precipitate. The black solution was then taken to dryness under vacuum, affording a black oil, which was treated by CH_2Cl_2 (20 mL) to give a black microcrystalline solid. Recrystallization from CH_3CN/Et_2O generated 0.165 g (52 %) product as black needle-like crystals. Anal. Calcd. for $C_{20}H_{49}Cl_4Fe_4N_3S_3$: C, 30.29; H, 6.23; N, 5.30. Found: C, 30.11; H, 6.19; N, 5.06.

$(Et_4N)_2[Fe_4(\mu_3\text{-}N^tBu)(\mu_3\text{-}Se)_3Cl_4]$ (45). To a solution of $(Et_4N)_2[Fe_4(\mu_3\text{-}Se)_4Cl_4]$ (0.412 g, 0.4 mmol) in CH_3CN (30 mL) was added $Fe_2(\mu\text{-}NH^tBu)_2(\mu\text{-}Se)[N(SiMe_3)_2]_2$ (0.273 g, 0.4 mmol) in THF (30 mL). The reaction mixture was stirred for 8 hours, and filtered through celite to remove a black precipitate. The black solution was then taken to dryness under vacuum, affording a black solid, which was treated by CH_2Cl_2 (20 mL) wash 4 to 5 times, to give a black microcrystalline solid. Recrystallization from CH_3CN/Et_2O generated 0.108 g (22 %) product as black plate-like crystals. Anal. Calcd. for $C_{20}H_{49}Cl_4Fe_4N_3S_3$: C, 30.29; H, 6.23; N, 5.30. Found: C, 30.11; H, 6.19; N, 5.06.

$(Et_4N)_2[Fe_4(\mu_3\text{-}N^tBu)_2(\mu_3\text{-}S)_2(SPh)_4]$ (43a). NaSPh (0.060 g, 0.6 mmol) was added to a solution of $(Et_4N)_2[Fe_4(\mu_3\text{-}N^tBu)_2(\mu_3\text{-}S)_2Cl_4]$ (0.141 g, 0.15 mmol) in CH_3CN (20 mL). The reaction mixture was stirred for 3 hours, and filtered through celite to remove precipitate. The black solution was then volume reduced to 10 mL and Et_2O introduced by vapor diffusion at –30 ºC for 2 d to give 0.112 g black crystals (76 %).

2.4.3 Electrochemical Analysis

Cyclic voltammograms were measured on Biologic SP-150 using platinum as working and counter electrodes, and a nonaqueous $Ag/AgNO_3$ (0.01 M) reference electrode. Measurements for compounds **42**, **43**, **44** were performed using a standard three-electrode cell and 0.1 M $(n\text{-}Bu_4N)(ClO_4)$

(TBAP) supporting electrolyte in MeCN (storage over activated alumina). Potentials were referenced internally to the ferrocene/ferrocenium ($Fc^{0/+}$) couple, then converted to the SCE scale ($Fc^{+/0}$ = +0.38 V vs SCE in 0.1 M TBAP/MeCN).[85]

2.4.4 X-Ray Crystallography

Crystals suitable for X-ray diffraction experiments were mounted on a glass fiber using Apiezon-M grease. Apiezon-M grease was pumped overnight and stored in the glovebox before use. Data were collected with graphite-monochromatized Mo Kα radiation (λ = 0.71 Å) on a Bruker APEX II diffractometer equipped with an MSC X- stream cryosystem at 200 K. Structures were solved by using SHELX-97.[86] Crystallographic data for products described in this chapter are summarized in Tables 2.11 and 2.12, respectively.

2.4.5 NMR and UV-Vis Spectroscopy

^{1}H NMR spectra were performed on Bruker 300 MHz spectrometers, with chemical shifts referenced to residual protiosolvent signals; UV-Vis spectra were recorded on a Varian Cary 5000 spectrophotometer; for clusters **42**, **43**, **44** and **45** concentrated solutions (MeCN) and 0.1 mm pathlength cells were used to minimize decomposition.

Table 2.11. Crystallographic data for clusters **42**, **43**, and **44**.

	Cluster 42	**Cluster 43**	**Cluster 44**
formula	$C_{20}H_{47}Fe_4N_4SCl_4$	$C_{24}H_{58}Fe_4N_4S_2Cl_4$	$C_{22}H_{52}Fe_4N_4S_3Cl_4$
fw	740.88	832.06	834.06
space group	*C*2/*c*	$P2_1/c$	$Pca2_1$
Z	8	4	4
a, Å	23.4155(10)	17.8185(12)	26.4805(11)
b, Å	20.7305(9)	11.3121(7)	10.7835(4)
c, Å	17.8411(13)	22.1301(14)	12.7847(5)
α, deg	90.00	90.00	90
β, deg	130.1660(10)	108.7950(10)	90
γ, deg	90.00	90.00	90
V, (Å^3)	6618.0(6)	4222.8(5)	3650.7(2)
ρ_{calc}, g/cm^3	1.487	1.309	1.517
θ_{max}, deg	30.39	22.83	28.68
total data, %	99.4	99.9	99.7
μ, mm^{-1}	2.120	1.717	2.041
R_1 (wR_2), %	3.30 (7.22)	4.98 (10.2)	3.79 (8.05)
S	1.023	0.978	1.072

Table 2.12. Crystallographic data for clusters **43a** and **45**.

	Cluster 43a	**Cluster 45**
formula	$C_{48}H_{78}Fe_4N_4S_6$	$C_{20}H_{49}Fe_4N_3Se_3Cl_4$
Fw	1126.90	933.70
space group	*Pca2*$_1$	*P*2$_1$2$_1$2$_1$
Z	4	4
a, Å	16.3518(7)	11.5384(12)
b, Å	17.5883(8)	14.1705(15)
c, Å	19.4253(9)	21.395(2)
α, deg	100.0540(10)	90
β, deg	94.3210(10)	90
γ, deg	90.5680(10)	90
V, (Å^3)	5483.8(4)	3498.3(6)
ρ_{calc}, g/cm^3	1.365	1.773
θ_{max}, deg	25.00	21.15
total data, %	99.8	99.8
μ, mm^{-1}	1.301	5.068
R_1 (wR_2), %	4.16 (5.89)	3.36 (6.86)
S	1.002	0.986

CHAPTER 3. DINUCLEAR IRON-AMIDE CLUSTERS

3.1 Introduction

Compounds $Fe_2(\mu\text{-}NH^tBu)_2[N(SiMe_3)_2]_2$ (**46**) and $Fe_2(\mu\text{-}NH^tBu)_2(\mu\text{-}S)[N(SiMe_3)_2]_2$ (**47**) are two unique dinuclear iron-amide clusters, which are also important synthetic precursors for $[Fe_4(N^tBu)_n(S)_{4-n}Cl_4]^z$ cubane complexes. The preparations of **46** and **47** have previously been reported by Duncan in the Lee lab, and here we investigate their properties in more detail. A number of relevant compounds will also be explored.

Cluster **46** contains three-coordinate trigonal planar iron centers, which can be found in a number of known compounds, and such complexes can be classified into three categories: (i) mononuclear; (ii) dinuclear; and (iii) trinuclear. In general, sterically hindered ligands have been employed to stabilize the coordinatively unsaturated mononuclear iron centers; such compounds $[FeCl\{Si(SiMe_3)_3\}_2]^-$, $Fe\{N(SiMe_3)_2\}_3$, and $[Fe\{N(SiMe_3)_2\}_2(THF)]$ are presented in Figure 3.1.[87, 88]

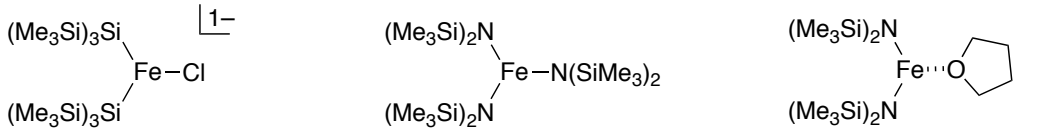

[FeCl{Si(SiMe$_3$)$_3$}$_2$]$^-$ **Fe{N(SiMe$_3$)$_2$}$_3$** **[Fe{N(SiMe$_3$)$_2$}$_2$(THF)]**

Figure 3.1. Mononuclear compounds with three-coordinate iron centers

Compared with mononuclear species, dinuclear trigonal planar species are more limited. Several examples[89-92] are presented in Figure 3.2 and can be divided into two classes: (i) homoleptic; and (ii) heteroleptic. A variety of ligand types have been found in the homoleptic dimers, such as amide in $[Fe_2(\mu\text{-}N(SiMe_3)_2)_2(N(SiMe_3)_2)_2]$ or $[Fe_2(\mu\text{-}NPh_2)_2(NPh_2)_2]$, selenolate in

$[Fe_2(\mu\text{-}Se(C_6H_2\text{-}2,4,6\text{-}Ph_3))_2(Se(C_6H_2\text{-}2,4,6\text{-}Ph_3))_2]$, boryloxide in $[Fe_2(\mu\text{-}OBMes_2)_2(OBMes_2)_2]$, and thiolate in $[Fe_2(\mu\text{-}S(2,4,6\text{-}{}^tBu_3C_6H_2))_2(S(2,4,6\text{-}{}^tBu_3C_6H_2))_2]$. Dimers in the heteroleptic class usually contain bis(trimethylsilyl)amide terminal ligands and different bridging ligands, such as phosphide in $[Fe_2(\mu\text{-}PMes_2)_2(N(SiMe_3)_2)_2]$, aryloxide in $[Fe_2(\mu\text{-}O(2,4,6\text{-}{}^tBu_3C_6H_2)_2(N(SiMe_3)_2)_2]$, and selenolate in $[Fe_2(\mu\text{-}Se(C_6H_2\text{-}2,4,6\text{-}Ph_3))_2(N(SiMe_3)_2)_2]$. Clusters $[Fe_2(\mu\text{-}N(SiMe_3)_2)_2(N(SiMe_3)_2)_2]$ and $[Fe_2(\mu\text{-}NPh_2)_2(NPh_2)_2]$ are constructed from Fe(II) centers and terminal and bridging amides and are more relevant to the compounds discussed in this chapter, although they contain homoleptic cores.

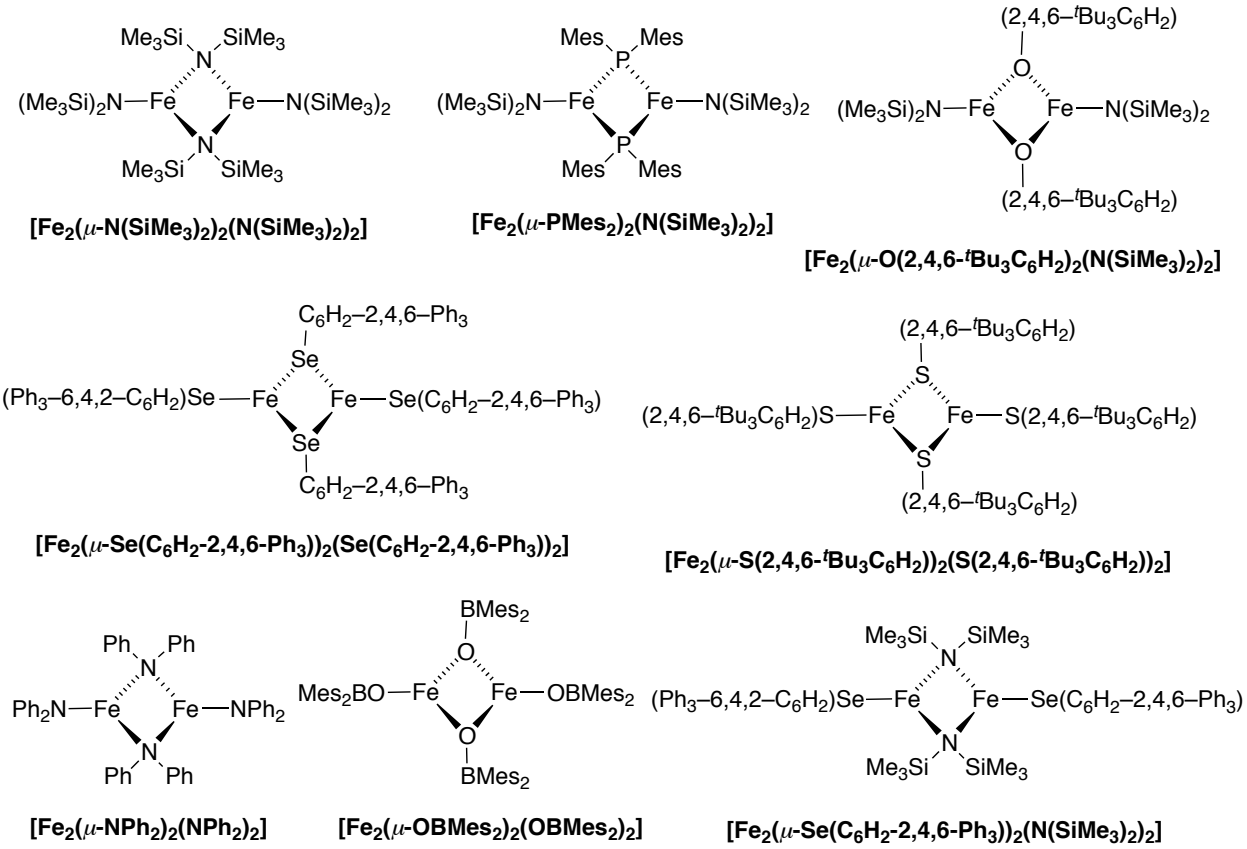

$[Fe_2(\mu\text{-}N(SiMe_3)_2)_2(N(SiMe_3)_2)_2]$ **$[Fe_2(\mu\text{-}PMes_2)_2(N(SiMe_3)_2)_2]$**

$[Fe_2(\mu\text{-}O(2,4,6\text{-}{}^tBu_3C_6H_2)_2(N(SiMe_3)_2)_2]$

$[Fe_2(\mu\text{-}Se(C_6H_2\text{-}2,4,6\text{-}Ph_3))_2(Se(C_6H_2\text{-}2,4,6\text{-}Ph_3))_2]$

$[Fe_2(\mu\text{-}S(2,4,6\text{-}{}^tBu_3C_6H_2))_2(S(2,4,6\text{-}{}^tBu_3C_6H_2))_2]$

$[Fe_2(\mu\text{-}NPh_2)_2(NPh_2)_2]$ **$[Fe_2(\mu\text{-}OBMes_2)_2(OBMes_2)_2]$** **$[Fe_2(\mu\text{-}Se(C_6H_2\text{-}2,4,6\text{-}Ph_3))_2(N(SiMe_3)_2)_2]$**

Figure 3.2. Dinuclear compounds with three-coordinate iron centers

The last category that contains three-coordinate iron centers is trinuclear complexes, which are constructed of two trigonal planar iron centers edge-fused to a central tetrahedral iron. These compounds

are rare and only three examples exist in the literature (Figure 3.3).[59, 93-97] $[Fe_3(\mu\text{-}N^tBu)_4(N(SiMe_3)_2)_2]$, $[Fe_3(\mu\text{-}OSi_2Me_5)_4(N(SiMe_3)_2)_2]$, and $[Fe_3(\mu\text{-}S(C_6H_2\text{-}2,4,6\text{-}i\text{Pr}_3))_4(N(SiMe_3)_2)_2]$ are all terminally ligated by bis(trimethylsilyl)amide, and bridged by imide, siloxide or thiolate respectively. The iron centers in these clusters with this special geometry can also be extended to other transition metals, such as manganese in $[Mn_3(\mu\text{-}NH(C_6H_3\text{-}2,6\text{-}i\text{Pr}_2))_4(N(SiMe_3)_2)_2]$, zinc in $[Zn_3(\mu\text{-}OSi_2Me_5)_4(N(SiMe_3)_2)_2]$ and nickel in $[Ni_3(\mu\text{-}O(C_6H_3\text{-}2,6\text{-}i\text{Pr}_2))_4(O(C_6H_3\text{-}2,6\text{-}i\text{Pr}_2))_2]$.

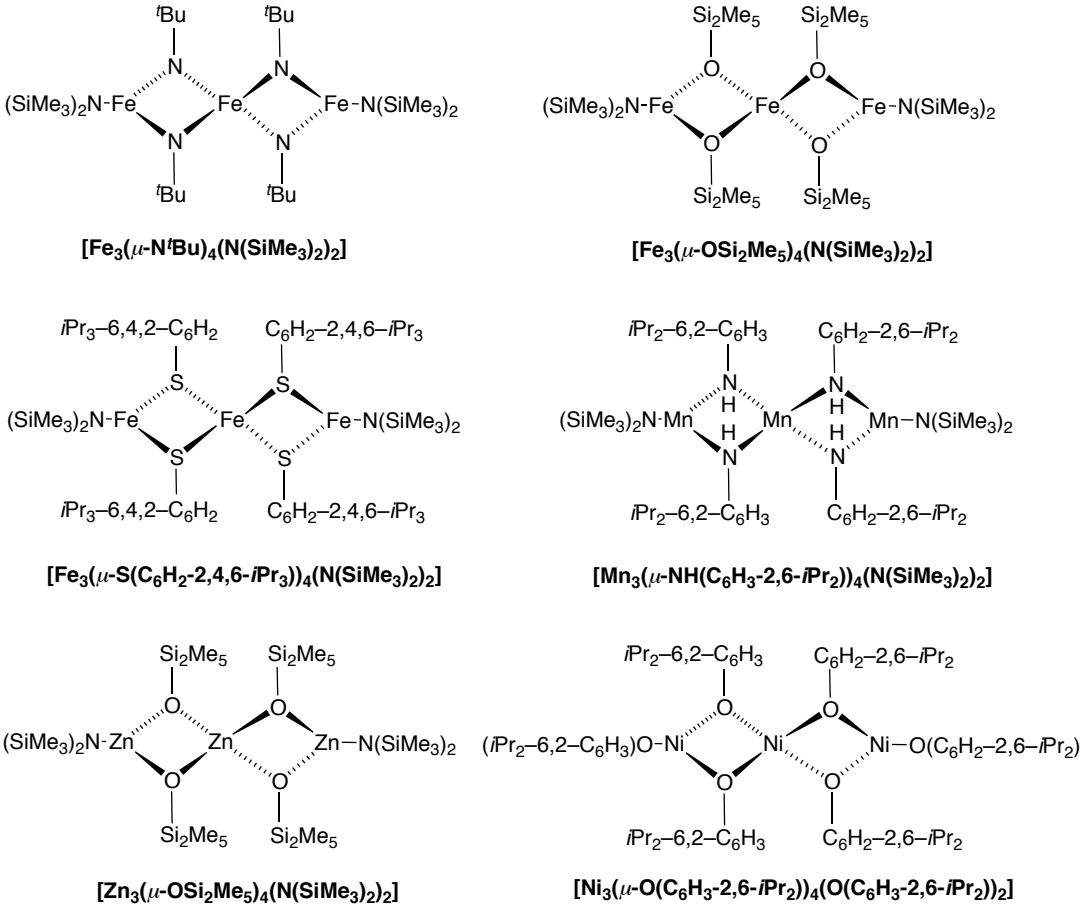

Figure 3.3. Trinuclear compounds with three-coordinate iron centers

Another structurally unusual compound is cluster **47**, which contains a confacial bitetrahedral geometry that has only been observed in several examples of late-transition-metal d^{8-10} systems. All the

known synthetic dinuclear confacial bitetrahedral complexes are presented in Figure. 3.4.[98-102]

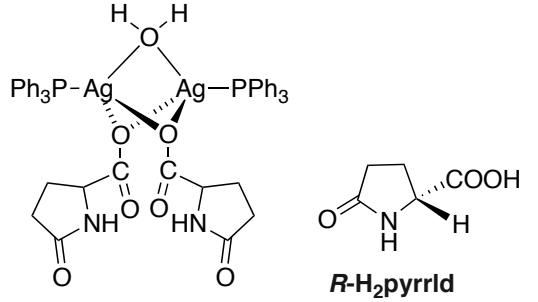

***R*-H_2pyrrld**

Ag_2(*R*-Hpyrrld)$_2$(H_2O)(PPh_3)$_2$

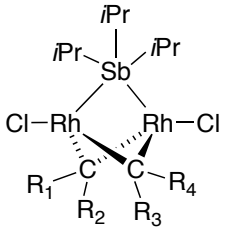

R_1	R_2	R_3	R_4
Ph	Ph	Ph	Ph
p-Tol	*p*-Tol	*p*-Tol	*p*-Tol
p-Tol	Ph	*p*-Tol	Ph
Ph	Ph	Ph	*p*-Tol
Ph	Ph	*p*-Tol	*p*-Tol

Rh_2Cl_2(μ-CR_1R_2)(μ-CR_3R_4)(μ-Sb*i*Pr$_3$)

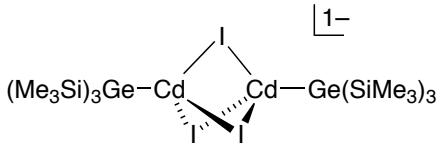

[Cd_2(μ-I)$_3$[Ge(SiMe$_3$)$_3$]$_2$]$^-$

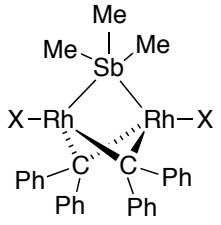

X = Br, I

Rh_2X_2(μ-CPh_2)$_2$(μ-$SbMe_3$)

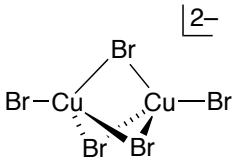

[Cu_2Br_5]$^{2-}$

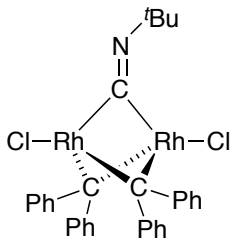

Rh_2Cl_2(μ-CPh_2)$_2$(μ-CN^{t}Bu)

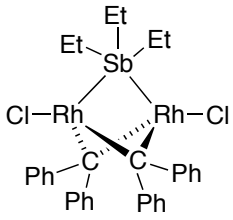

Rh_2Cl_2(μ-CPh_2)$_2$(μ-$SbEt_3$)

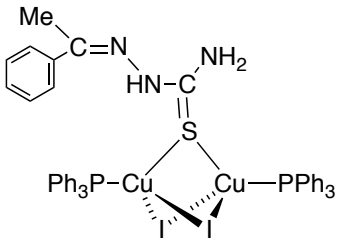

Cu_2(μ-I)$_2$(μ-S-Haptsc)(PPh_3)$_2$

Figure 3.4. Synthetic dinuclear confacial bitetrahedral complexes

The structure of the dinuclear complex [Ag_2(*R*-Hpyrrld)$_2$(H_2O)(PPh_3)$_2$] is constructed of two Ag(I) centers, two PPh_3 terminal ligands, two bridging Hpyrrld$^-$ ligands and one bridging water molecule. A series of clusters Rh_2Cl_2(μ-CR_1R_2)(μ-CR_3R_4)(μ-Sb*i*Pr$_3$) is made from a mononuclear precursor *trans*-[RhCl(C_2H_4)(Sb*i*Pr$_3$)$_2$]. Treatment of cluster Rh_2Cl_2(μ-CPh_2)$_2$(μ-Sb*i*Pr$_3$) with one equivalent of CN^{t}Bu yields the isocyanide complex Rh_2Cl_2(μ-CPh_2)$_2$(μ-CN^{t}Bu). The Sb*i*Pr$_3$ ligand of Rh_2Cl_2(μ-CPh_2)$_2$(μ-Sb*i*Pr$_3$)

can also be replaced by $SbMe_3$ or $SbEt_3$ to give the dinuclear complexes $Rh_2Cl_2(\mu\text{-}CPh_2)_2(\mu\text{-}SbMe_3)$ and $Rh_2Cl_2(\mu\text{-}CPh_2)_2(\mu\text{-}SbEt_3)$. $Cu_2(\mu\text{-}I)_2(\mu\text{-}S\text{-}Haptsc)(Ph_3P)_2$ is another triple heterobridging complex, in which two iodine atoms and one sulfur atom of the thiosemicarbazone ligand bridge two copper atoms, and each copper atom is terminally ligated by the phosphorus atom from PPh_3. The $[Cd_2(\mu\text{-}I)_3[Ge(SiMe_3)_3]_2]^-$ core consists of two tetrahedrally coordinated cadmium atoms with three iodine atoms in trigonal bridging positions and two germanium atoms in terminal positions. The last confacial bitetrahedral core $[Cu_2Br_5]^{2-}$ contains the delocalized $(Cu^{1.5+})_2$ pair and is made by the reduction of $CuBr_2$.

3.2 Results and Discussion

The preparation of iron-amide complexes started from a ferrous compound, $Fe[N(SiMe_3)_2]_2$ (**23**). Compound **23** reacted with aryl- or alkylamines to form heteroleptic dimers or trimers. The oxidation states of iron atoms in these dimers are 2Fe(II), thus they may further react with some oxidants, such as elemental sulfur, selenium and iodine. These reactions formed sulfido-bridged, selenido-bridged and iodo-bridged dimers that contain mixed iron-amide-sulfide/selenide/iodide cores. The reaction routes are summarized in Scheme 3.1 and the results of this study are presented here.

Scheme 3.1. Reaction scheme for the preparation of iron-amide clusters

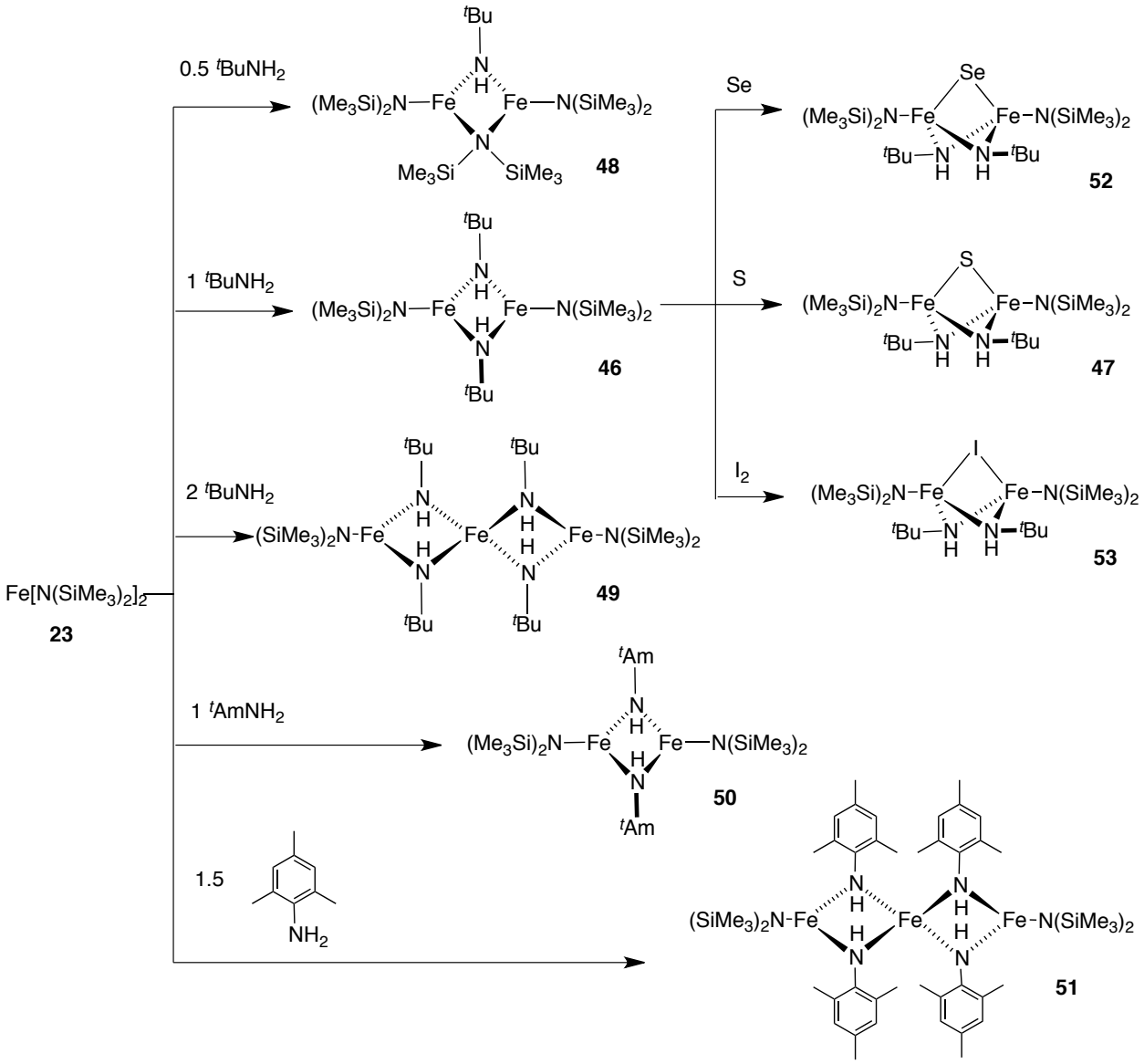

3.2.1 Protonolysis by *tert*-Butylamine

$Fe[N(SiMe_3)_2]_2$ (**23**) was originally prepared by a direct ligand exchange of $FeCl_2$ and $Li[N(SiMe_3)_2]$ in Et_2O. The reasons for using **23** as the precursor are as follows: (i) $[N(SiMe_3)_2]^-$ is a sterically-hindered ligand that may allow greater control over the coordination environment of the metal center. (ii) $[N(SiMe_3)_2]^-$ can be easily replaced by other ligands via protonolysis. Compound **23** is a

mononuclear cluster in solution at ambient temperature, as proven by molecular weight determination and further supported by variable-temperature ^{1}H NMR investigations. However, the X-ray crystallographic studies revealed **23** contains a dinuclear structure with two bridging and two terminal amide groups in the solid state, which can be explained by the equilibrium, 2 $Fe[N(SiMe_3)_2]_2 \rightleftharpoons [Fe[N(SiMe_3)_2]_2]_2$.[103] Compound **23** dissolves in C_6H_6 to give a green solution, that reacts with 1 equivalent of ^{t}BuNH$_2$ with lightening of the solution color to yield a neutral ferrous heteroleptic dimer $Fe_2(\mu\text{-}NH^tBu)_2[N(SiMe_3)_2]_2$ (**46**) in quantitative conversion. This reaction is achieved by substitution of the $[N(SiMe_3)_2]^-$ with NH^tBu^- ligand. Although there is a markedly unfavorable *pKa* difference between ^{t}BuNH$_2$ and $(Me_3Si)_2NH$,[104] proton transfer still occurs during the preparation of cluster **46**. We believe that this transformation is driven by additional stabilization associated with the *tert*-butylamide bridging ligands. This reaction needs to be heated overnight to finish the ligand substitution at reasonable rates. A time course reaction study has been performed to monitor cluster formation by ^{1}H NMR spectroscopy, which is shown in Figure 3.5. The reaction of 1 equivalent of ^{t}BuNH$_2$ with compound **23** was performed in C_6D_6 and heated at 45 ºC. At first, we observed five independent paramagnetic signals that, after time, the five signals diminished, with development of two new signals assignable to compound **46** (^{t}Bu: 18H, $SiMe_3$: 36H).

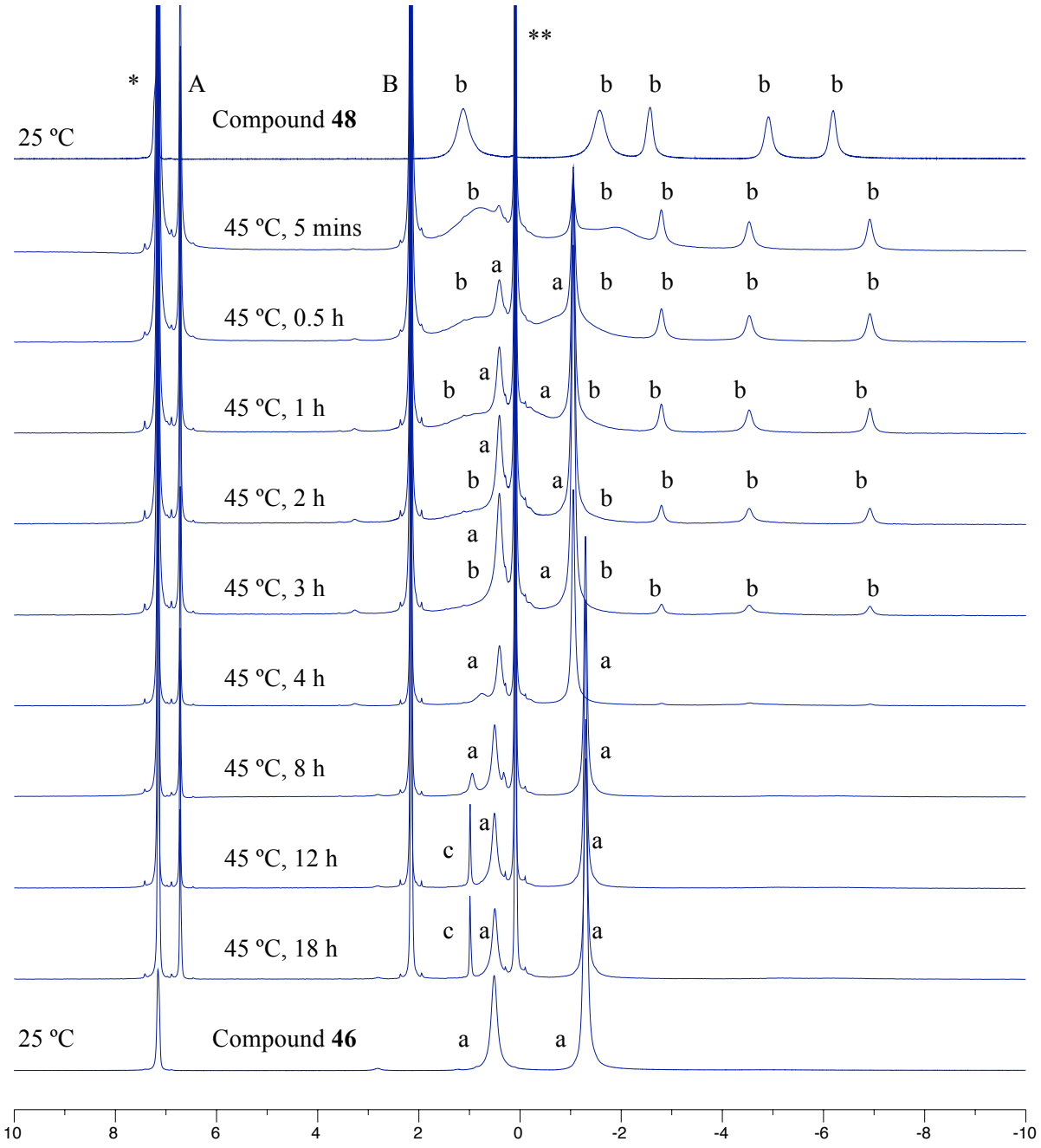

Figure 3.5. ^{1}H NMR spectra (300 MHz) monitoring cluster formation of **46** at 45 ºC. Residual protio signal of C_6D_6 is marked by *; HMDSA is marked by **, internal calibrant mesitylene is marked by A and B; compound **46** is marked by (a); compound **48** is marked by (b) and slightly excess $^{t}BuNH_2$ is marked by c.

In order to identify and isolate this reaction intermediate, the addition of 0.5 equivalent of $^{t}BuNH_2$ to compound **23** was tested under the same reaction conditions as the synthesis of **46**. We found that only one of the two bridging amide ligands was replaced by the $NH^{t}Bu^{-}$ group, and a new mono-substituted complex $Fe_2(\mu\text{-}NH^{t}Bu)[\mu\text{-}N(SiMe_3)_2][N(SiMe_3)_2]_2$ (**48**, Figure 3.6) was synthesized. The ^{1}H NMR spectrum of **48**, which is shown in Figure 3.5 and summarized in Table 3.1, corresponds to the spectra of the intermediate shown in the 1:1 reaction of **23** and $^{t}BuNH_2$. The reaction of **23** and 0.5 equivalent of $^{t}BuNH_2$ is stoichiometrically correct for the generation of cluster **48**, which is proposed in Equation 3.1.

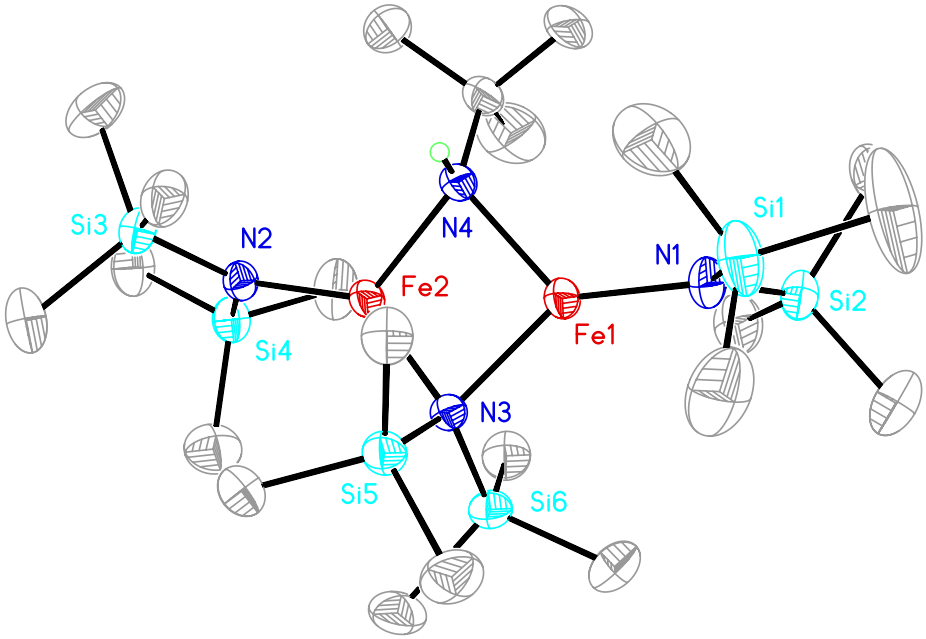

Figure 3.6. Structure of $Fe_2(\mu\text{-}NH^{t}Bu)[\mu\text{-}N(SiMe_3)_2][N(SiMe_3)_2]_2$ (**48**) with thermal ellipsoids (50% probability level) and selected atom labels. Non-amido hydrogen atoms are omitted. The *tert*-butyl group is disordered, and only the major component is shown.

$$2\ Fe(N\{SiMe_3\}_2)_2 + {}^{t}BuNH_2 \longrightarrow Fe_2(NH^{t}Bu)(N\{SiMe_3\}_2)_3 + HN(SiMe_3)_2 \qquad \text{(eq 3.1)}$$

Table 3.1. ^{1}H NMR spectroscopic data for clusters **48**

Compound	^{1}H NMR (C_6D_6, δ ppm)
48	1.08 (18 br), -1.62 (18 br), -2.59 (9 br), -4.96 (9 br), -6.19 (9 br)

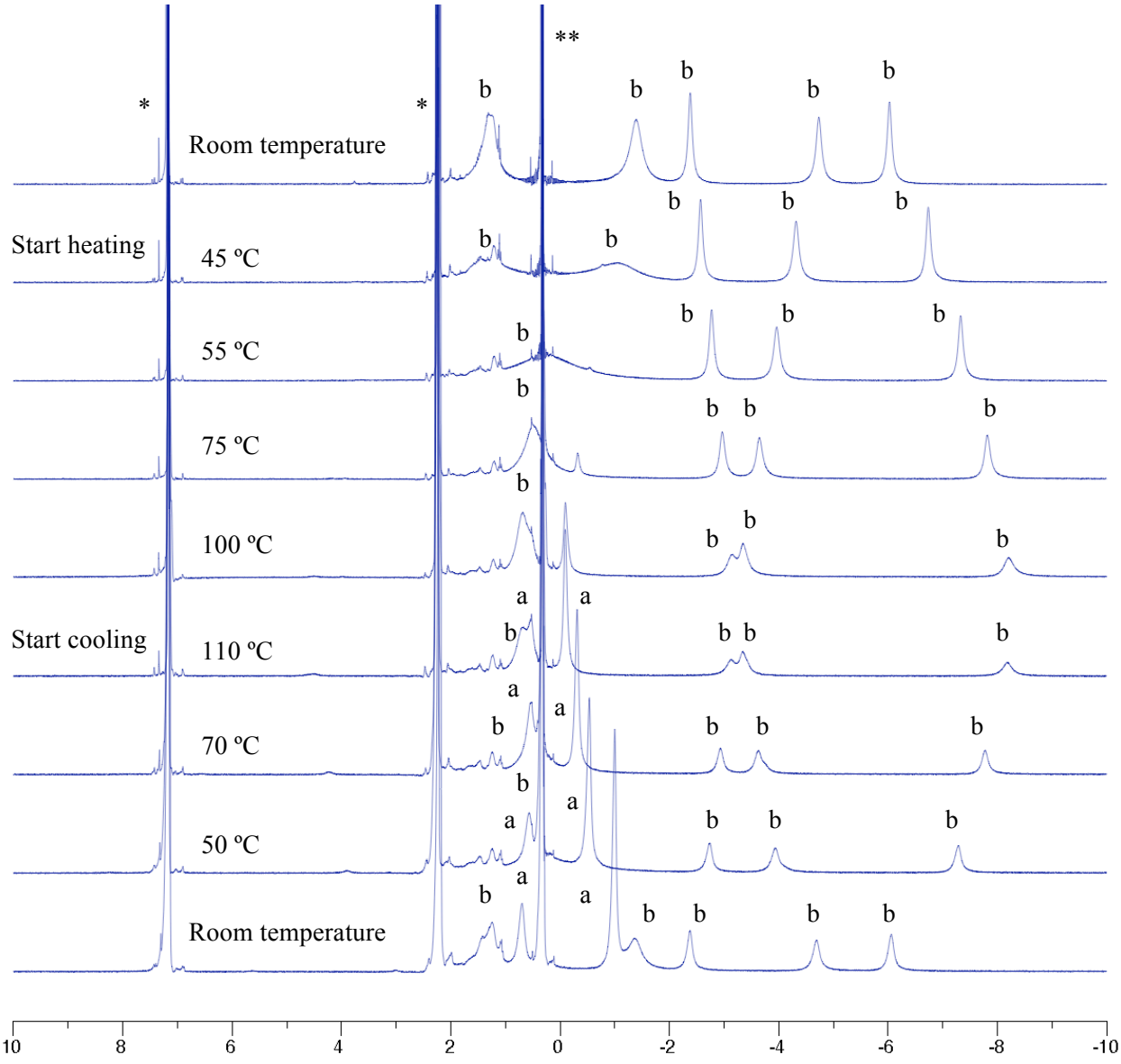

Figure 3.7. ^{1}H NMR spectra (300 MHz) monitoring ligand rotation in compound **48** at different temperatures. Residual protio signals of deuterated *o*-xylene are marked by *; internal calibrant HMDSO is marked by **; compound **46** is marked by (a); and compound **48** is marked by (b).

The structure shown in Figure 3.6 is consistent with the solution ^{1}H NMR spectrum assuming hindered rotation of terminal amides leading to four different chemical environments for the trimethylsilyl groups. To further study this compound, the temperature-dependent ^{1}H NMR spectra were investigated. The **48** was dissolved in deuterated *o*-xylene and the solution was heated to 110 ºC, ^{1}H NMR spectra indicated that two left signals started to become broad and coalesced at 55 ºC, with the chemical shifts of the three other signals changing positions upon heating. When the temperature was raised to 75 ºC after heating for 3 hours, complexes $Fe[N(SiMe_3)_2]_2$ (**23**) (the chemical shift of **23** is at 65ppm, and is not shown in the spectra for clarity) and $Fe_2(\mu\text{-}NH^tBu)_2[N(SiMe_3)_2]_2$ (**46**) were detected in the spectra. We believe that cluster **48** was unstable and disproportionated at a high temperature, and the proposed balanced reaction is shown is Equation 3.2.

$$2\ Fe_2(NH^tBu)(N\{SiMe_3\}_2)_3 \longrightarrow 2\ Fe(N\{SiMe_3\}_2)_2 + Fe_2(NH^tBu)_2(N\{SiMe_3\}_2)_2 \quad \text{(eq 3.2)}$$

We already found that 0.5 equivalent and 1 equivalent of ^{t}BuNH$_2$ reacted with compound **23** to give cluster **42** and cluster **41** in C_6H_6 respectively. The addition of 2 equivalents of ^{t}BuNH$_2$ to **23** in THF results in a product mixture outcome compared to the C_6H_6 reaction systems. The crude product mixture can be separated by recrystallization using *n*-pentane/HMDSO vapor diffusion. The first fraction crystallized out of the solution was $Fe_3(\mu\text{-}NH^tBu)_4[N(SiMe_3)_2]_2$ (**49**, Figure 3.8), which is a trinuclear array of two trigonal planar iron centers and one tetrahedral iron center with *tert*-butylamide bridges and terminal trimethylsilylamide ligands. Complex **46** was found as the co-product of this reaction. Although the full mass balance for the synthesis of cluster **49** is still unknown, we believe the excess ^{t}BuNH$_2$ and coordination solvent THF are critical for this reaction. In the X-ray crystal structure of **49**, although all the bridging *tert*-butyl groups are *trans*-disposed in the local $[Fe_2N_2]$ rhombic plane and the [Fe2Fe3] rhomb is in perfect order, there are two different NH^{t}Bu orientations associated with the [Fe1Fe2] rhomb. One

orientation consists of N3, N4, and their *tert*-butyl groups. These are disposed to form an approximately S_4 point group (methyl groups are ignored) for the overall molecular symmetry of the trimer (Figure 3.9a). Another position includes N3'H^{t}Bu, N4'H^{t}Bu, which orient themselves differently with N3H^{t}Bu and N4H^{t}Bu to form an approximately D_2 point group (methyl groups are ignored) (Figure 3.9b). It is notable that two different structures occupy the same position in the same lattice.

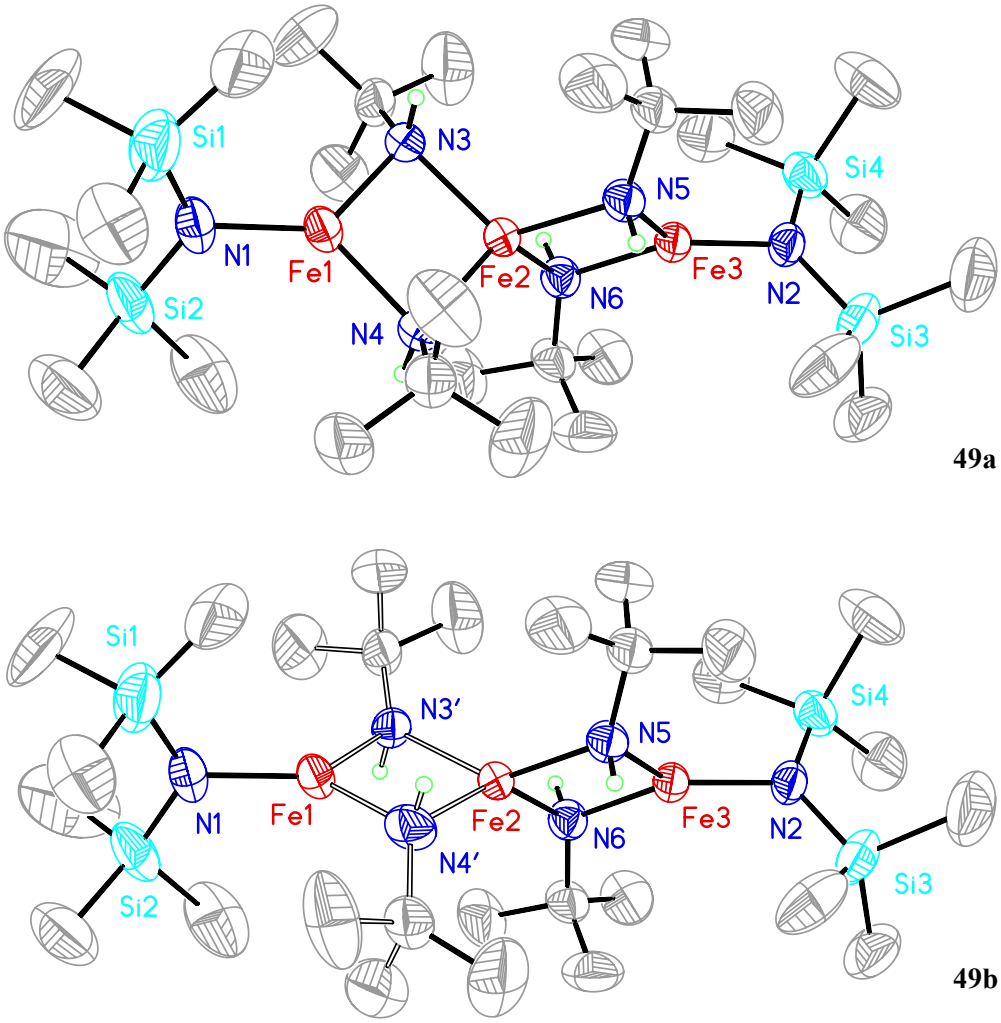

Figure 3.8. Two structures of $Fe_3(\mu\text{-}NH^tBu)_4[N(SiMe_3)_2]_2$ (**49a, 49b)** with thermal ellipsoids (50% probability level) and selected atom labels. Non-amido hydrogen atoms are omitted.

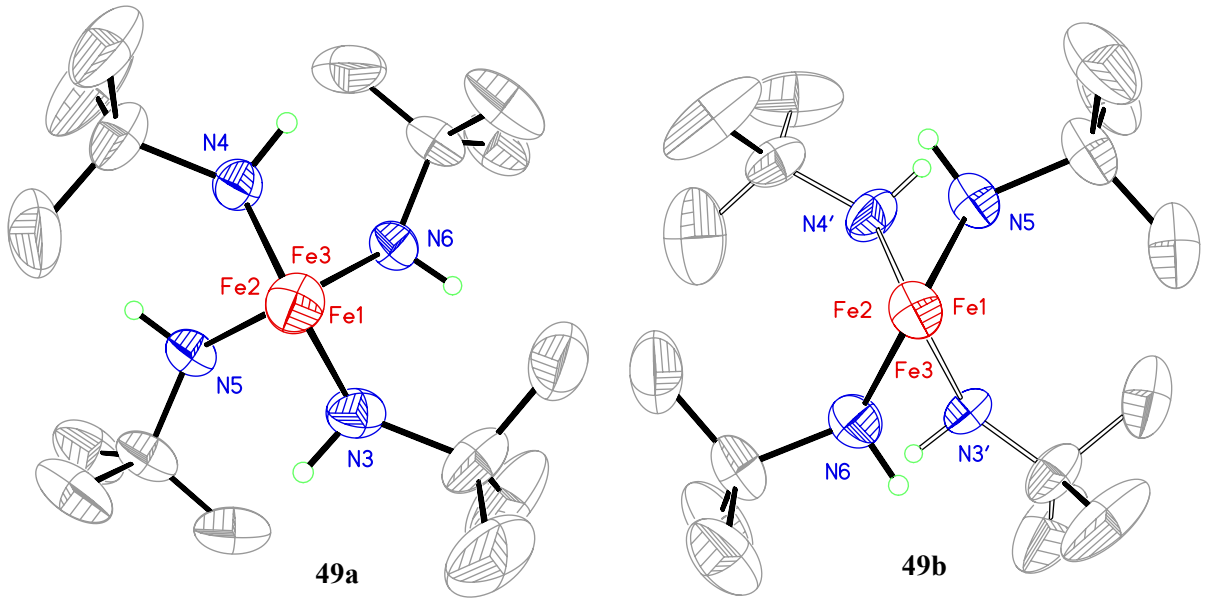

Figure 3.9. Two structures of $Fe_3(\mu\text{-}NH^tBu)_4[N(SiMe_3)_2]_2$ (**49a 49b**) with thermal ellipsoids (50% probability level) and selected atom labels. Non-amido hydrogen atoms are omitted. These two structures are viewed through Fe1-Fe2-Fe3 axis and terminal amides are not shown for clarity.

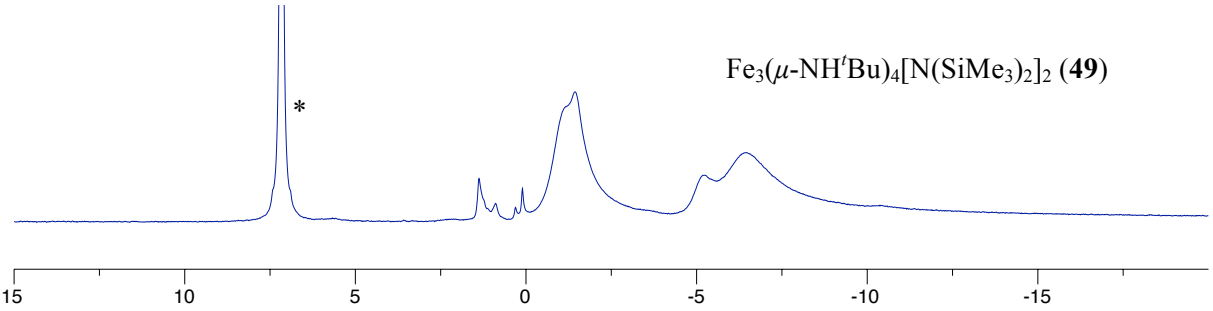

Figure 3.10. ^1H NMR spectra (300 MHz) of clusters **49**. Residual protio signal of C_6D_6 is marked by *.

The ^1H NMR spectrum of cluster **49** is shown in Figure 3.10. Superposition of the two different structures in **49** made this spectrum too complicated to interpret. However, temperature-dependent NMR spectroscopy is proposed to assign each chemical shift and such research is still under investigation.

Several ^{1}H NMR scale experiments have been performed to examine the cluster reactivity and formation of compounds $Fe_2(\mu\text{-}NH^tBu)_2[N(SiMe_3)_2]_2$ (**46**), $Fe_2(\mu\text{-}NH^tBu)[\mu\text{-}N(SiMe_3)_2][N(SiMe_3)_2]_2$ (**48**) and $Fe_3(\mu\text{-}NH^tBu)_4[N(SiMe_3)_2]_2$ (**49**). The following observations are noted:

(i) ^{1}H NMR scale reactions showed that the cluster **48** reacted with 0.5 equivalent of ^{t}BuNH$_2$ at room temperature to yield complex **46** cleanly.

(ii) **46** did not react with ^{t}BuNH$_2$ in C_6H_6 to form **49** at either room temperature or 55 ° C.

(iii) $Fe[N(SiMe_3)_2]_2$ (**23**) reacted with 2 equivalents of ^{t}BuNH$_2$ in C_6H_6 at 55 ºC overnight only led to complex **46**, and there is no evidence for cluster **49**. Trinuclear cluster **49** was only generated in THF solution.

(iv) **23** does not react with complex **46** in C_6H_6 at 55 ºC as proposed in Equation 3.3. Instead, the reverse reaction has been found performed at 55 ºC (Equation 3.2).

$$Fe_2(N\{SiMe_3\}_2)_4 + Fe_2(NH^tBu)_2(N\{SiMe_3\}_2)_2 \not\rightarrow 2\ Fe_2(NH^tBu)(N\{SiMe_3\}_2)_3 \quad \text{(eq 3.3)}$$

It is concluded that cluster **46** is the most stable of these three iron *tert*-butylamide compounds. Once it is formed, it neither exchanges core ligands with $Fe[N(SiMe_3)_2]_2$, nor further reacts with ^{t}BuNH$_2$ to generate more complicated clusters. Also, the coordinating solvent plays an important role in the preparation of trimer **49**, which is generated by a pathway different from the synthesis of dimer **46**, and cluster **46** is not a reaction intermediate to compound **49**.

3.2.2 Protonolysis by other Alkylamines

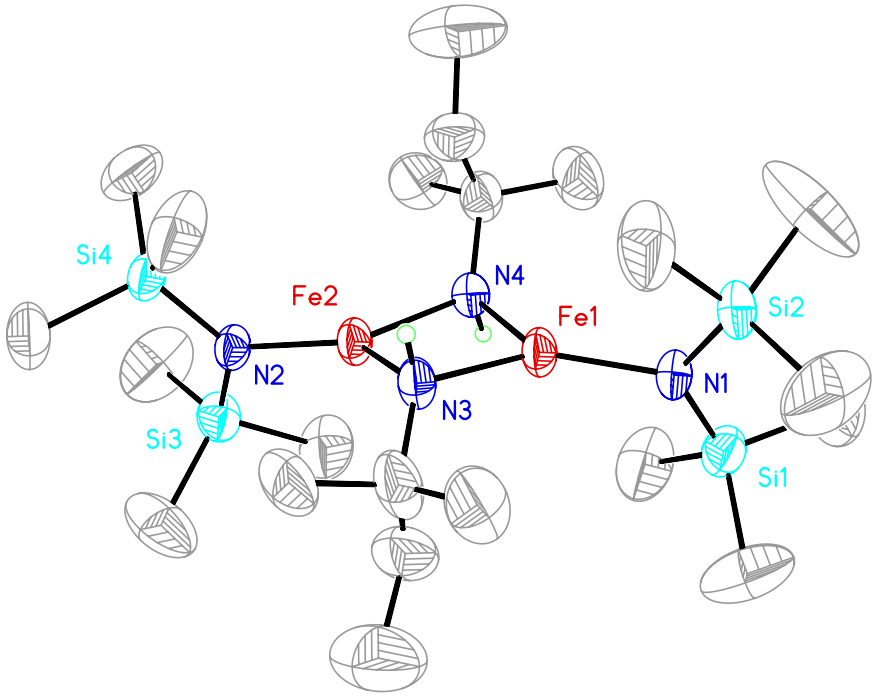

Figure 3.12. Structure of $Fe_2(\mu\text{-}NH^tAm)_2[N(SiMe_3)_2]_2$ (**50**) with thermal ellipsoids (50% probability level) and selected atom labels. Non-amido hydrogen atoms are omitted. *tert*-Amyl groups are disordered, and only the major component is shown.

$$2\ Fe(N\{SiMe_3\}_2)_2 + 2\ {}^tAmNH_2 \longrightarrow Fe_2(NH^tAm)_2(N\{SiMe_3\}_2)_2 + 2\ HN(SiMe_3)_2 \quad \text{(eq 3.4)}$$

tert-Amylamine is another alkylamine that has been reacted with compound **23**. When *tert*-amylamine is reacted with **23** in a 1:1 stoichiometry in C_6H_6, a lighter, transparent green solution formed, from which crystalline $Fe_2(\mu\text{-}NH^tAm)_2[N(SiMe_3)_2]_2$ (**50**, Figure 3.12) can be isolated in quantity. The hypothetical reaction stoichiometry is presented in Equation 3.4. The reaction conditions and chemistry for cluster formation of compound **50** is analogous to the preparation of complex **46** since *tert*-butylamine and *tert*-amylamine share similar structures and they are both primary amines with tertiary

substituted carbon attached to nitrogen. From our experience in amine protolysis, we found out that only primary amines with tertiary substituted carbon centers will lead to successful cluster formation. Other alkylamines with hydrogen at the α-carbon position, such as benzylamine and isopropylamine, reacted with compound **23** to give black solutions, instead of green. The products generated from these reactions are ^{1}H NMR silent and cannot be crystallized. To further analyze the amine protolysis process, gas chromatography will be used to identify the reaction mixture products and such protocols are still under investigation. The ^{1}H NMR spectrum of cluster **50** is shown in Figure 3.11 and summarized in Table 3.2.

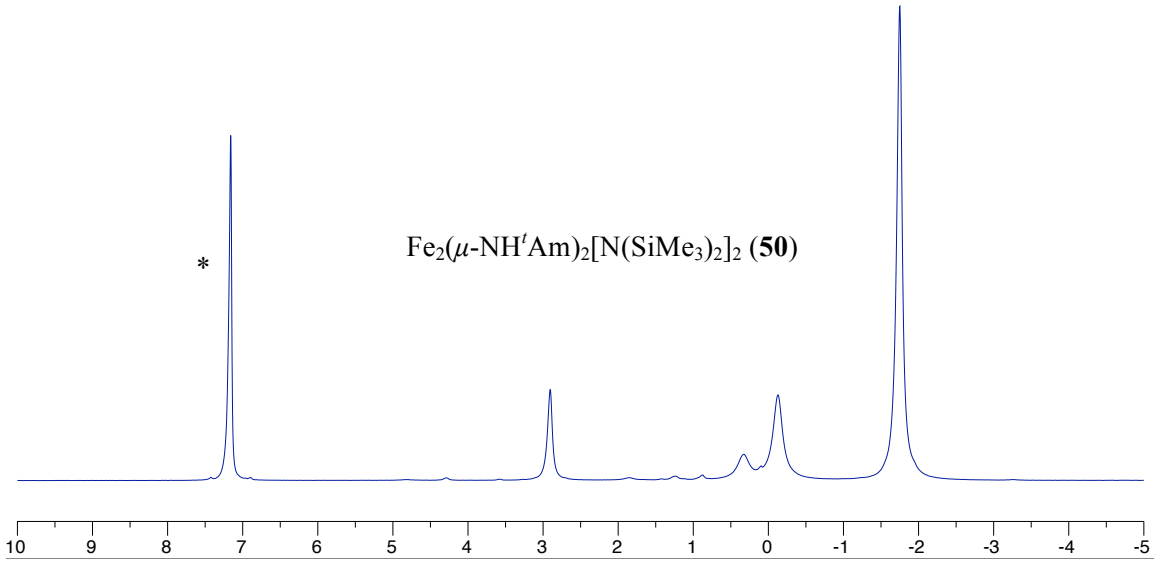

Figure 3.11. ^{1}H NMR spectra (300 MHz) of cluster **50**. Residual protio signal of C_6D_6 is marked by *.

Table 3.2. ^{1}H NMR spectroscopic data for cluster **50**.

Compound	^{1}H NMR (C_6D_6, δ ppm)
50	2.90 (6 br), 0.35 (4 br), -0.15 (12 br), -1.72 (36 br)

3.2.3 Protonolysis by Arylamine

The protolysis of complex **23** can also be extended to arylamines, such as 2,4,6-trimethylaniline. Compared with *tert*-butylamine, 2,4,6-trimethylaniline is more acidic. The cluster assembly process changed dramatically: (i) reaction times decreased (from hours to minutes); (ii) reaction was achieved at room temperature versus heating at 45 ºC. Compound **23** and 2,4,6-trimethylaniline were dissolved in C_6H_6 solvent separately, and the amine solution was added dropwisely into the **23** C_6H_6 solution. The green color of the solution immediately darkened, and the triiron mesitylamide cluster $Fe_3(\mu\text{-NHMes})_4[N(SiMe_3)_2]_2$ (**51**, Figure 3.13) was formed as the predominant product. Although the NMR spectrum of this reaction crude is contaminated by other minor components, **51** can be isolated as dark green crystalline material. In this reaction system, the diiron mesitylamide cluster does not appear to form even at the 1:1 ratio of compound **23** and 2,4,6-trimethylaniline as presented in Equation 3.5.

$$2\ Fe(N\{SiMe_3\}_2)_2 + 2\ MesNH_2 \not\rightarrow Fe_2(NHMes)_2(N\{SiMe_3\}_2)_2 + HN(SiMe_3)_2 \qquad \text{(eq 3.5)}$$

We believe that the strong acidity of the arylamine facilitated the further cluster aggregation. It is notable that compared with the two different structures in trinuclear cluster **49**, compound **51** exists only with one NHMes orientation, which is similar to cluster **49b** (Figure 3.14). Other arylamines, such as *p*-toluidine and aniline have been reacted with **23**, but both yielded black oily materials, which are ^{1}H NMR silent and cannot be crystallized as well-defined solid material, and further analyses are still under investigation. The ^{1}H NMR spectra of cluster **50** is shown in Figure 3.15; although it is relatively clean, the chemical shifts are still difficult to assign, and temperature-dependent NMR experiments are proposed to give a more defined spectrum.

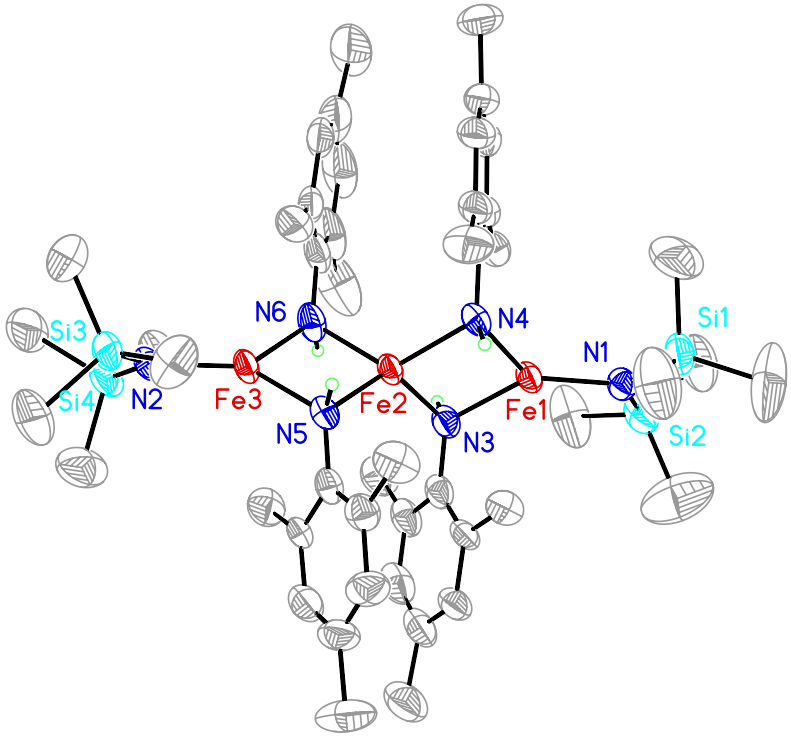

Figure 3.13. Structure of $Fe_3(\mu\text{-NHMes})_4[N(SiMe_3)_2]_2$ (**51**) with thermal ellipsoids (50% probability level) and selected atom labels. Non-amido hydrogen atoms are omitted.

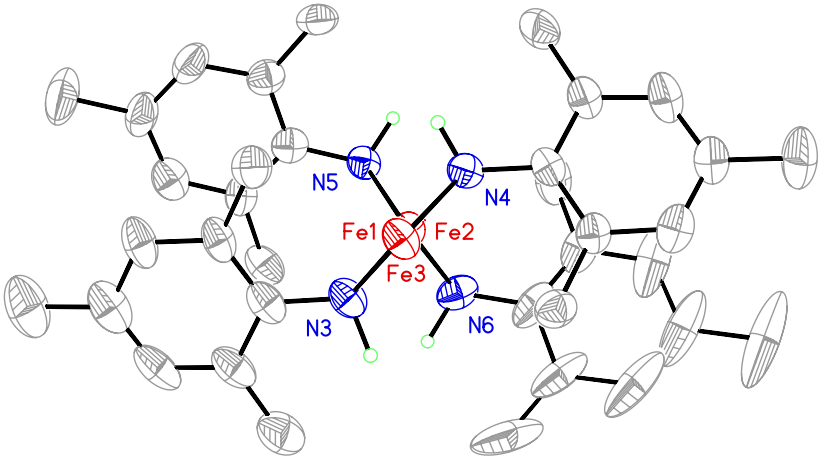

Figure 3.14. Structure of $Fe_3(\mu\text{-NHMes})_4[N(SiMe_3)_2]_2$ (**51**) with thermal ellipsoids (50% probability level) and selected atom labels. Non-amido hydrogen atoms are omitted. The structure is viewed through Fe1-Fe2-Fe3 axis and terminal amides are not shown for clarity.

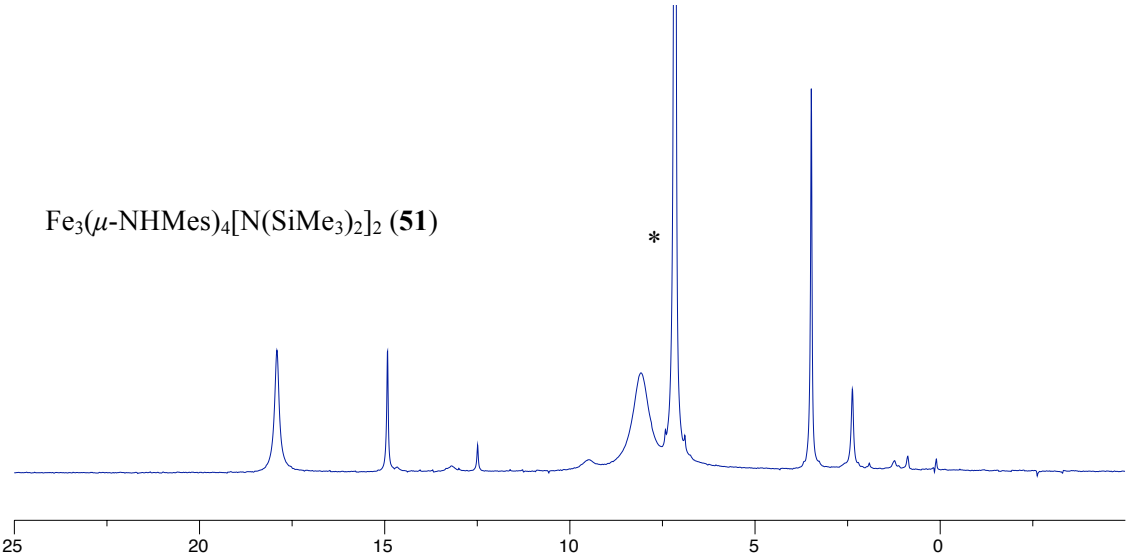

Figure 3.15. ^{1}H NMR spectra (300 MHz) of cluster **51**. Residual protio signal of C_6D_6 is marked by *.

3.2.4 Oxidative addition to $Fe_2(\mu\text{-}NH^tBu)_2[N(SiMe_3)_2]_2$ (46)

The addition of elemental sulfur to a green solution of **46** in C_6H_6 yielded the sulfido-bridged, all-ferric $Fe_2(\mu\text{-}NH^tBu)_2(\mu\text{-}S)[N(SiMe_3)_2]_2$ (**47**), which is also the precursor for clusters $[Et_4N]_2[Fe_4(\mu_3\text{-}N^tBu)_2(\mu_3\text{-}S)_2Cl_4]$ and $[Et_4N]_2[Fe_4(\mu_3\text{-}N^tBu)(\mu_3\text{-}S)_3Cl_4]$ in chapter 2; **47** is formed quantitatively in solution, but its crystalline form can only be isolated in ca. 40% yield, due to the high solubilities of **47** in inert, nonpolar solvents. Product **47** can also be prepared effectively in one pot without isolation of the intermediate ferrous dimer **46** with no loss in yield, and the crude product **47** is suitable for subsequent reaction directly.

Red elemental selenium was tested to oxidize cluster **46**. Another dinuclear ferric cluster $Fe_2(\mu\text{-}NH^tBu)_2(\mu\text{-}Se)[N(SiMe_3)_2]_2$ (**52**, Figure 3.16) has been synthesized and isolated in ca. 35% yield. Compared to the sulfide addition reaction, integrating the selenide core ligand into **46** required heating overnight to complete the conversion (Equation 3.6). The reaction of **46** with red selenium was performed in C_6H_6 and heated at 45 ºC for 18 hours, and some grey powder precipitated out of the solution. The grey

powder is believed to result from decomposition of red selenium at high temperature. As grey selenium does not react with cluster **46** and heating is unavoidable, excess red selenium is necessary for the clean preparation of cluster **52**, which also contains the unusual confacial bitetrahedral geometry.

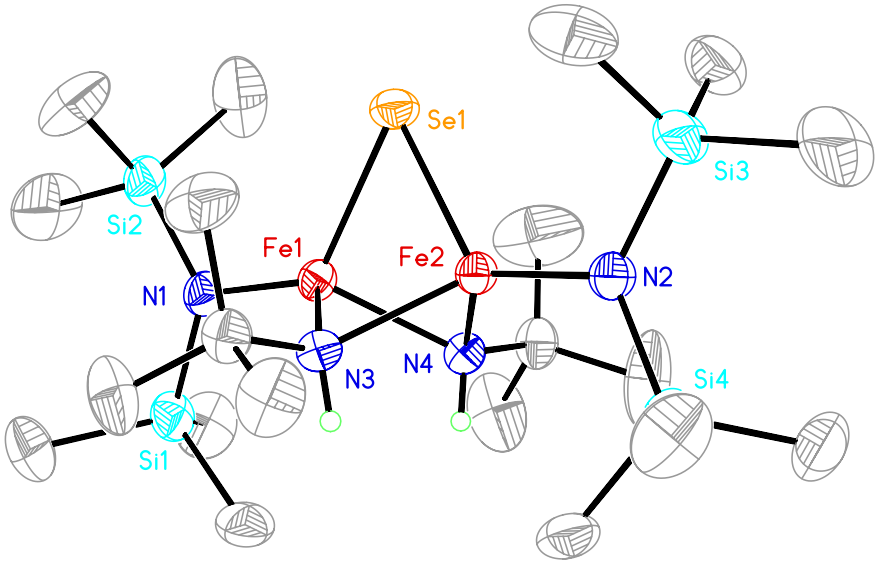

Figure 3.16. Structure of $Fe_2(\mu\text{-}NH^tBu)_2(\mu\text{-}Se)[N(SiMe_3)_2]_2$ (**52**) with thermal ellipsoids (50% probability level) and selected atom labels. Non-amido hydrogen atoms are omitted.

$$Fe_2(NH^tBu)_2(N\{SiMe_3\}_2)_2 + Se \longrightarrow Fe_2(NH^tBu)_2(Se)(N\{SiMe_3\}_2)_2 \qquad \text{(eq 3.6)}$$

Furthermore, iodine is another element that has been found to react with cluster **46**. The addition of 0.5 equivalent I_2 in C_6H_6 solution to compound **46** results in a instant color change from green to black. The solution was stirred for 2 hours and the iodo-bridged cluster $Fe_2(\mu\text{-}NH^tBu)_2(\mu\text{-}I)[N(SiMe_3)_2]_2$ (**53**, Figure 3.17) crystallized by *n*-pentane/HMDSO vapor diffusion at −30 °C. This compound shares the same structure with clusters **47** or **52**, but, it contains Fe(II)/Fe(III) mixed oxidation states compared with the previous all-ferric clusters.

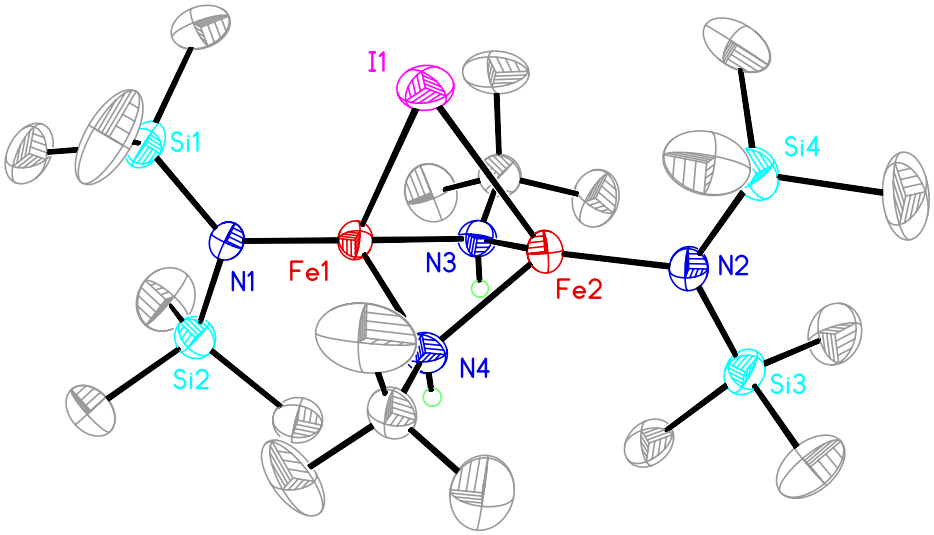

Figure 3.17. Structure of $Fe_2(\mu\text{-}NH^tBu)_2(\mu\text{-}I)[N(SiMe_3)_2]_2$ (**53**) with thermal ellipsoids (50% probability level) and selected atom labels. Non-amido hydrogen atoms are omitted.

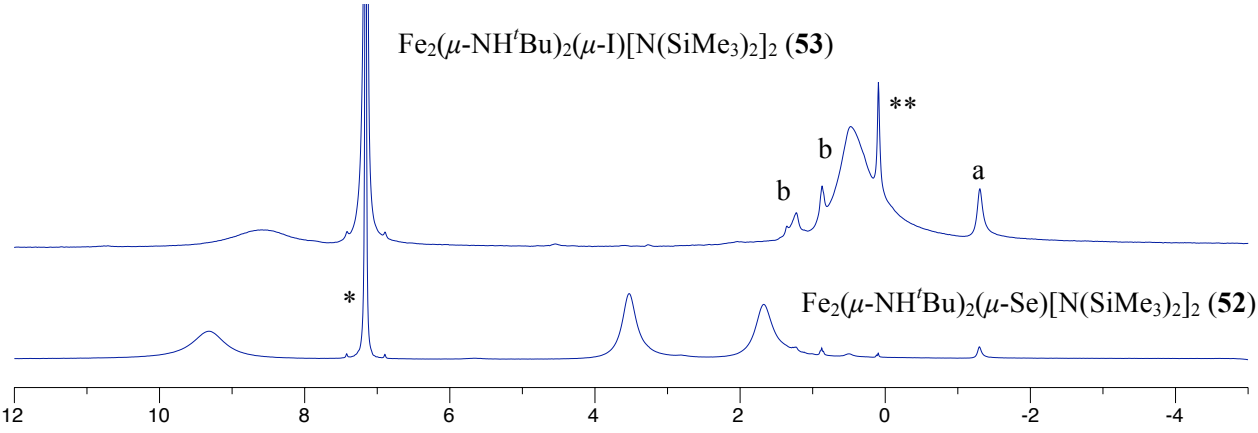

Figure 3.18. ^{1}H NMR spectra (300 MHz) of clusters **52** and **53**. Residual protio signal of C_6D_6 is marked by *. HMDSO is marked by **, residual *n*-pentane is marked by b, and contaminant **46** is marked by a.

Cluster **52** exhibits a well defined isotropically shifted ^{1}H NMR spectrum that is consistent with its solid state structure (Figure 3.16 and Table 3.3). The spectrum of **52** has three peaks with the same integral ratio, which indicates that the rotation of terminal amides is restricted on the NMR spectroscopic

time scale. Although the spectrum of **53** is contaminated by cluster **46** and residual solvent, the chemical shifts of **53** can still be assigned as presented in Table 3.3.

Table 3.3. ^{1}H NMR spectroscopic data for clusters **52** and **53**.

Compound	^{1}H NMR (C_6D_6, δ ppm)
52	9.31 (18 br), 3.53 (18 br), 1.68 (18 br)
53	8.64 (18 br), 0.53 (36 br)

3.2.5 Cluster Structures

The structures of iron-amide clusters can be divided into three categories: trigonal planar dimer, linear trimer and confacial bitetrahedral dimer. The first one contains two trigonal planar iron centers that are edge-fused through two μ_2-amide bridges and terminal amides to complete the ligand sets. Metrics for the crystal structures of $Fe_2(\mu\text{-}NH^tBu)[\mu\text{-}N(SiMe_3)_2][N(SiMe_3)_2]_2$ (**48**) and $Fe_2(\mu\text{-}NH^tAm)_2[N(SiMe_3)_2]_2$ (**50**) that adopt this geometry are summarized in Table 3.4. This cluster type can be viewed as an $[Fe_2N_2]$ rhombic motif and it is approximately planar. There are two different bridging ligand types *tert*-butylamide and bis(trimethylsilyl)amide in cluster **48** and the Fe-NH^{t}Bu distance (average: 2.055 Å) is slightly shorter than Fe-N(SiMe$_3$)$_2$ distance (average: 2.074 Å). In cluster **50**, the nitrogen centers of terminal amides are approximately planar, and this silyamide plane is nearly perpendicular with the $[Fe_2N_2]$ core.

The second cluster type contains the linear trinuclear core, which can be found in clusters $Fe_3(\mu\text{-}NH^tBu)_4[N(SiMe_3)_2]_2$ (**49**) and $Fe_3(\mu\text{-}NHMes)_4[N(SiMe_3)_2]_2$ (**51**) and their metrics are presented in Table 3.5. These complexes are constructed of two trigonal planar iron centers edge-fused to a central tetrahedral iron by four μ_2-bridging amide nitrogens, forming two $[Fe_2N_2]$ planes. It is notable that cluster

49 contains two structures, the first one consisting of N3H^{t}Bu and N4H^{t}Bu disposed to form an approximately S_4 point group (methyl groups are ignored), while the second one includes N3'H^{t}Bu and N4'H^{t}Bu, disposed to form an approximately D_2 point group (methyl groups are ignored). Within the first geometry, the two rhomb [Fe_2N_2] planes are nearly perpendicular to each other at 90.4°, while the angle between the two [Fe_2N_2] planes in the second structure is bent from the right angle at 121.4°. The previously discussed complex [$Fe_3(\mu$-$OSi_2Me_5)_4(N(SiMe_3)_2)_2$] adopts the first structure type, and compounds **51** and [$Fe_3(\mu$-$S(C_6H_2$-2,4,6-iPr$_3$))$_4(N(SiMe_3)_2)_2$] are formed as the second cluster geometry. The μ_2-amide bridges are not symmetric, with Fe-N bond distances to the central tetrahedreal iron being longer than those to the outer trigonal planar iron centers. With the presence of sterically hindered mesityl groups in cluster **51**, the aryl rings are approximately perpendicular to the [Fe_2N_2] cores and the four aryl rings are almost parallel to each other. Compared with arylamide compound **51**, the [Fe_2N_2] cores in alkylamide cluster **49** are relatively compressed: Fe–N and Fe···Fe contacts of compound **49** are slightly shorter while N···N distances are roughly the same with cluster **51** (average distances: Fe–N, 2.041 Å; Fe···Fe, 2.753 Å; N···N, 3.014 Å in compound **49** versus Fe–N, 2.067 Å; Fe··· Fe, 2.823 Å; N··· N, 3.011 in compound **51**).

Two tetrahedral iron sites face-fused through two μ_2-bridging amides and one μ_2-bridging selenide/iodide construct the third type of cluster structure. Relevant metrics for $Fe_2(\mu$-NH^{t}Bu$)_2(\mu$-Se$)[N(SiMe_3)_2]_2$ (**52**) and $Fe_2(\mu$-NH^{t}Bu$)_2(\mu$-I$)[N(SiMe_3)_2]_2$ (**53**) are summarized in Table 3.6. Compared with the other confacial bitetrahedral cluster **47**, the Fe–X contacts (Fe–S: 2.233 Å, Fe–Se: 2.3656 Å and Fe–I: 2.7463 Å) are longer than the Fe–N contacts (average 2.054 Å in cluster **47**, average 2.051 Å in cluster **52**, and average 2.047 Å in cluster **53**). Also the Fe–X bond distances are Fe–I > Fe–Se > Fe–S and the Fe···Fe separations are **53** > **52** > **47**. The Fe–S/Se/I–Fe angles (average

66.69°/62.232°/56.826°) are compressed versus the Fe–N–Fe angles (average 73.41° in cluster **47**, average 74.40° in cluster **52** and average 79.32° in cluster **53**). The terminal NSi_2 planes in complex **52** are close to coplanar with the central [Fe_2Se] plane.

Table 3.4. Selected interatomic distances (Å) and angles (deg) in $Fe_2(\mu\text{-}NH^tBu)[\mu\text{-}N(SiMe_3)_2][N(SiMe_3)_2]_2$ (**48**) and $Fe_2(\mu\text{-}NH^tAm)_2[N(SiMe_3)_2]_2$ (**50**).

	48	**50**
Fe(1/2)-N(1/2)	1.9039(19)/1.9031(18)	1.9179(13)/1.9149(13)
Fe(1)-N(3/4)	2.041(3)/2.017(3)	2.0714(12)/2.0763(13)
Fe(2)-N(3/4)	2.032(3)/2.014(3)	2.051(3)/2.059(3)
Fe(1)…Fe(2)	2.6976(5)	2.7659(3)
N(3)…N(4)	3.009(4)	2.995(3)
N(1)-Si(1/2)	1.712(2)/1.716(2)	1.7220(15)/1.7237(15)
N(2)-Si(3/4)	1.711(2)/1.716(2)	1.7261(14)/1.7288(14)
N(4)-C(19)		1.513(4)
N(3)-Si(5/6)		1.7702(13)/1.7696(14)
N(3/4)-C(30/40)	1.485(4)/1.506(4)	
N(1/1/4)-Fe(1)-N(3/4/3)	133.18(10)/131.15(10)/95.65(11)	138.36(6)/126.63(9)/93.18(9)
N(2/2/4)-Fe(2)-N(3/4/3)	133.42(10)/130.52(10)/96.05(11)	139.20(5)/125.05(10)/92.81(10)
C(19)-N(4)-Fe(1/2)		123.0(2)/121.0(2)
C(40)-N(4)-Fe(1/2)	122.0(2)/121.2(2)	
C(30)-N(3)-Fe(1/2)	121.7(2)/121.7(2)	
Si(1/3)-N(1/2)-Si(2/4)	126.05(11)/125.29(11)	122.76(8)/121.47(8)
Si(5/6)-N(3)-Fe(1)		116.65(7)/109.84(6)
Si(5/6)-N(3)-Fe(2)		110.51(6)/114.82(7)
Si(5)-N(3)-Si(6)		116.95(7)
Fe(1)-N(3/4)-Fe(2)	82.94(10)/84.02(11)	83.65(5)/84.60(12)
Si(1/2)-N(1)-Fe(1)	117.21(11)/116.73(11)	117.64(8)/119.57(8)

Si(3/4)-N(2)-Fe(2)	117.37(11)/117.32(10)	120.04(7)/118.37(7)
	Planarity	
[Fe(1,2),N(3,4)]	0.0770	0.1633

Table 3.5. Selected interatomic distances (Å) and angles (deg) in $Fe_3(\mu\text{-}NH^tBu)_4[N(SiMe_3)_2]_2$ (**49**) and $Fe_3(\mu\text{-}NHMes)_4[N(SiMe_3)_2]_2$ (**51**).

	49	**51**
Fe(1/3)-N(1/2)	1.904(3)/1.913(3)	1.905(5)/1.908(5)
Fe(4/6)-N(7/8)	1.909(3)/1.907(3)	1.910(5)/1.902(5)
Fe(1/2)-N(3)	2.024(6)/2.053(5)	2.047(5)/2.058(5)
Fe(1/2)-N(4)	2.056(5)/2.058(5)	2.064(5)/2.088(5)
Fe(2/3)-N(5)	2.065(3)/2.012(3)	2.079(5)/2.069(5)
Fe(2/3)-N(6)	2.067(3)/2.005(3)	2.080(5)/2.052(5)
Fe(4/5)-N(9)	2.033(4)/2.078(4)	2.060(5)/2.066(5)
Fe(4/5)-N(10)	2.017(4)/2.050(4)	2.052(5)/2.069(5)
Fe(5/6)-N(11)	2.064(3)/2.009(3)	2.059(5)/2.051(5)
Fe(5/6)-N(12)	2.071(3)/2.007(3)	2.061(5)/2.059(5)
Fe(1/2)…Fe(2/3)	2.7569(10)/2.7498(10)	2.8289(12)/2.8438(12)
Fe(4/5)…Fe(5/6)	2.7567(10)/2.7486(10)	2.8141(11)/2.8054(11)
N(3/5)…N(4/6)	3.027(7)/3.006(5)	3.007(7)/3.008(7)
N(9/11)…N(10/12)	3.019(6)/3.009(5)	3.015(7)/3.010(7)
N(1)-Si(1/2)	1.701(4)/1.726(4)	1.723(6)/1.713(5)
N(2)-Si(3/4)	1.703(4)/1.714(4)	1.718(6)/1.713(6)
N(7)-Si(5/6)	1.714(4)/1.714(4)	1.731(5)/1.711(5)
N(8)-Si(7/8)	1.717(4)/1.714(4)	1.725(6)/1.702(6)
N(3/4)-C(30/40)	1.503(7)/1.496(6)	
N(5/6)-C(50/60)	1.499(5)/1.497(5)	
N(3/4)-C(301/401)		1.432(8)/1.427(7)
N(5/6)-C(501/601)		1.422(8)/1.442(9)

N(9/10)-C(90/100)	1.493(5)/1.519(6)	
N(11/12)-C(110/120)	1.503(5)/1.496(5)	
N(9/10)-C(901/1001)		1.436(8)/1.435(8)
N(11/12)-C(111/121)		1.432(8)/1.430(8)
N(1/1/4)-Fe(1)-N(3/4/3)	133.05(19)/131.13(17)/95.8(2)	134.8(2)/131.2(2)/93.99(19)
N(7/7/10)-Fe(4)-N(9/10/9)	131.54(15)/132.06(15)/96.39(16)	132.3(2)/133.2(2)/94.27(19)
N(2/2/6)-Fe(3)-N(5/6/5)	132.38(14)/130.74(14)/96.88(13)	135.2(2)/131.0(2)/93.7(2)
N(8/8/12)-Fe(6)-N(11/12/11)	132.96(14)/129.96(14)/97.01(13)	134.9(2)/130.9(2)/94.18(19)
N(3/4)-Fe(2)-N(5/6)	118.3(2)/117.0(2)	125.5(2)/125.2(2)
N(9/10)-Fe(5)-N(11/12)	118.30(15)/117.96(16)	125.6(2)/126.9(2)
N(3/5)-Fe(2)-N(4/6)	94.9(2)/93.35(13)	92.97(19)/92.62(19)
N(9/11)-Fe(5)-N(10/12)	94.00(16)/93.38(13)	93.59(19)/93.86(19)
C(30)-N(3)-Fe(1/2)	120.3(4)/128.8(4)	
C(40)-N(4)-Fe(1/2)	117.7(4)/128.7(4)	
C(50)-N(5)-Fe(2/3)	129.4(3)/120.4(3)	
C(60)-N(6)-Fe(2/3)	128.5(3)/120.5(3)	
C(90)-N(9)-Fe(4/5)	118.4(3)/128.1(3)	
C(100)-N(10)-Fe(4/5)	118.4(3)/127.5(3)	
C(110)-N(11)-Fe(5/6)	128.4(3)/119.9(2)	
C(120)-N(12)-Fe(5/6)	128.7(3)/119.1(3)	
C(301)-N(3)-Fe(1/2)		122.4(4)/119.6(4)
C(401)-N(4)-Fe(1/2)		123.4(4)/120.7(4)
C(501)-N(5)-Fe(2/3)		119.7(4)/125.0(4)
C(601)-N(6)-Fe(2/3)		118.1(4)/125.5(5)
C(901)-N(9)-Fe(4/5)		124.9(4)/116.5(4)
C(101)-N(10)-Fe(4/5)		126.6(4)/117.4(4)
C(111)-N(11)-Fe(5/6)		121.5(4)/123.3(4)
C(121)-N(12)-Fe(5/6)		120.6(4)/123.7(4)
Si(1/3)-N(1/2)-Si(2/4)	126.6(2)/126.2(2)	125.8(3)/124.4(3)
Si(5/7)-N(7/8)-Si(6/8)	126.1(2)/126.7(2)	125.4(3)/126.1(3)

Fe(1)-N(3/4)-Fe(2)	84.16(18)/85.1(2)	87.1(2)/85.90(19)
Fe(2)-N(5/6)-Fe(3)	84.84(12)/84.93(13)	86.57(19)/87.0(2)
Fe(4)-N(9/10)-Fe(5)	84.21(16)/85.34(15)	86.00(19)/86.13(19)
Fe(5)-N(11/12)-Fe(6)	84.86(13)/84.74(12)	86.09(18)/85.83(18)
Si(1/2)-N(1)-Fe(1)	118.6(2)/114.8(2)	116.5(3)/117.7(3)
Si(3/4)-N(2)-Fe(3)	116.7(2)/117.18(19)	116.6(3)/118.8(3)
Si(5/6)-N(7)-Fe(4)	117.0(2)/116.9(2)	114.8(3)/118.5(3)
Si(7/8)-N(8)-Fe(6)	116.44(19)/116.8(2)	116.3(3)/117.5(3)
	Planarity	
[Fe(1,2),N(3,4)]	0.0209	0.0129
[Fe(2,3),N(5,6)]	0.0046	0.0212
[Fe(4,5),N(9,10)]	0.0166	0.0046
[Fe(5,6),N(11,12)]	0.0047	0.0134

Table 3.6. Selected interatomic distances (Å) and angles (deg) in $Fe_2(\mu\text{-}NH^tBu)_2(\mu\text{-}Se)[N(SiMe_3)_2]_2$ (**52**) and $Fe_2(\mu\text{-}NH^tBu)_2(\mu\text{-}I)[N(SiMe_3)_2]_2$ (**53**), in the first column Q = Se, and in the second column Q = I.

	52	**53**
Fe(1/2)-Q(1)	2.3706(3)/2.3606(3)	2.7182(4)/2.7754(4)
Fe(1/2)-N(1/2)	1.885(15)/1.8893(15)	1.890(2)/1.898(2)
Fe(1)-N(3/4)	2.0586(15)/2.0419(15)	2.027(2)/2.023(2)
Fe(2)-N(3/4)	2.0526(15)/2.0515(15)	2.075(2)/2.066(2)
Fe(1)…Fe(2)	2.4802(4)	2.6144(5)
N(1)-Si(1/2)	1.7348(17)/1.7382(17)	1.737(2)/1.727(2)
N(2)-Si(3/4)	1.7401(17)/1.7320(17)	1.724(2)/1.727(2)
N(3/4)-C(13/17)	1.498(2)/1.497(2)	1.494(3)/1.497(3)
N(1/3/4)-Fe(1)-Q(1)	125.15(5)/92.98(4)/93.28(5)	122.59(7)/93.37(7)/92.47(7)
N(2/3/4)-Fe(2)-Q(1)	124.32(5)/93.42(4)/93.33(5)	124.20(7)/90.70(7)/89.90(7)
N(1/1/4)-Fe(1)-N(3/4/3)	123.89(7)/126.62(7)/83.37(6)	124.83(9)/127.50(9)/85.43(9)
N(2/2/4)-Fe(2)-N(3/4/3)	126.65(7)/124.53(7)/83.28(6)	126.95(9)/129.09(10)/83.13(9)

Fe(1)-Q(1)-Fe(2)	62.232(10)	56.826(11)
C(17)-N(4)-Fe(1/2)	128.25(12)/127.92(12)	129.36(18)/129.23(18)
C(13)-N(3)-Fe(1/2)	126.92(12)/129.85(12)	129.30(17)/130.17(18)
Si(1/3)-N(1/2)-Si(2/4)	124.04(9)/124.08(9)	123.01(12)/124.81(13)
Fe(1)-N(3/4)-Fe(2)	74.21(5)/74.59(5)	79.18(8)/79.48(8)
Si(1/2)-N(1)-Fe(1)	118.17(9)/117.75(9)	118.66(12)/118.22(11)
Si(3/4)-N(2)-Fe(2)	117.05(9)/118.87(9)	117.90(12)/117.29(12)

3.2.6 Spectroscopic Properties

Electronic absorption spectroscopic data of iron-amide clusters **46**, **48**, and **49** are summarized in Table 3.7. All the compounds were measured in *n*-pentane. The solution electronic absorption spectra of these dinuclear clusters displayed multiple intense charge-transfer bands at violet to blue energies and almost no absorption in the rest of the visible range. Electronic absorption spectra of **47**, **52** and **53** (Table 3.8) are characterized by intense charge-transfer bands in the near-violet region and trail off into the visible region, which explains why they are black in solution.

Table 3.7. Electronic absorption spectroscopic data for clusters **46**, **47**, **48**, **49**, **52** and **53**.

Compound	electronic abs: λ_{max}, nm (ε_M, L $mol^{-1} \cdot cm^{-1}$)
46	207 (14300), 277 (14300), 395 (300)
47	224 (7100), 285 (6900), 402 (200)
48	262 (17500)
49	205 (11600), 277 (11000)
52	286 (11700), 348 (8800), 439 (4800)
53	245 (10300), 282 (10900), 383 (6200), 493 (3800)

Figure 3.17. Comparative electronic absorption spectra of clusters **46**, **48** and **49** in *n*-pentane

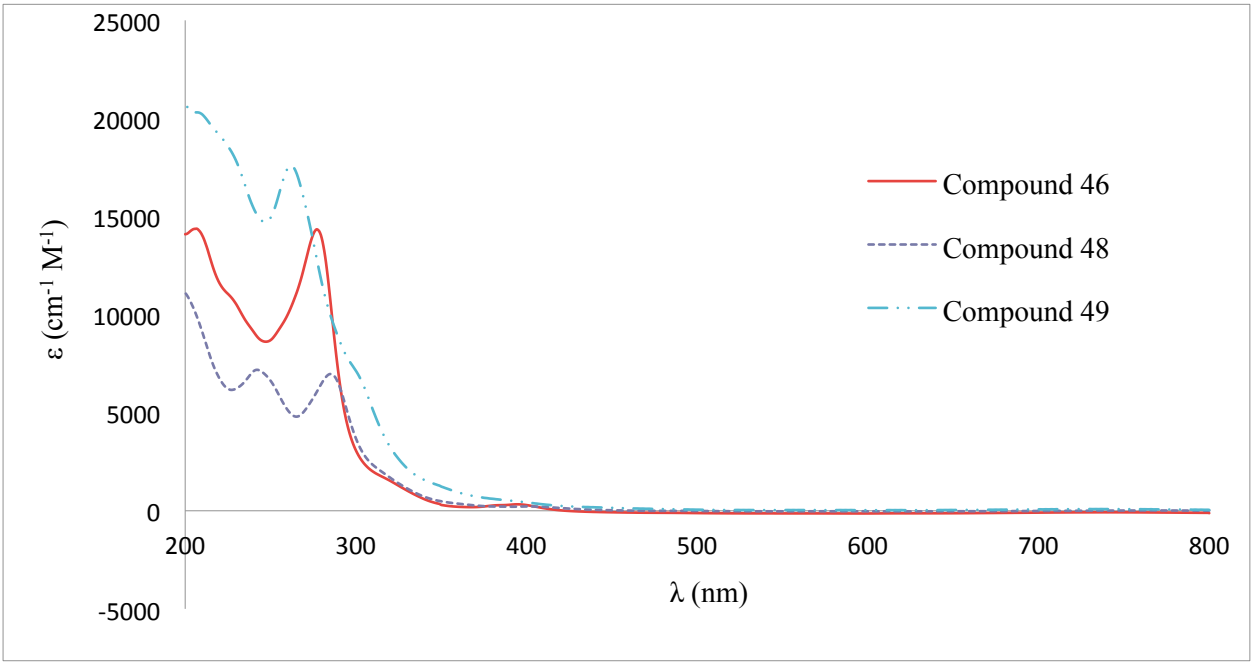

Figure 3.18. Comparative electronic absorption spectra of clusters **47**, **52** and **53** in *n*-pentane

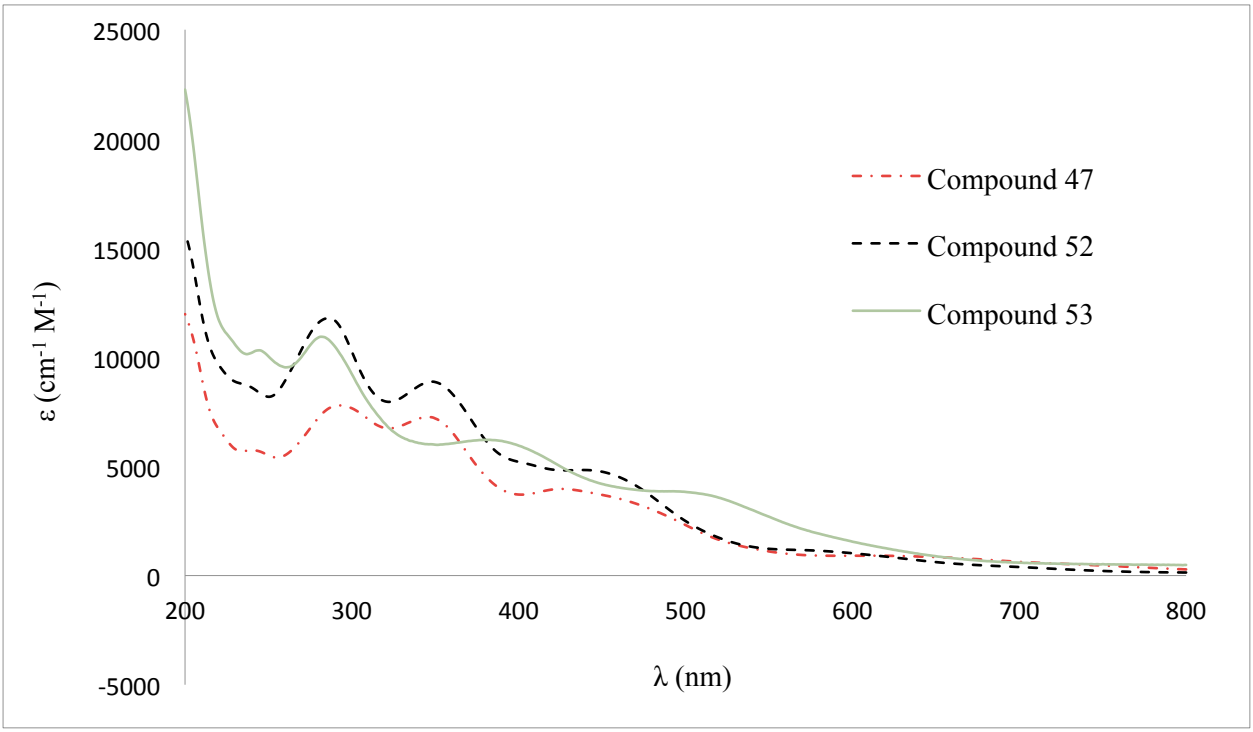

3.3 Experimental Section

3.3.1 General Experimental Method

Most of the procedures used in this study were outlined in Chapter 2, Section 2.3.1; *tert*-butylamine, *tert*-amylamine and 2,4,6-trimethylaniline were distilled from CaH_2, then degassed and kept in the glovebox before use.

Compounds in this chapter are extremely reactive and unstable, and may decompose over time, even crystalline form and under N_2 atmosphere. Compounds were therefore stored at −20 ºC to enhance stability. Even under these conditions, compound **50** still faced the problem of decomposing after removal from the mother liquor.

3.3.2 Preparation of Compounds

$Fe_2(\mu\text{-}NH^tBu)[\mu\text{-}N(SiMe_3)_2][N(SiMe_3)_2]_2$ (48). Neat $^tBuNH_2$ (0.042 mL, 0.4 mmole) was added to a green solution of $Fe[N(SiMe_3)_2]_2$ (0.301 g, 0.8 mmole) in C_6H_6 (20 mL). The solution was heated to 45ºC for 12 hours to yield a dark green solution. The solvent was removed in vacuo, and the dried material was dissolved in *n*-pentane, filtered, concentrated in vacuo, and cooled to −20 ºC with vapor diffusion of HMDSO to yield light green crystals. Total yield: 0.275 g (60.8%).

$Fe_3(\mu\text{-}NH^tBu)_4[N(SiMe_3)_2]_2$ (49). Neat $^tBuNH_2$ (0.168 mL, 1.6 mmole) was added to a blue solution of $Fe[N(SiMe_3)_2]_2$ (0.301 g, 0.8 mmole) in THF (20 mL), causing an immediate color-darkening. The solution was heated to 45ºC for 12 hours to yield a dark green solution. The solvent was removed in vacuo, and the dried material was dissolved in *n*-pentane, filtered, concentrated in vacuo, and cooled to −20 ºC with vapor diffusion of HMDSO. This reaction generated a mixture material of cluster **49** and

cluster $Fe_2(\mu\text{-}NH^tBu)_2[N(SiMe_3)_2]_2$ (**46**). However, the target compound **49** can be separated by crystallization. The first crop of product out of the solution is cluster **49**, as light green needle crystals and cluster **46** crystallized later. Total yield: 0.105 g (35.2%).

$Fe_2(\mu\text{-}NH^tAm)_2[N(SiMe_3)_2]_2$ (50). Neat $^tAmNH_2$ (0.098 mL, 0.8 mmole) was added to a green solution of $Fe[N(SiMe_3)_2]_2$ (0.301 g, 0.8 mmole) in C_6H_6 (20 mL). The solution was heated to 45ºC for 12 hours to yield a dark green solution. The solvent was removed in vacuo, and the dried material was dissolved in *n*-pentane, filtered, concentrated in vacuo, and cooled to −20 ºC with vapor diffusion of HMDSO to yield light green crystals. Total yield: 0.225 g (52.8%).

$Fe_3(\mu\text{-}NHMes)_4[N(SiMe_3)_2]_2$ (51). Neat 2,4,6-trimethylaniline (177 mg, 4.8 mmole) was dissolved in C_6H_6 (10 mL) and added to a green solution of $Fe[N(SiMe_3)_2]_2$ (1.506 g, 4.0 mmole) in C_6H_6 (20 mL) dropwise, causing an immediate color-darkening. The solution was stirred for 12 h to yield a dark green solution. The solvent was removed in vacuo, and the dried material was dissolved in *n*-pentane, filtered, concentrated in vacuo, and cooled to −20 ºC with vapor diffusion of HMDSO to yield dark green plate-like crystals. Total yield: 0.775 g (41.5%).

$Fe_2(\mu\text{-}NH^tBu)_2(\mu\text{-}Se)[N(SiMe_3)_2]_2$ (52). Neat $^tBuNH_2$ (0.500 mL, 4.0 mmole) was added to a green solution of $Fe[N(SiMe_3)_2]_2$ (1.524 g, 4.0 mmole) in benzene (30 mL). The solution was heated to 45 ºC for 8 h to yield a dark green solution. Se_8 (2.140 g, 4.0 mmole) was then added into the solution, followed by stirring at 45 ºC for 12 h. The brownish-orange solution was dried in vacuo to afford a black material, which was dissolved in *n*-pentane (12 mL), filtered, and set for evaporation with HMDSO at –20 ºC for 5 d to generate black crystals. The crystals were collected by filtration, rinsed with cold HMDSO (3 x 1 mL), and dried in vacuo for 2 h, to yield 0.588 g (44.9 %).

$Fe_2(\mu\text{-}NH^tBu)_2(\mu\text{-}I)[N(SiMe_3)_2]_2$ (53). I_2 (82 mg, 2.0 mmole) was dissolved in C_6H_6 (10 mL) to

form a purple solution and then added to a green solution of $Fe_2(\mu\text{-}NH^tBu)_2[N(SiMe_3)_2]_2$ (**46)** (1.506 g, 4.0 mmole) in C_6H_6 (20 mL), causing an immediate color-darkening, followed by stirring at or 4 h. The brownish-black solution was dried in vacuo to afford a black material, which was dissolved in *n*-pentane (12 mL), filtered, and set for evaporation with HMDSO at –20 ºC for 4 d to generate black crystals. The crystals were collected by filtration, rinsed with cold HMDSO (3 x 1 mL), and dried in vacuo for 2 h, to 0.448 g (34.2 %).

3.3.3 X-ray Crystallography

General crystallographic procedures were described in Chapter 2, Section 2.3.3. Single crystals suitable for X-ray diffraction analysis were obtained from the following conditions and solvents: *n*-pentane/HMDSO vapor diffusion at −30 °C (**48**, **49**, **50**, as light green plates; **51**, as dark green needles; **52**, **53,** as black blocks). Essential crystallographic data for compounds in this chapter are summarized in Table 3.8 and 3.9. Disordered coordinated molecules were found in the structures of **48, 49,** and **50**.

3.3.4 NMR and UV-Vis Spectroscopy

^{1}H NMR spectra were performed on Bruker 300 MHz spectrometers, with chemical shifts referenced to residual protiosolvent signals; UV-Vis spectra were recorded on a Varian Cary 5000 spectrophotometer; for all the clusters discussed in this chapter, concentrated solutions (*n*-pentane) and 0.1 mm pathlength cells were used to minimize decomposition.

Table 3.8. Crystallographic data for compounds **48**, **50** and **53**

	48	**50**	**53**
formula	$C_{22}H_{64}Fe_2N_4Si_6$	$C_{22}H_{60}Fe_2N_4Si_4$	$C_{20}H_{56}Fe_2N_4Si_4I$
fw	665.01	604.8	703.65
space group	P2(1)/c	*C*2/*c*	$P2_1/n$
Z	2	2	4
a, Å	9.0003(4)	10.5480(5)	16.6153(6)
b, Å	14.7448(7)	11.6888(6)	9.2670(4)
c, Å	15.1053(7)	15.9348(8)	23.3513(9)
α, deg	80.6310(10)	78.5270(10)	90
β, deg	85.3580(10)	71.7570(10)	100.0050(10)
γ, deg	84.9780(10)	82.4330(10)	90
V, (Å^3)	1965.72(16)	1823.53(16)	3540.8(2)
ρ_{calc}, g/cm^3	1.124	1.101	1.320
θ_{max}, deg	30.07	30.01	29.26
total data, %	98.6	98.8	99.8
μ, mm^{-1}	0.937	0.942	1.841
R_1 (wR_2), %	3.53 (6.79)	4.77 (11.99)	2.7 (7.06)
S	1.777	1.012	1.032

Table 3.9. Crystallographic data for compounds **49**, **51** and **52**

	49	**51**	**52**
formula	$C_{28}H_{76}Fe_3N_6Si_4$	$C_{48}H_{84}Fe_3N_6Si_4$	$C_{20}H_{56}Fe_2N_4Si_4Se$
fw	776.86	1025.12	655.71
space group	*Pbca*	$P\overline{1}$	P2(1)/n
Z	16	4	4
a, Å	17.088(5)	16.4201(15)	16.4943(6)
b, Å	22.888(7)	16.4851(15)	9.0935(3)
c, Å	47.093(15)	22.763(2)	23.5967(8)
α, deg	90.00	103.626(2)	90.00
β, deg	90.00	104.0130(10)	101.6310(10)
γ, deg	90.00	95.7500(10)	90.00
V, (Å^3)	18418(10)	5728.7(9)	3466.6(2)
ρ_{calc}, g/cm^3	1.121	1.189	1.256
θ_{max}, deg	25.00	25.00	29.78
total data, %	99.8	99.2	99.8
μ, mm^{-1}	1.060	0.868	2.039
R_1 (wR_2), %	5.21 (11.36)	7.17 (16.75)	3.11 (7.50)
S	1.050	1.055	1.018

CHAPTER 4. CONCLUSION AND FUTURE WORK

4.1 Relationship between Iron-Amide, Iron-Imide-Sulfide Clusters and FeMo-cofactor in Nitrogenase

In this project, we have developed effective synthetic pathways to the selective preparation of dinuclear and tetranuclear clusters with heteroligated cores. Methods for building these heteroligated cores were unknown prior to this work. The tetranuclear compounds discussed in this thesis contain weak-field Fe-NR-S cores, which are similar to the FeMo cofactor Mo-Fe-S-X environment, that may be potentially useful in the study of cofactor chemistry both for the development of synthetic approaches to the cofactor structure, and for the understanding of the cofactor properties. Although the substrate binding site and the structural relationship between the resting state enzyme and catalytically-active forms remain uncertain, iron centers are widely accepted to be the sites where dinitrogen binding and reduction occur. The study of nitrogen containing iron-sulfur clusters may help to define the intermediate forms of the cofactor during catalysis. Among all the $[Fe_4(N^tBu)_n(S)_{4-n}Cl_4]^z$ cubane complexes we have generated, $(Et_4N)_2[Fe_4(\mu_3\text{-}N^tBu)(\mu_3\text{-}S)_3Cl_4]$ **(44)** is the first synthetic cluster to represent the corresponding heteroligated $[Fe_4S_3X]$ subunit in the FeMo cofactor structure (if X = N). Cluster **44** offers an opportunity to compare the chemical and physical properties of a well-defined synthetic system against the actual biometallocluster.

4.2 Synthetic Considerations

The synthetic route to iron-amide clusters $Fe_2(\mu\text{-}NH^tBu)[\mu\text{-}N(SiMe_3)_2][N(SiMe_3)_2]_2$ (**48**), $Fe_3(\mu\text{-}NH^tBu)_4[N(SiMe_3)_2]_2$ (**49**), $Fe_2(\mu\text{-}NH^tAm)_2[N(SiMe_3)_2]_2$ (**50**) and $Fe_3(\mu\text{-}NHMes)_4[N(SiMe_3)_2]_2$ (**51**)

was achieved by protolytic substitution of $Fe[N(SiMe_3)_2]_2$ with different amines. The successful syntheses of these heteroleptic dimers or trimers depend on: (i) The nature of the amines. We found that the effective preparation of iron-amide clusters requires certain primary amines with tertiary substituents. (ii) Solvent adoption. Trimer **49** only formed in THF, while other compounds can be synthesized in C_6H_6, *n*-pentane or THF. (iii) Stoichiometry. Clusters **46**, **48** and **49** are prepared by the reaction of $Fe[N(SiMe_3)_2]_2$ with $^tBuNH_2$ in a ratio of 2:1, 1:1 and 1:2 respectively. The syntheses of clusters $Fe_2(\mu\text{-}NH^tBu)_2(\mu\text{-}Se)[N(SiMe_3)_2]_2$ (**52**) and $Fe_2(\mu\text{-}NH^tBu)_2(\mu\text{-}I)[N(SiMe_3)_2]_2$ (**53**) were accomplished by oxidative addition of elemental selenium and iodine with $Fe_2(\mu\text{-}NH^tBu)_2[N(SiMe_3)_2]_2$ (**46**) to form the new complexes with confacial bitetrahedral iron centers.

The dinuclear complexes $Fe_2(\mu\text{-}NH^tBu)_2[N(SiMe_3)_2]_2$ (**46**) and $Fe_2(\mu\text{-}NH^tBu)_2(\mu\text{-}S)[N(SiMe_3)_2]_2$ (**47**) are used for the preparation of $[Fe_4(N^tBu)_n(S)_{4-n}Cl_4]^z$ cubane complexes. The detailed descriptions of these tetranuclear clusters formation pathways are still unknown. These cubane clusters have been established to be compositionally stable, although they decompose slowly in solution and ligand exchange has been found in the cluster formation process. The cubane products do not undergo intercluster core-ligand exchange.

4.3 Iron-amide and Iron-imide-sulfide Cluster Properties

A class of weak-field iron-aimde clusters has been investigated. Three basic structure types have been found by X-ray crystallography study: (i) diiron clusters bridged by two μ_2-amide ligands; (ii) diiron clusters bridged by two μ_2-amide and one μ_2-selenide or iodide ligand; and (iii) linear triiron clusters bridged by four μ_2-amide ligands. For the tetranuclear iron-imide-sulfide clusters, four tetrahedral iron centers are bridged by mixed μ_3-sulfide and μ_3-imide core ligands, and capped with chloride terminal

ligands. The structural and coordination environments of the $[Fe_4(N^tBu)_n(S)_{4-n}Cl_4]^z$ cubane complexes are similar to those seen in all-sulfide and all-imide clusters, respectively. The ^1H NMR spectra indicate these nitrogen-containing iron-sulfur compounds are paramagnetic and contain high spin iron centers.

4.4 Future Work

The successful syntheses of the dinuclear iron-amide and tetranuclear iron-imide-sulfide clusters with heteroligated cores may provide logical pathways to other heteroligands that may more closely resemble the X ligand in the FeMo cofactor, such as carbide or oxide. In addition, these clusters may also be used to construct higher-nuclearity clusters.

With regard to the existing work, both iron-amide and iron-imide-sulfide systems are starting points for further investigation. For the syntheses of iron-amide clusters, we have demonstrated that only certain amines react with $Fe[N(SiMe_3)_2]_2$ to stabilize and generate the heteroleptic dimers, while the other aryl- and alkylamines result in uncharacterizable products. The identification of parent compounds and decomposition products by gas chromatographic analysis would be important to further understand the reaction mechanism and optimize reaction conditions.

The complexes described in Chapter 2 (except **43a**) are all capped with chloride terminal ligands, and they were found to slowly decompose in solution. Also, these clusters are difficult to isolate due to the presence of contaminant clusters with comparable solubilities. The substitution of their terminal ligands with thiolate may not only improve their stability, but may also assist in the separation of the compounds. Furthermore, based on the electrochemistry data summarized in Table 2.6, some of the clusters exhibited reversible or quasi-reversible electrochemical processes, which indicate the possible existence of clusters with different oxidation states from those discussed here. The reaction of oxidizing and reducing agents

with current clusters appears promising.

4.5 Final words

The development of iron-amide and iron-imide-sulfide clusters with weak-field iron centers has demonstrated several interesting and informative points related to FeMo cofactor chemistry, including Fe-N bond properties and partial synthetic analogues. Although iron-sulfur analogue chemistry is now a mature subject in large part, almost no work on analogue clusters with mixed iron-imide-sulfide cores has previously been accomplished. Our research is to explore the chemistry of the mixed Fe-NR-S cores in weak-field heteroligated environments to gain insight into cofactor properties.

References

1. Seefeldt, L. C.; Hoffman, B. M.; Dean, D. R. *Annu. Rev. Biochem*. **2009**, *78*, 701.
2. Stewart, W. D. P. *Ann. Rev. Microbiol*. **1973**, *27*, 283.
3. Kozuch, S.; Shaik, S. *J. Phys. Chem. A* **2008**, *112*, 6032.
4. Barney, B. M.; Yurth, M. G.; Dos Santos, P. C.; Dean, D. R.; Seefeldt, L. C. *J. Biol. Inorg. Chem.* **2009**, *14*, 1015.
5. Hoffman, B. M.; Dean, D. R.; Seefeldt, L. C. *Acc. Chem. Res.* **2009**, *42*, 609.
6. Peters, J. W.; Szilagyi, R. K. *Curr. Opin. Chem. Biol.* **2006**, *10*, 101.
7. Burgess, B. K.; Lowe, D. *J. Chem. Rev.* **1996**, *96*, 2983.
8. Hernandez, J. A; George, S. J.; Rubio, L. M. *Biochemistry* **2009**, *48*, 9711
9. Barney, B. M.; Yurth, M. G.; Dos Santos, P. C.; Dean, D. R.; Seefeldt, L. C. *J. Biol. Inorg. Chem.* **2009**, *14*, 1015.
10. Mayer, S. M.; Lawson, D. M.; Gormal, C. A.; Roe, S. M.; Smith, B. E. *J. Mol. Biol*. **1999**, *292*, 871.
11. Peters, J. W.; Stowell, M. H. B.; Soltis, S. M.; Finnegan, M. G.; Johnson, M. K.; Rees, D. C. *Biochemistry* **1997**, *36*, 1181.
12. Lee, C. C.; Blank, M. A.; Fay, A. W.; Yoshizawa, J. M.; Hu, Y.; Hodgson, K. O.; Hedman, B.; Ribbe, M. W. *Proc. Natl. Acad. Sci. U.S.A.* **2009**, *106*, 18474.
13. Kim, J.; Rees, D. C. *Science* **1992**, *257*, 1677.
14. Kim, J.; Rees, D. C. *Nature* **1992**, *260*, 553.
15. Hu, Y.; Fay, A. W.; Lee, C. C.; Yoshizawa, J; Ribbe, M. W. *Biochemistry* **2008**, *47*, 3973.

16. Einsle, O.; Tezcan, F. A.; Andrade, S. L.; Schmid, B.; Yoshida, M., Howard, J. B.; Rees, D. C. *Science* **2002**, *297*, 1696.

17. Lovell, T.; Li, J.; Liu, T.; Case, D.; Noodleman, L. *J. Am. Chem. Soc.* **2001**, *123*, 12392.

18. Dance, I. *Chem. Commun.* **2003**, 324.

19. Hinnemann, B.; Nørskov, J. K. *J. Am. Chem. Soc.* **2003**, *125*, 1466.

20. Hoffman, B. M. *Proc. Natl. Acad. Sci. U.S.A.* **2003**, *100*, 3575.

21. Hoffman, B. M. *Acc. Chem. Res.* **1991**, *24*, 164.

22. Lippard, S. J.; Berg, J. M. *Principles of Bioinorganic Chemistry*; University Science Books: Mill Valley, CA, **1994**.

23. Zheng, L.; Dean, D. R. *J. Biol. Chem.* **1994**, *269*, 18723.

24. Burgess, B. K. *Chem. Rev.* **1990**, *90*, 1377.

25. Ibers, J. A.; Holm, R. H. *Science* **1980**, *209*, 223.

26. Rao, P. V.; Holm, R. H. *Chem. Rev.* **2004**, *104*, 527.

27. Averill, B. A.; Herskovitz, T.; Holm, R. H.; Ibers, J. A. *J. Am. Chem. Soc.* **1973**, *95*, 3523.

28. Lane, R. W.; Ibers, J. A.; Frankel, R. B.; Holm, R. H. *Proc. Natl. Acad. Sci. U.S.A.* **1975**, *72*, 2868.

29. Tsukihara, T.; Fukuyama, K.; Tahara, H.; Katsube, Y.; Matsuura, Y.; Tanaka, N.; Kakudo, M.; Wada, K.; Matsubara, H. *J. Biochem. (Tokyo)* **1978**, *84*, 1645.

30. Herskovitz, T.; Averill, B. A.; Holm, R. H.; Ibers, J. A.; Phillips, W. D.;Weiher, J. F. *Proc. Natl. Acad. Sci. U.S.A.* **1972**, *69*, 2437.

31. Sieker, L. C.; Adman, E.; Jensen, L. H. *Nature* **1972**, *235*, 40.

32. DePamphilis, B. V.; Averill, B. A.; Herskovitz, T.; Que, L., Jr.; Holm, R. H. *J. Am. Chem. Soc.* **1974**, *96*, 4159.

33. Bobrik, M. A.; Que, L., Jr.; Holm, R. H. *J. Am. Chem. Soc.* **1974**, *96*, 285.

34. Robbins, A. H.; Stout, C. D. *Proteins: Struct., Funct. Genet.* **1989**, *5*, 289.

35. Zhou, J.; Holm, R. H. *J. Am. Chem. Soc.* **1995**, *117*, 11353.

36. Kennedy, M. C.; Kent, T. A.; Emptage, M.; Merkle, H.; Beinert, H.; Munck, *E. J. Biol. Chem.* **1984**, *259*, 14463.

37. Hagen, K. S.; Watson, A. D.; Holm, R. H. *J. Am. Chem. Soc.* **1983**, *105*, 3905.

38. Wolff, T. E.; Power, P. P.; Frankel, R. B.; Holm, R. H. *J. Am. Chem. Soc*. **1980**, *102*, 4694.

39. Palermo, R. E.; Singh, R.; Bashkin, J. K.; Holm, R. H. *J. Am. Chem. Soc*. **1984**, *106*, 2600.

40. Armstrong, W. H.; Mascharak, P. K.; Holm, R. H. *Inorg. Chem.* **1982**, *21*, 1699.

41. Mascharak, P. K.; Armstrong, W. H.; Mizobe, Y.; Holm, R. H. *J. Am. Chem. Soc*. **1983**, *105*, 475.

42. Armstrong, W. H.; Holm, R. H. *J. Am. Chem. Soc*. **1981**, *103*, 6246.

43. Huang, J.; Goh, C.; Holm, R. H. *Inorg. Chem*. **1997**, *36*, 356.

44. Armstrong, W. H.; Mascharak, P. K.; Holm, R. H. *J. Am. Chem. Soc.* **1982**, *104*, 4373.

45. Zhou, J.; Holm, R. H. *J. Am. Chem. Soc.* **1995**, *117*, 11353.

46. Raebiger, J. W.; Crawford, C. A.; Zhou, J.; Holm, R. H. *Inorg. Chem*. **1997**, *36*, 994.

47. Kovacs, J. A.; Holm, R. H. *J. Am. Chem. Soc.* **1986**, *108*, 340.

48. Kovacs, J. A.; Holm, R. H. *Inorg. Chem.* **1987**, *26*, 702.

49. Kovacs, J. A.; Holm, R. H. *Inorg. Chem.* **1987**, *26*, 711.

50. Osterloh, F.; Achim, C.; Holm, R. H. *Inorg. Chem.* **2001**, *40*, 224.

51. Zhang, Y.; Zuo, J.-L.; Zhou, H.-C.; Holm, R. H. *J. Am. Chem. Soc.* **2002,** *124*, 14292.

52. Zuo, J.-L.; Zhou, H.-C.; Holm, R. H. *Inorg. Chem.* **2003**, *42*, 4624.

53. Ohki, Y.; Ikagawa, Y.; Tatsumi, K. *J. Am. Chem. Soc*. **2007**, *129*, 10457.

54. Ohki, Y.; Sunada Y.; Honda, M.; Katada, M.; Tatsumi, K. *J. Am. Chem. Soc*. **2003**, *125*, 4052.

55. Ohki, Y.; Imada M.; Murata, A.; Sunada, Y.; Ohta, S.; Honda, M.; Sasamori, T.; Tokitoh, N.; Katada, M.; Tatsumi. K. *J. Am. Chem. Soc*. **2009**, *131*, 13168.

56. Peters, J. W.; Szilagyi, R. K *Curr. Opin. Chem. Biol.* **2006**, *10***,** 101.

57. Verma, A. K.; Lee, S. C. *J. Am. Chem. Soc.* **1999,** *121,* 10838.

58. Duncan, J. S.; Nazif, T. N.; Verma, A. K.; Lee, S. C. *Inorg. Chem.* **2003**, *42*, 1211.

59. Duncan, J. S.; Traub, M. C.; Lee, S. C., manuscript in preparation

60. Link, H.; Fenske, D. *Z. Anorg. Allg. Chem.* **1999**, *625*, 1878.

61. Bennett, M. V.; Stoian, S.; Bominaar, E. L.; Munck, E.; Holm, R. H. *J. Am. Chem. Soc.* **2005**, *127*, 12378.

62. Bennett, M. H.; Holm, R. H. *Angew. Chem. Int. Ed.* **2006**, *45*, 5613.

63. Zhang, Y.; Holm, R. H. *Inorg. Chem.* **2004,** *43,* 674

64. Berlinguette, C. P.; Holm, R. H. *J. Am. Chem. Soc.* **2006,** *128,* 11993

65. Zhang, Y.; Holm, R. H. *J. Am. Chem. Soc.* **2003,** *125,* 3910

66. Hlavinka, M. L.; Miyaji, T.; Staples, R. J.; Holm, R. H. *Inorg. Chem.* **2007,** *46,* 9192

67. Couvanis, D.; Salifoglou, A.; Kanatzidis, M. G.; Simopoulos, A.; Papefthymiou, V. *J. Am. Chem. Soc.* **1984**, *106*, 6081.

68. Ballmann, J.; Albers, A.; Demeshko, S.; Dechert, S.; Bill, E.; Bothe, E.; Ryde, U.; Meyer, F. *Angew. Chem., Int. Ed.* **2008**, *47*, 9537.

69. Pryadun, R.; Holm, R. H. *Inorg. Chem.* **2008**, *47*, 3366.

70. Zhang, Y.; Holm, R. H. *J. Am. Chem. Soc.* **2003**, *125*, 3910.

71. Verma, A. K.; Nazif, T. N.; Achim, C.; Lee, S. C. *J. Am. Chem. Soc.* **2000**, *122,* 11013.

72. Chu, C. T. W.; Gall, R. S.; Dahl, L. F. *J. Am. Chem. Soc*. **1982**, *104*, 737.

73. Chu, C. T. W.; Lo, F. Y.; Dahl, L. F. *J. Am. Chem. Soc.***1982**, *104*, 3409.

74. Lee, S. C.; Holm, R. H. *Proc. Natl. Acad. Sci. U.S.A*. **2003**, *100*, 3595.

75. Holm, R. H. *Acc. Chem. Res.* **1995**, *67*, 217.

76. Xiao, Y.; Fisher, K.; Smith, M. C.; Newton, W. E.; Case, D. A.; George, S. J.; Wang, H.; Sturhahn, W.; Alp, E. E.; Zhao, J.; Yoda, Y.; Cramer, S. P. *J. Am. Chem. Soc.* **2006**, *128*, 7608.

77. Wong, G. B.; Bobrik, M. A.; Holm, R. H. *Inorg. Chem.* **1978**, *17*, 578.

78. Chen, X.-D.; Duncan, J. S.; Verma, A. K.; Lee, S. C. *J. Am. Chem. Soc.* **2010,** *132,* 15884.

79. Duncan, J. S.; Zdilla, M. J.; Lee, S. C. *Inorg. Chem*. **2007**, *46*, 1071.

80. Lee, S. C.; Holm, R. H. *Chem. Rev*. **2004**, *104*, 1135.

81. Sharp, C. R.; Duncan, J. S.; Lee, S. C. *Inorg. Chem.* **2010**, *49*, 6697.

82. Yu, S.; Papaefthymiou, G. C.; Holm. R. H. *Inorg. Chem.* **1991**, *30*, 3416.

83. Kern, R. J. *Inorg. Nucl. Chem.* **1962**, *24*, 1105.

84. Schaumann, E.;Wrided, U.; Ehlers, J. *Synth. Commun.* **1980**, 907.

85. Connelly, N. G.; Geiger, W. E. *Chem. Rev.* **1996**, *96,* 877.

86. Sheldrick, G. M. *Acta Crystallogr., Sect. A: Found, Crystallogr.* **2008**, *A64*, 112.

87. Alvarez, S. *Coord. Chem. Rev.* **1999,** *195,* 13

88. Olmstead, M. M.; Power, P. P.; Shoner, S. C. *Inorg. Chem.* **1991,** *30,* 2547

89. Chen, H.; Power, P. P.; Shoner, S. C. *Inorg. Chem.* **1991,** *30,* 2884

90. Hauptmann, R.; Kliss, R.; Henkel, G. *Angew. Chem., Int. Ed. Engl.* **1999,** *38,* 377

91. Power, P. P.; Shoner, S. C. *Angew. Chem., Int. Ed. Engl.* **1991,** *30,* 330

92. Bartlett, R. A.; Ellison, J. J.; Power, P. P.; Shoner, S. C. *Inorg. Chem.* **1991,** *30,* 2888

93. Frederick M.; MacDonnell, L.; Karin, R,; Effrey, J.; Ellison, R.; Holm, R. H.; Power. P. *Inorg. Chem.* **1995**, *34*, 1815.

94. Fedotova, Y.; Zhezlova, E. V.; Mushtina, T. G.; Kornev, A. N.; Chesnokova, T. A.; Fukin, G. K.; Zakharov, L. N.; Domrachev. G. A. *Russ. Chem. Bul.* **2003**, *52*, 414.

95. Kennepohl, D.; Brooker, S.; Shedldrick, G.; Roesky, H. Z. *Naturforsh., B: Chem. Sci.* **1992**, *47*, 9.

96. Campora, J.; Reyes, M.; Mereiter, K. *Organometallics*, **2002**, *21*, 1014.

97. Driess, M.; Merz, K; Rell, S. *Eur. J. Inorg. Chem.* **2000**, 2517.

98. Pechmann, T.; Brandt, C. D.; Werner, H. *Chem. Commun.* **2003,** 1136.

99. Lobana, T. S.; Khanna, S.; Butcher, R. J.; Hunter, A. D.; Zeller, M. *Inorg. Chem.* **2007,** *46,* 5826.

100. Noguchi, R.; Sugie, A.; Okamoto, Y.; Hara, A.; Nomiya, K. *Bull. Chem. Soc. Jpn.* **2005,** *78,* 1953.

101. Horn, C.; Dance, I.; Craig, D.; Scudder, M.; Bowmaker, G. *J. Am. Chem. Soc.* **1998,** *120,* 10549.

102. Mallela, S. P.; Schwan, F.; Geanangel, R. A. *Inorg. Chem.* **1996,** *35,* 745.

103. Olmstead, M. M.; Power, P. P.; Znorg. S. *C. Chem.* **1991**, *30*, 2547.

104. Bordwell, F. G. *Acc. Chem. Res.* **1988**, *21*, 456.